Leibniz-Institut für Katalyse e.V. an der Universität Rostock

Fundamentals determining activity and product selectivity in the oxidative coupling of methane over MnO_x-M_2WO_4/SiO_2 (M=Na, K, Rb, or Cs)

Dissertation

In Kumulativer Form

zur Erlangung des akademischen Grades

Doctor rerum Naturalium (Dr. rer. Nat.)

der Mathematisch-Naturwissenschaftlichen Fakultät

der Universität Rostock

vorgelegt von

Anna Zanina

geb. am 16.01.1994 in Irkutsk, Russland

Rostock, 2023

https://doi.org/10.18453/rosdok_id00004386

Die vorliegende Arbeit entstand in der Zeit von Juli 2020 bis Februar 2023 am Leibniz-Institut für Katalyse e.V. an der Universität Rostock unter der Betreuung von Prof. Dr. Evgenii V. Kondratenko (Leiter der Themengruppe „Reaktionsmechanismen“).

This thesis was performed in the Leibniz Institute for Catalysis at the University of Rostock in the period from July 2020 to February 2023 and was supervised by Prof. Dr. Evgenii V. Kondratenko (the group leader of “Reaction mechanisms”).

1. Gutachter

Prof. Dr. Evgenii V. Kondratenko

Leibniz-Institut für Katalyse e.V., 18059 Rostock, Germany

2. Gutachter

Prof. Dr. Reinhard Schomäcker

Institute of Chemistry, TU Berlin, 10623 Berlin, Germany

Tag der Einreichung: 10.03.2023

Tag der mündlichen Prüfung: 06.06.2023

Prüfungsrechtliche Erklärung

Ich, Anna Zanina, versichere, dass ich die Arbeit selbständig verfasst, nicht anderweitig für Prüfungszwecke vorgelegt, alle benutzten Quellen und Hilfsmittel angegeben sowie wörtliche und sinngemäße Zitate als solche gekennzeichnet habe.

Plagiarism Declaration in Accordance with Examination Rules

I herewith declare that I have worked on this thesis independently. Furthermore, it was not submitted to any other examining committee. All sources and aids used in this thesis, including literal and analogous citations, have been identified.

Rostock, March 2023

Acknowledgment

First of all, I would like to express my sincere gratitude to my supervisor, Prof. Dr. Evgenii V. Kondratenko, for the unique opportunity to conduct the present dissertation in his group at the Leibniz Institute for Catalysis. I am extremely grateful for his constant support and unwavering guidance, helpful and productive discussions, invaluable insights into the topic, and inspiring motivation.

I would like to thank Prof. Dr. Reinhard Schomäcker for kindly agreeing to review this thesis.

My special thanks go to all colleagues who contributed to the scientific results of this work. I would like to thank Dr. Vita A. Kondratenko for performing TAP experiments and for great help in discussions and writing, Dr. Henrik Lund for performing many sophisticated in situ XRD experiments. I would also like to thank all the people from the technical support of LIKAT.

For financial support, I would like to thank the German Research Foundation. This work was performed within the framework of a Sino-German project. Therefore, I would like to thank all the collaborators, Prof. Guiyuan Jiang, Dr. Yuming Li, Jianshu Li, Juan Chen, Kai Wu, and Lin Xu, for our cooperative work.

Furthermore, I would like to thank all my colleagues in the Catalyst Discovery and Reaction Engineering Department. I am very grateful to the head of the department, Dr. David Linke, for his warm welcome to the department and all his help. Many thanks to all my colleagues, Karin Buchholz, Dr. Mariana Armbruster, Dr. Uwe Rodemerck. Dr. Tatiana Otroshchenko, Dr. Zeynep Aydin, Dr. Andrey Skrypnik, Dr. Qingxin Yang, Dr. Dan Zhao, Laura Kraußer, Nils Ortner, Aleksandr Fedorov, and Qiyang Zhang, for all their help and support over the past three years.

My deepest and heartfelt thanks are extended to my parents, Nina and Vadim, who have been my best role models and have always supported and cheered me up. And finally, I am indebted to my partner, Denis Makhmutov, who has been by my side all these years, from the beginning of our journey in chemistry, and with whom we have made it to this point together. He has not only been a great moral support during the last three years, but has also tirelessly helped me in all aspects of my work. I have been very fortunate to work with him together. I am eternally grateful to him for everything.

Zusammenfassung

Die steigende Nachfrage nach Ethylen erfordert neue Ansätze für seine Herstellung. Das Steamcracken oder das katalytische Cracken verschiedener Erdölfraktionen, das derzeit das wichtigste Verfahren zur Ethylenherstellung darstellt, verbraucht aufgrund seines endothermen Charakters viel Energie, verursacht hohe CO_2-Emissionen und ist von den Erdölressourcen abhängig. Vor diesem Hintergrund ist die oxidative Kopplung von Methan (OCM) zu C_2-Kohlenwasserstoffen (C_2H_6 und C_2H_4) ein attraktiver Weg zur Verwendung von Methan, das in großen Mengen in Erdgas und Biogas vorhanden ist. Neben einer hohen Aktivität und Selektivität muss ein geeigneter OCM-Katalysator eine Langzeitstabilität bei hohen Temperaturen (700-900 °C) aufweisen. Der MnO_x-Na_2WO_4/SiO_2-Katalysator erfüllt diese Anforderungen. Die unzureichende Kenntnis der Grundlagen, die für ein maßgeschneidertes Katalysatordesign erforderlich sind, schränkt jedoch weitere Verbesserungen dieses Katalysatorsystems ein, die für eine potenzielle industrielle Anwendung notwendig sind. Einer der Gründe dafür sind die Einschränkungen der in situ/operando Charakterisierungstechniken aufgrund der schwierigen Reaktionsbedingungen. Kürzlich vorgeschlagene mechanistische Konzepte, die auf der Beteiligung von MnO_x-Phasen, Gittersauerstoff von Na_2WO_4 und Na-WO_x-Stellen basieren, werden noch kontrovers diskutiert. Die Rolle adsorbierte Sauerstoffspezies wird oft übersehen, obwohl sie, wie in dieser Studie gezeigt wurde, eine wichtige Rolle spielen.

Ein systematischer Multimethodenansatz, der in dieser Arbeit entwickelt und angewandt wurde, ermöglichte neue Einblicke in den Mechanismus der Produktbildung, der aktiven Phasen und der Sauerstoffspezies in der OCM-Reaktion über (MnO_x)-M_2WO_4/SiO_2 (M=Na, K, Rb oder Cs). Unter Verwendung von O_2 (O_2-OCM) oder N_2O (N_2O-OCM) als Oxidationsmittel wurde festgestellt, dass monoatomare Spezies für die selektive Umwandlung von Methan in C_2-Kohlenwasserstoffe verantwortlich sind. Ihre Konzentration kann durch die Verwendung von N_2O als Oxidationsmittel kontrolliert werden, und/oder durch die Zugabe von H_2O, das an der Zersetzung von unselektiven zweiatomigen Sauerstoffspezies beteiligt ist, die aus Sauerstoff in der Gasphase gebildet werden. In situ/operando UV-vis-Messungen haben gezeigt, dass der Oxidationszustand von MnO_x in MnO_x-Na_2WO_4/SiO_2 in der N_2O-OCM etwas niedriger ist als in der O_2-OCM. Dies führt zu einer Isolierung von Gittersauerstoffstellen, was auch für die selektive Methanumwandlung von Vorteil ist.

Impulsexperimente in Abwesenheit und Anwesenheit von Sauerstoff haben gezeigt, dass der Gittersauerstoff von M_2WO_4/SiO_2 (M=Na, K, Rb oder Cs) nicht in der Lage ist, Methan selektiv in C_2-Kohlenwasserstoffe umzuwandeln, sondern nur in CO_x-Produkte mit geringer Reaktivität bildet. Somit

wurde festgestellt, dass adsorbierte Sauerstoffspezies, die aus der Gasphase stammen, sowohl für die Methanaktivierung (C–H-Bindungsspaltung) als auch für die Produktbildung wesentlich sind. Eine besondere Rolle der geschmolzenen Na_2WO_4- oder MnO_x-Phase(n) für die selektive Bildung von C_2-Kohlenwasserstoffen konnte nicht bestätigt werden. Es wurde jedoch festgestellt, dass die Aktivität dieser Katalysatoren von der Elektronegativität der Alkalimetalle abhängt. Es wurde daher vorgeschlagen, dass die elektronischen Eigenschaften der M_2WO_4/SiO_2-Katalysatoren für die Bildung adsorbierter Sauerstoffspezies entscheidend sind, die folglich die Katalysatoraktivität beeinflussen.

Um die Art der Sauerstoffspezies, die an der Methanaktivierung beteiligt sind, und die Rolle von Alkalimetall und MnO_x zu bestimmen, wurde eine systematische Vergleichsuntersuchung der trimetallischen MnO_x-M_2WO_4/SiO_2 (M=Na, K, Rb oder Cs) und der M_2WO_4/SiO_2-Katalysatoren durchgeführt. Im Gegensatz zu diesen kann der Gittersauerstoff der trimetallischen Katalysatoren Methan selektiv in C_2-Kohlenwasserstoffe umwandeln. Die adsorbierten Sauerstoffspezies spielen jedoch sowohl bei bi- als auch bei trimetallischen Katalysatoren eine entscheidende Rolle. Es wurde kein Einfluss des Alkalimetalls in MnO_x-M_2WO_4/SiO_2 auf die Aktivität und die C_2-Kohlenwasserstoffselektivität festgestellt. Die höhere Aktivität des MnO_x-haltigen Katalysators im Vergleich zu M_2WO_4/SiO_2 (M=Na, K, Rb oder Cs) wurde durch eine höhere Umsatzfrequenz der aktiven Stellen erklärt.

Abstract

With the increasing demand for ethylene, new approaches to its production are required. Steam or catalytic cracking of different oil fractions, which is currently the main process used to produce ethylene, consumes a lot of energy due to its endothermic nature, resulting in high CO_2 emissions and depends on oil resources. From this perspective, the oxidative coupling of methane (OCM) to C_2-hydrocarbons (C_2H_6 and C_2H_4) is an attractive way to valorize methane, which is available in large amounts in natural gas and biogas. Apart from high activity and selectivity, a suitable OCM catalyst must have long-term stability at high temperatures (700-900 °C). The MnO_x-Na_2WO_4/SiO_2 catalyst fulfils these requirements. However, the insufficient knowledge of fundamentals required for tailored catalyst design limits further improvements of this catalytic system, which are necessary for potential industrial application. One of the reasons for this situation is the limitations of in situ/operando characterization techniques due to severe reaction conditions. Recently proposed mechanistic concepts based on the involvement of MnO_x phases, lattice oxygen of Na_2WO_4 and Na-WO_x sites are still controversially discussed. The role of adsorbed oxygen species is often overlooked, although they play an important role as demonstrated in the present study.

A systematic and multi-technique approach developed and applied in this work enabled to provide new insights into the mechanism of product formation, active phases, and oxygen species in the OCM reaction over (MnO_x)-M_2WO_4/SiO_2 (M=Na, K, Rb, or Cs). Using O_2 (O_2-OCM) or N_2O (N_2O-OCM) as oxidants, monoatomic oxygen species were concluded to be responsible for the selective conversion of methane into C_2-hydrocarbons. Their concentration can be controlled by using N_2O as an oxidant and/or by adding of H_2O that is involved in decomposition of unselective biatomic oxygen species formed from gas-phase oxygen. In situ/operando UV-vis measurements revealed that the oxidation state of MnO_x in MnO_x-Na_2WO_4/SiO_2 is slightly lower in the N_2O-OCM than in the O_2-OCM. This results in isolation of lattice oxygen sites, which is also beneficial for the selective methane conversion.

Pulse experiments in the absence and presence of oxygen showed that lattice oxygen of M_2WO_4/SiO_2 (M=Na, K, Rb, or Cs) is unable to selectively convert methane into C_2-hydrocarbons, but forms CO_x products exclusively, however, with low reactivity. Thus, adsorbed oxygen species originating from gas-phase oxygen were established to be essential both for methane activation (C–H bond cleavage) and product formation. No exceptional role of molten Na_2WO_4 or MnO_x phase(s) for the selective formation of C_2-hydrocarbons was confirmed. However, the activity of these catalysts was found to be dependent on the electronegativity of alkali metals. Thus, it was proposed that the electronic properties of the

M_2WO_4/SiO_2 catalysts define the formation of adsorbed oxygen species that consequently affects the catalyst activity.

To determine the kind of oxygen species participating in methane activation and the role of alkali metal and MnO_x, a systematic comparative study of the trimetallic MnO_x-M_2WO_4/SiO_2 (M=Na, K, Rb, or Cs) and their MnO_x-free counterparts was performed. In contrast to the M_2WO_4/SiO_2 catalysts, lattice oxygen of the trimetallic counterparts can selectively convert methane into C_2-hydrocarbons. However, adsorbed oxygen species play a crucial role for both bi- and trimetallic catalysts. No effect of alkali metal in MnO_x-M_2WO_4/SiO_2 on activity and C_2-hydrocarbons selectivity was observed. The higher activity of the MnO_x-containing catalyst compared to M_2WO_4/SiO_2 (M=Na, K, Rb, or Cs) was explained by a higher turnover frequency of active sites.

Contents

1. Introduction 1

1.1. Industrial routes of methane conversion 1

1.2. Direct routes of methane conversion 3

1.2.1. Non-oxidative coupling of methane. 4

1.2.2. Oxidative coupling of methane 5

1.3. What is known about the promising MnO_x-Na_2WO_4/SiO_2 catalyst? 13

1.3.1. Preparation methods/phase composition of MnO_x-Na_2WO_4/SiO_2 13

1.3.2. Role of SiO_2 phase in MnO_x-Na_2WO_4/SiO_2 14

1.3.3. Enhancing effect of water on catalyst activity and product selectivity 15

1.3.4. Proposed active phase/species 16

2. Objectives and outline 19

2.1. Objectives 19

2.2. Outline 20

3. Results 21

3.1. Effects of N_2O and water on activity and selectivity in the oxidative coupling of methane over MnO_x-Na_2WO_4/SiO_2: role of oxygen species. 21

3.2. The role of adsorbed and lattice oxygen species in product formation in the oxidative coupling of methane over M_2WO_4/SiO_2 (M=Na, K, Rb, or Cs) 26

3.3. Performance-defining factors of MnO_x-M_2WO_4/SiO_2 (M=Na, K, Rb or Cs) catalysts in oxidative coupling of methane 31

4. Conclusions 36

5. Outlook 37

6. References 38

7. Publications 47

8. Curriculum vitae 146

List of abbreviations

CL-OCM – chemical looping oxidative coupling of methane

DFT – density functional theory

EPR – electron paramagnetic resonance

FTO – Fischer-Tropsch-to-olefins

GTL – gas-to-liquids

GTM – gas-to-methanol

IWI – incipient wetness impregnation

KIE – kinetic isotope effect

MSA – methanesulfonic acid

MTO – methanol-to-olefins

NG – natural gas

NOCM – non-oxidative coupling of methane

OCM – oxidative coupling of methane

PSA – pressure swing adsorption

SC – steam cracking

SG – sol-gel

SSITKA – steady-state isotopic transient kinetic analysis

TPSR – temperature programmed surface reaction

UOP – Universal Oil Products

XANES – X-ray absorption near edge structure

XPS – X-ray photoelectron spectroscopy

XRD – X-Ray diffraction

XRD-CT – X-ray diffraction computed tomography

1. Introduction

1.1. Industrial routes of methane conversion

Methane is the simplest hydrocarbon that is the main constituent of natural gas, biogas, shale gas, or gas clathrates. According to the annual statistical review of British Petroleum in 2021, proven reserves of natural gas are $190 \cdot 10^{12}$ m^3 (oil reserves - $244 \cdot 10^9$ tons) [1]. At the same time, proven reserves of shale gas in the USA and China are $2.7 \cdot 10^{12}$ m^3 and $2.0 \cdot 10^{12}$ m^3, respectively, while estimated unproven reserves can be up to hundreds of trillions of cubic meters [2, 3]. Meanwhile, the deposits of methane hydrates are estimated to be between $2 \cdot 10^{14}$ m^3 and $3 \cdot 10^{18}$ m^3, which is many times the reserves of conventional oil, natural gas, and coal combined [4, 5]. These enormous reserves of methane make it the most available and affordable carbon source for the petrochemical industry. However, methane deposits are often located in remote areas, that causes difficulties related to its transportation. As a consequence, methane is flared on site (ca. $144 \cdot 10^9$ m^3/year), resulting in unnecessary CO_2 emissions [6].

Despite the large reserves of methane and its potential to become the major feedstock for the chemical industry, methane is mainly combusted (about 90%) for heating purposes and power generation. Nevertheless, there are a few large-scale processes that use methane to produce value-added products. The largest one is the production of synthesis gas (syngas, a mixture of CO and H_2). Syngas can be produced by steam reforming, dry reforming or partial oxidation of methane according to equations 1-3, respectively [7]. Steam reforming of methane is the mature technology used worldwide. As this reaction is endothermic, the process is conducted at 750-850 °C over Ni-containing catalysts [8, 9]. The main applications of syngas include ammonia (to the largest extent), methanol and Fischer-Tropsch syntheses [10] (Figure 1.1).

$$CH_4 + H_2O \rightleftharpoons CO + 3H_2 \qquad \Delta H°_{298K} = 206 \text{ kJ/mol} \tag{1}$$

$$CH_4 + CO_2 \rightleftharpoons 2CO + 2H_2 \qquad \Delta H°_{298K} = 247 \text{ kJ/mol} \tag{2}$$

$$CH_4 + 0.5O_2 \rightleftharpoons CO + 2H_2 \qquad \Delta H°_{298K} = -36 \text{ kJ/mol} \tag{3}$$

The production of methanol is a well-established technology around the globe, e.g., the Lurgi gas-to-methanol (GTM) process [11]. Cu-ZnO-Al_2O_3 catalysts are typically applied at 270-300 °C and a pressure of 50-100 bar. Methanol is also used to produce the highly demanded ethylene and propylene through the methanol-to-olefins (MTO) technology, which was originally jointly licensed by UOP and Norsk Hydro. Nowadays, several other companies (Lurgi, Exxon Mobil, SINOPEC, etc.) have developed

their technologies of MTO process. The MTO reaction is carried out over acidic zeolite catalysts (ZSM-5, SAPO-34) at 350-400 °C and atmospheric pressure [12].

Syngas is also used in the Fischer-Tropsch synthesis (FTS) to produce higher hydrocarbons. Adjusting the selectivity of FTS predominantly towards light olefins (ethylene and propylene) could be an alternative way to produce these value-added products (Fischer-Tropsch-to-olefins, FTO). Currently, Fischer-Tropsch synthesis is utilized for the production of liquid hydrocarbons (GTL gas-to-liquids process), e.g., Shell plants in Malaysia, Peral GTL in Qatar and another plant in Qatar owned by Qatar Petroleum [13]. For FTO to be used on an industrial scale, the problem of low selectivity to target light olefins needs to be overcome.

Natural gas is also the main feedstock for acetylene production, that has been originally carried out using an electric arc as the energy source [14]. Later, a process based on partial oxidation of natural gas was developed [15]. However, the demand for acetylene has decreased over the years as light olefins are currently produced from crude oil [16, 17].

Methane can also be used to produce halogenated hydrocarbons. The reaction between methane and molecular Cl_2 or Br_2 (eq. 4) can be carried out either non-catalytically (thermally/photo-initiated) or catalytically [18, 19]. The former approach cannot provide high selectivity and results in a mixture of halogenated products. In the presence of heterogeneous catalysts, methane reacts with hydrogen halides (HCl, HBr) in the presence of oxygen under relatively mild conditions (300-500 °C, atmospheric pressure) (eq. 5) [20, 21]. The obtained methyl halides can be further converted into lower olefins (eq. 6). Harmful and expensive HX can be recycled for the methyl halide production. However, the olefins obtained in this way require additional purification for their further use in polymerization reactions. The main barriers to large-scale implementation of halogen-mediated methane conversion are the toxicity of the precursors used and their corrosiveness, which poses a major challenge for the choice of reactor material. In addition, this process includes several steps for the production of value-added chemicals, which contributes to higher costs and does not provide obvious economic benefits [22, 23].

$$CH_4 + X_2 \rightarrow CH_3X + HX\ (Cl, Br) \quad (4)$$

$$CH_4 + HX + 0.5O_2 \rightarrow CH_3X + H_2O \quad (5)$$

$$nCH_3X \rightarrow \frac{n}{6}C_2H_4 + \frac{n}{9}C_3H_6 + \frac{n}{12}C_4H_8 + nHX\ (Cl, Br) \quad (6)$$

Another large-scale use of methane is the production of hydrogen cyanide by the Andrussow process. This process is based on the reaction of methane and ammonia in the presence of oxygen over Pt-Rh

gauze catalysts [24]. Methane and ammonia can also be converted non-oxidatively into HCN and H_2 over noble metal catalysts according to the BMA- or Degussa process [25, 26]. This reaction is highly endothermic and requires temperatures above 1100°C.

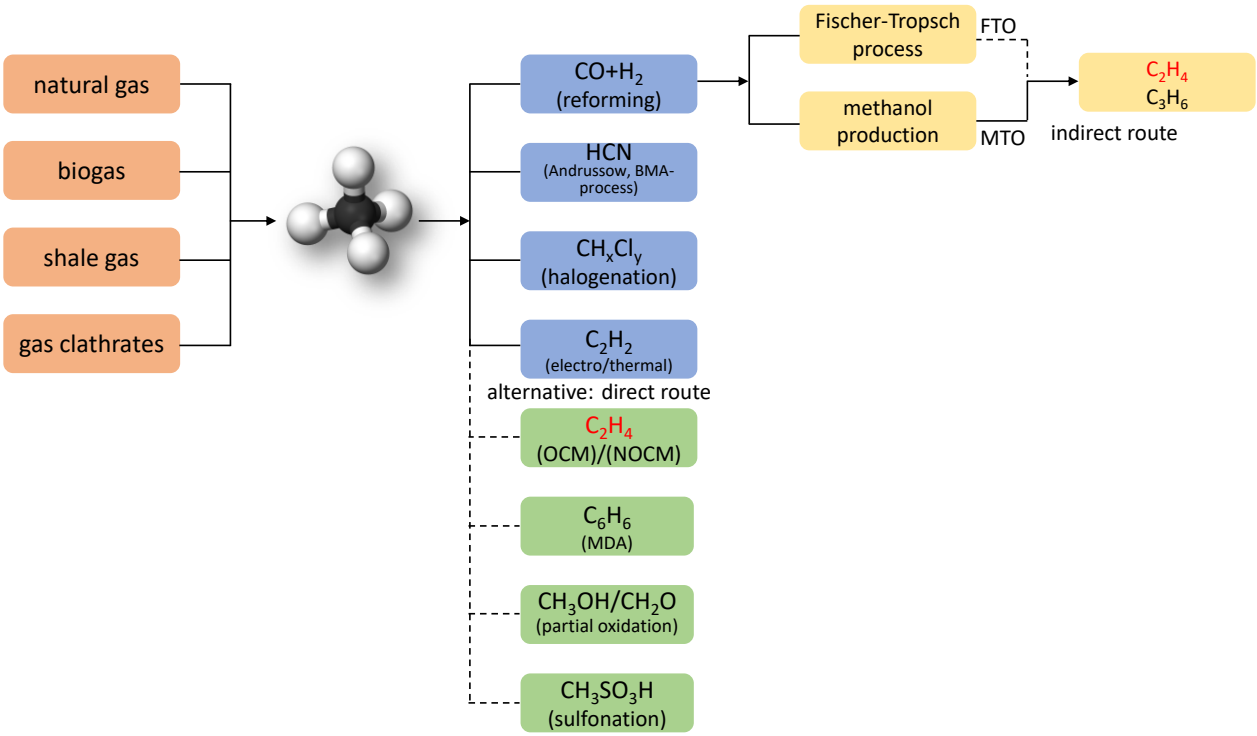

Figure 1.1. Sources of methane as well as products formed from this hydrocarbon on a large scale (blue boxes) or in research laboratories (green boxes). Industrial processes based on CH_4 and leading to ethylene are also shown.

1.2. Direct routes of methane conversion

A direct large-scale process to produce light olefins such as ethylene or propylene substantial for petrochemistry is steam cracking of oil-derived feedstocks (often naphtha). The dependence on crude oil is one of the drawbacks of this process, as oil reserves are limited. In addition, the olefins production causes more than 200-300 million tons of CO_2 emissions annually (or 1-2 tons of CO_2 per ton of olefins) [27, 28]. Therefore, it is highly desirable to produce ethylene more sustainably and from a more available source, which can be methane [29]. Ethane and ethylene can be produced through oxidative or non-oxidative coupling of methane, which is introduced and thoroughly discussed in Sections 1.2.1 or 1.2.2.

Aromatics can also be produced directly from methane through methane dehydroaromatization (MDA) without the use of oxidants according to eq. 7. This reaction is highly endothermic and is typically carried out at temperatures above 700 °C, with graphitic carbon being the most thermodynamically

favorable product. The main problems of this process are related to rapid coke formation and low per pass catalyst productivity [30].

$$6CH_4 \rightleftharpoons C_6H_6 + 9H_2 \qquad \Delta H°_{298K} = 532 \text{ kJ/mol} \qquad (7)$$

In the presence of an oxidizing agent, methane can be converted directly into methanol or formaldehyde. Non-catalytically, the reaction of methane with oxygen at temperatures of ca. 500 °C and at high pressures (30-200 bar) leads to methanol. The formation of formaldehyde is more favorable at lower pressures. MFI zeolites containing catalytically active CuO_x, MoO_x or FeO_x (or combinations thereof) or heteropolyacids were found to be the most active catalysts for the partial oxidation of methane to methanol [31]. A catalyst can significantly improve the activity; however, as methane conversion increases, the selectivity to CO_2 also increases, preventing high yields of methanol [32].

Recently, the company Grillo reported the synthesis of methanesulfonic acid (MSA) from methane and sulfur trioxide (oleum) at about 100 bar and 50 °C with the addition of an electrophilic MSA initiator (less than 1%). The determined yield of the target product is about 99% [33]. This promising technology has been already acquired by BASF, the largest manufacturer of MSA [34].

1.2.1. Non-oxidative coupling of methane

Direct conversion of methane to ethylene is possible in the absence or in the presence of gas-phase oxygen (non-oxidative or oxidative coupling of methane). The non-oxidative coupling of methane allows to avoid overoxidation of the desired products, but is an endothermic process (eq. 8, 9). The free Gibbs energy of the methane conversion into ethane and hydrogen (eq. 8) almost does not change in a wide temperature range (up to 1300 °C), while it becomes significantly lower for the formation of ethylene at higher temperatures (eq. 9) [35]. It is important to note that the formation of aromatics or polyaromatics is even more probable than the formation of aliphatic hydrocarbons [30]. In other words, the MDA reaction would be preferable to the non-oxidative coupling of methane to ethane/ethylene. Typically, the latter reaction is conducted in a two-step homologation of methane reaction. The first step is methane adsorption and formation of carbonaceous species on the catalyst surface, the second step is the formation of higher hydrocarbons upon their reaction with fed hydrogen [36-39]. Highly selective formation of C_2-hydrocarbons (>90%) was observed over Pt-Bi/ZSM-5 catalyst at 600-700 °C, while methane conversion was around 2% [40]. The conversion of methane to C_2-hydrocarbons is limited by the equilibrium, so the maximum possible methane conversion to C_2H_6 at 900 °C is 4.8% [35]. An extremely promising catalyst for non-oxidative coupling of methane was proposed by Bao's group, namely, lattice confined single-

site Fe supported on SiO_2 [41]. It was possible to selectively convert methane (ca. 32%) to ethylene (52.7%), benzene (22.5%) and naphthalene (25.8%). Importantly, no coke formation was observed over 60 hours on methane stream. Such high performance could not be achieved in further studies; however, it was noted that the Fe/SiO_2 catalyst does not favor significant coke deposition [42-44].

$$2CH_4 \rightleftharpoons C_2H_6 + H_2 \qquad \Delta H°_{298K} = 65 \text{ kJ/mol} \qquad (8)$$

$$2CH_4 \rightleftharpoons C_2H_4 + 2H_2 \qquad \Delta H°_{298K} = 202 \text{ kJ/mol} \qquad (9)$$

$$CH_4 \rightleftharpoons C + 2H_2 \qquad \Delta H°_{298K} = 75 \text{ kJ/mol} \qquad (10)$$

1.2.2. Oxidative coupling of methane

The oxidative coupling of methane (OCM) to C_2H_6 and C_2H_4 (C_2-hydrocarbons) opens a direct route to methane valorization, avoiding its initial conversion into syngas. The possibility of such conversion was first reported in 1982 by Bhasin and Keller [45]. As it can be seen from the report of the Web of Science platform for keywords "Oxidative coupling of methane" (Figure 1.2), the interest in this reaction in academia can be observed in two waves. The peak of the first wave happened in the mid-1990s, while the second wave is occurring in the 2020s, and it is not clear how this trend will change in the future.

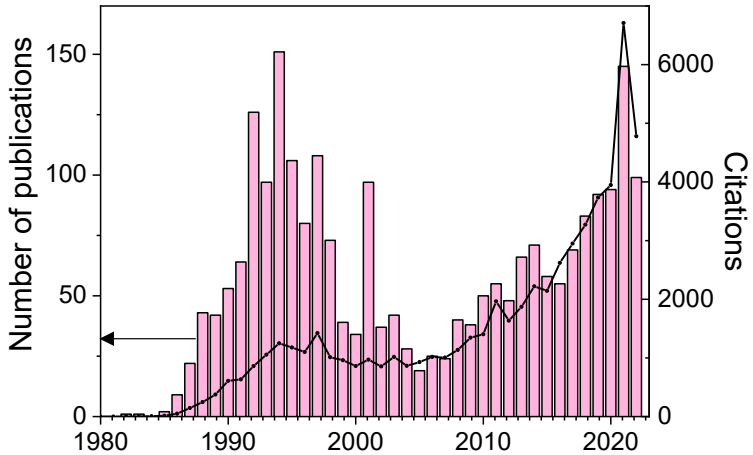

Figure 1.2. Publications (bars) and citation report (line) generated by the Web of Science platform for the search "Oxidative coupling of methane" in 1980-2022.

The motivation for the new wave of research comes from the annually increasing demand for ethylene (today's production is at $150\text{-}160 \cdot 10^6$ tons/year) and growing price of oil. According to the techno-economic evaluation of the OCM viability carried out by Spallina et al., its real implementation depends on the price of natural gas (NG). For example, the production of ethylene by OCM in Saudi Arabia, where the price of NG and electricity is low, can already be an alternative to steam cracking (SC). The

most expensive part of production in both processes is the refrigeration units for product separation, but SC was calculated to be twice cheaper in capital expenditure compared to OCM. The difference in ethylene cost between the conventional SC process and the best OCM scenario in Europe was found to be 374 €/ton of ethylene (835 €/ton vs. 1209 €/ton). An ethylene yield of 50% in the OCM reaction was identified as necessary to compete with the SC process (ethylene price drops to 876 €/ton) [46]. The predictive techno-economic analysis, also oriented to the European market, showed that the OCM technology can become an alternative to the SC route in 2030-2035 if the price of naphtha changes more significantly than the price of NG. The analysis was based on known kinetics developed for the La_2O_3/CaO catalyst. The lowest price of ethylene by OCM was calculated to be 1514 €/ton (market price in October 2021 was 1190 €/ton [47]) when it is produced at 850 °C, $CH_4/O_2 = 3$ and methane conversion and C_2-hydrocarbons selectivity are 32% and 44%, respectively (yield 14%). It was shown that these conditions do not provide the highest possible yield, but the lowest price. Moreover, ensuring higher selectivity to C_2-hydrocarbons would rather be more impactful on the ethylene price than achieving higher methane conversion for the same yield [48].

Siluria Technology is the US-based company attempting to develop an industrial process on the basis of OCM. The company owns the first demonstration plant located in La Porte, Texas [49]. In their reports, they underlined their focus on adapting OCM for mid- or small-scale production ($<0.15\cdot10^6$ tons/year), trying to make the process more economically attractive by replacing expensive cryogenic distillation for product separation with pressure swing adsorption (PSA). If the OCM reaction can be industrially viable at such scale, it would be advantageous since SC is only used in mega-scale production (scale of crackers is typically $0.5\cdot10^6$-$1.5\cdot10^6$ tons of ethylene), while typical conversion to polymers requires $0.05\cdot10^6$-$0.15\cdot10^6$ tons of ethylene [50, 51]. Using a high throughput experimental tool, Siluria claimed to test hundreds of catalyst compositions. As they stated, it was possible to find a catalyst that can stable operate under the required pressure (5-10 bar), at lower than typical temperatures (several hundred lower) for a long time (years). The unique nanostructured catalysts could belong to the catalyst family prepared by the company's patented technology for making nanowires of mixed oxides by the virus-template method [52, 53].

In the presence of gas-phase oxygen in the OCM reaction, both methane conversion into the desired C_2H_4 and C_2H_6 products (eq. 11, 12) as well as methane the oxidation to carbon oxides (eq. 13, 14) are exothermic processes. Thus, it is possible to achieve higher degrees of methane conversion in comparison with the NOCM reaction. However, since the formation of carbon oxides is thermodynamically more favorable than the desired products, it is challenging to produce them selectively from methane.

$$2CH_4 + 0.5O_2 \rightleftharpoons C_2H_6 + H_2O \quad \Delta H°_{298K} = -177 \text{ kJ/mol} \tag{11}$$

$$2CH_4 + O_2 \rightleftharpoons C_2H_4 + 2H_2O \quad \Delta H°_{298K} = -282 \text{ kJ/mol} \tag{12}$$

$$CH_4 + 1.5O_2 \rightleftharpoons CO + 2H_2O \quad \Delta H°_{298K} = -520 \text{ kJ/mol} \tag{13}$$

$$CH_4 + 2O_2 \rightleftharpoons CO_2 + 2H_2O \quad \Delta H°_{298K} = -803 \text{ kJ/mol} \tag{14}$$

1.2.2.1. Modes of OCM operation

There are several ways to carry out the OCM reaction. In a continuous mode of operation, methane and oxygen are fed together. In this case, non-reducible catalysts can be used (see Section 1.2.2.2). To avoid the side reactions, the reaction is typically operated under oxygen-lean conditions, where the CH_4/O_2 ratio is much higher than the stoichiometric ratio of 2 (for C_2H_4) or 4 (for C_2H_6). According to the OCM analysis performed by Green et al. [54], the upper limit of C_2-hydrocarbons formation in the co-feeding mode is 28%. For this purpose, a catalyst must be superior to those already known.

Methane and oxygen can also be fed separately in a periodic mode, i.e., a chemical looping (CL-OCM) concept [55, 56]. Product formation proceeds with participation of catalyst lattice oxygen reacting with fed CH_4. The removed lattice oxygen is then replenished by treating a catalyst with O_2. The advantages of this operation are that (i) air can be used for the reoxidation step instead of expensive O_2, since no separation of the oxidizing agent from the effluent is required, (ii) the absence of O_2 in the gas phase can result in improved selectivity to C_2-hydrocarbons due to a lower contribution of undesired reactions. In this case, however, the reaction is limited by the amount of oxygen stored by the catalyst.

Another concept aimed at maximizing the yield of C_2-hydrocarbons is the use of membrane reactors. In this mode of operation, oxygen is supplied through a permeable material along the reaction zone [57, 58]. Such concept allows oxygen to be distributed uniformly along the reactor as compared to a co-feeding mode in a fixed-bed reactor, where oxygen concentration is high at an inlet and gradually decreases in downstream located catalyst layers [59]. Importantly, methane and gas-phase oxygen are not in the direct contact, that eliminates unselective homogeneous reactions. As it was shown in [60], the selectivity to ethylene was exceptionally high using the $Ba_{0.5}Sr_{0.5}Co_{0.8}Fe_{0.2}O_{3-\delta}$ membrane reactor. It was possible to achieve the C_2H_4/C_2H_6 ratio of 12, while the same value for the fixed-bed reactor was about 1. However, despite the mentioned advantages of this concept, the maximum C_2 yield obtained in a membrane reactor is comparable or even lower (ca. 10-20%) than that obtained in a conventional fixed-bed reactor [61-65].

1.2.2.2. Catalysts for OCM

Catalysts for the OCM reaction can be divided into 4 groups, namely, (i) non-reducible metal oxides, (ii) reducible metal oxides, (iii) solid electrolytes, and (iv) halogen-containing catalysts [66]. The first three groups are suitable for continuous operation, periodic operation, and membrane reactor, respectively. The halogen-containing catalysts demonstrate high performance in OCM (reported yield 30-35% over MnO_x-containing catalysts doped with LiCl or NaCl) [67, 68]. Such performance was explained by higher methyl radical formation due to the participation of halogen radicals [69]. However, the main disadvantages of such materials are low stability due to the leaching of halogens and harmful impact on equipment due to corrosion.

Among the non-reducible catalysts, alkaline earth and rare earth metal oxides were found to be particularly active in OCM. MgO doped with Li, first proposed by Lunsford's group [70], is one of the most frequently studied catalysts. Doping of MgO with other alkali metals results in lower activity and selectivity [71, 72]. Despite the promising performance, the Li/MgO system is not stable for many hours under OCM conditions. One of the reasons for this is the loss of Li-component, as volatile LiOH or Li_2SiO_3 can be formed during the reaction. The latter can be formed by interaction of Li_2O with the quartz material of a reactor or quartz particles commonly used for catalyst dilution [73]. Regarding the active sites over Li/MgO, there are two major assumptions. The $[Li^+O^-]$ centers detected by EPR spectroscopy were proposed by the group of Lunsford as sites for methyl radical formation [74-76]. Conversely, it was suggested that $[Li^+O^-]$ centers can promote the formation of F-centers (oxygen vacancies) responsible for CH_4 activation [77, 78]. This assumption implies that MgO itself is an active catalyst in OCM, and its performance is controlled by the morphology of the catalyst surface. The role of Li is a structural promoter that can affect the microstructure of MgO [79-81]. Another example of popular non-reducible catalysts is La_2O_3 promoted with alkaline earth metal oxides (e.g., SrO) [82]. Doping of La_2O_3 supposedly results in either i) the formation of oxygen defects when La^{+3} is promoted by aliovalent Sr^{2+} ions or ii) the presence of SrO increases the overall basicity of the material. By tailoring the nanostructure of the La_2O_3 oxide, the operating temperatures can be significantly reduced. As it was shown in [83], CH_4 conversion > 25% and C_2-hydrocarbons selectivity >35% could be achieved at 450 °C over La_2O_3 nanorods, while a similar degree of methane conversion was achieved only at 650 °C over La_2O_3 nanoparticles or La_2O_3 bulk catalysts. Contrarily, it was found that among differently dimensional La_2O_3, the 2D structures (nanosheets) are the most active at low temperature [84]. It was shown that 14% of the C_2 yield can be achieved at 500 °C. The unique properties of nanostructured metal oxides appear to be promising for future industrial applications. For example, Siluria Technologies has

patented a method for preparing nanowires that are active and selective at low temperatures in OCM [52, 53].

One of the most studied redox catalysts is MnO_x-Na_2WO_4/SiO_2, which will be discussed in the Section 1.3. The main feature of redox catalysts is the mobility of lattice oxygen; therefore, they could be suitable for periodic mode of operation. Catalysts containing MnO_x have been found to be promising candidates for CL-OCM [55, 56, 85, 86]. The most recent studies devoted to this concept reported $FeMnO_3$-Na_2WO_4 [87], Mg_6MnO_8 doped with Na, W and P [88], $CaMnO_3$ and Na_2WO_4 [89], $Na_2WO_4/Mn_2O_3/SiO_2$ doped with TiO_2 [90]. All the materials are considered to be active due to the redox transitions of Mn^{+n} species.

1.2.2.3. Mechanism

OCM mechanism is a network of homo- and heterogeneous pathways that complicates its study. Scheme 1 shows possible pathways of methane conversion into selective and unselective products. As it was shown by kinetic studies with CH_4/CD_4, the formation of only symmetric hydrocarbons (C_2H_6, CD_3CH_3, C_2D_6 or C_2H_4, CD_2CH_2 and C_2D_4) indicates the formation of C_2H_6 by the coupling of two methyl radicals with its dehydrogenation to form ethylene [91]. The abstraction of H from CH_4 and the subsequent formation of a methyl radical is a heterogeneous step, whereas the coupling of methyl radicals is often ascribed to be a homogeneous reaction. The formation of methyl, ethyl, and allyl radicals from CH_4, C_2H_6, and C_3H_8, respectively, over various oxides was observed by EPR matrix isolation spectroscopy, while no formation of vinyl radical from C_2H_4 was detected [92]. The formation of undesired CO_x can occur heterogeneously on a catalyst surface or homogeneously in the gas-phase.

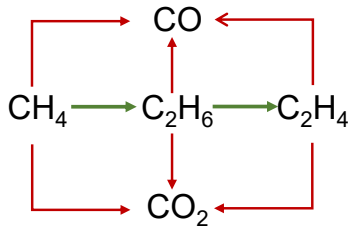

Scheme 1. A general scheme of possible pathways in the OCM reaction. Green and red arrows indicate selective and unselective reactions, respectively.

1.2.2.4. Methane activation

Methane activation is a great challenge for heterogeneous catalysis. This alkane is a symmetric molecule with very low HOMO and high LUMO [93] and possesses neither acidic nor basic properties (pKa~40). The cleavage of the strong and weakly polarized C–H bond (439 kJ/mol) is the main challenge

for methane activation [23]. Ethane is formed in the gas phase by coupling of two methyl radicals. As mentioned above, the formation of methyl radical was proved by EPR matrix isolation spectroscopy in several studies [92, 94, 95]. Many kinetic works considered the activation of methane as an exclusively heterogeneous process. However, as stated in the work of Takanabe et al. [96-98], methane activation can also occur in the gas phase by OH radicals.

The cleavage of C–H bond(s) in methane can occur via heterolytic or homolytic pathways. The former is typical for strongly basic sites, where methyl carbanion formed first is paired with a metal cation, while proton is bound to oxygen. The homolytic breaking is the reaction with oxygen, forming superoxide species and releasing methyl radical into the gas phase. Because strongly basic catalysts are typically non-reducible alkaline earth or rare earth metal oxides, gas-phase oxygen can be an electron acceptor in the formation of methyl radical [99]. As it was noted by Lunsford et al. [100], two types of active sites were observed over basic Ba/MgO catalysts, namely those that can activate methane via heterolytic C–H cleavage and the others - via homolytic. The concentration of the former was found to be lower than that of the latter, and moreover, due to their highly basic nature, they are easily poisoned by CO_2. Homolytic activation, i.e. the transfer of hydrogen atom, can proceed via O^-, which can easily accept an electron from hydrogen. Methane does not adsorb on a surface, and methyl radical is simultaneously released into gas phase. As it was calculated, homolytic activation is thermodynamically more favorable than heterolytic activation [101].

1.2.2.5. Oxygen activation and oxygen speciation

The role of oxygen species involved in product formation and/or oxygen activation in the OCM reaction is often omitted or underrepresented. Meanwhile, it is one, if not the most important aspect revealing of which can provide fundamentals for purposeful design of selective catalysts and selecting the mode of their operation.

As shown for the OCM reaction over non-reducible metal oxides in the absence of gas-phase oxygen, their lattice oxygen can barely contribute to methane conversion [102]. This implies the involvement of oxygen species formed from gas-phase oxygen. Oxygen activation is an electron-acceptor process consisting of several steps, namely, oxygen coordination (adsorption), electron transfer, dissociation, and incorporation into lattice according to the sequence 15 [103]:

$$O_2\,(g) \leftrightharpoons [O_2]_{ads} \overset{+e^-}{\leftrightharpoons} [O_2^-]_{ads} \leftrightharpoons [O^-]_{ads} \overset{+e^-}{\leftrightharpoons} [O^{2-}]_{lat} \qquad (15)$$

Oxygen species existing in an equilibrium state on a catalyst surface can be divided into two groups: weakly adsorbed species [O_2^-] and [O_2^{2-}] (molecular biatomic: superoxide and peroxide species) and strongly bound less electrophilic oxygen species, which are [O^-] and [O^{2-}]. The former species are proposed to be responsible for unselective methane oxidation to carbon oxides due to their high electrophilic nature. In [104], La_2O_3 was doped by aliovalent promoters, which made it possible to create different concentrations of anion vacancies, as determined by ionic conductivity measurements. The selectivity to C_2-hydrocarbons was found to be dependent on the conductivity: the higher the conductivity, the higher the selectivity. To explain this dependence, it was proposed that high ionic conductivity is beneficial for transformation of molecular biatomic adsorbed oxygen species into lattice species that are selective. It should, however, be noted that the role of oxygen species with different numbers of atoms (bi- or monoatomic) in selective and unselective reactions is still controversially discussed. Paramagnetic biatomic superoxide O_2^- species detected by EPR over Y_2O_3-CaO were concluded to be active sites for OCM [105]. The formation of superoxide species at room or elevated temperatures was further demonstrated in [106]. It was proposed that O_2^- is a likely active species for CH_4 activation, which can also produce O_2^{2-} or O^- species. The involvement of peroxide species (O_2^{2-}) in the selective conversion of methane was intensively studied by the group of Otsuka [107, 108]. It was proposed that biatomic peroxo species can be formed by the direct adsorption of gas-phase oxygen or exist on the surface of peroxides such as Na_2O_2, SrO_2 or BaO_2. The formation of C_2-hydrocarbons was observed over these peroxides even in the absence of gas-phase oxygen at above 300 °C. The same role was assigned to peroxo oxygen species, which were also detected by XPS over $BaPbO_3$ ($Ba^{+2}Pb^{+2}[O_2^{2-}]O^{-2}$), which is active and selective in OCM at 875 °C (C_2 yield 14-18%) [109]. A higher ability to form hydrocarbons over BaO/La_2O_3 was similarly explained by the presence of O_2^{2-} and its probable decomposition into other active species (O_2^- or O^-) [110]. DFT calculations by Neurock et al. [111, 112] confirmed that O_2^{2-} species are responsible for the formation of methyl radicals. However, according to these calculations, the most active oxygen species should be anionic O^-. Moreover, as it was noted by Li et al. [113], the transition state of CH_4 activation at such O_2^{2-} species on La_2O_3 was not shown and the reaction mechanism included only two steps, omitting the elimination of H_2O and regeneration of active sites. Thus, according to the studies reevaluating the role of peroxides, it was shown by DFT analysis by considering cluster model of La_2O_3 that undetected O^{2-} may play an even more important role than the detected O_2^{2-} species [113, 114].

As mentioned above, selective OCM materials can rapidly transfer an electron to adsorbed oxygen species [O_2^{n-}] followed by their incorporation into lattice [O^{2-}] [103, 115]. The assumption that biatomic

species are unselective, while monoatomic ones are selective, was justified in various OCM studies using O_2 or N_2O as oxidant (Figure 1.3) [116-118]. The decomposition of the latter mainly yields monoatomic oxygen species (eq. 16) [119].

$$N_2O + * \rightarrow O* + N_2 \quad (16)$$

Where *-coordinatively unsaturated center/anion vacancy.

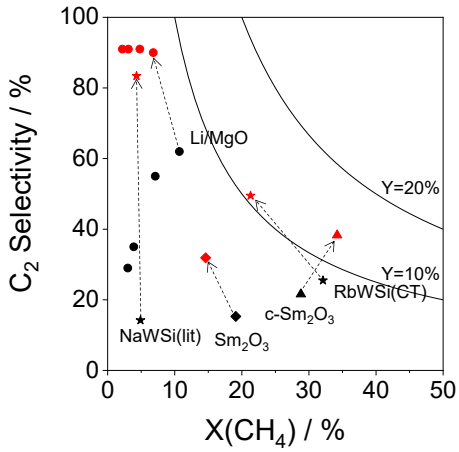

Figure 1.3. Comparison of selected catalysts in O_2-OCM (black) and N_2O-OCM (red) from [120] (●, Li/MgO 635-680 °C), [121] (♦, Sm_2O_3 710 °C), [122] (▲, c-Sm_2O_3 740 °C), [123] (★, NaWSi(lit), RbWSi(CT) 800 °C).

1.2.2.6. Alternative oxidants

As mentioned above, not only O_2 but also N_2O or S_2 can be used as oxidants in OCM. N_2O-OCM is even more thermodynamically favorable than O_2-OCM. Catalyst activity is defined by a kinetically controlled oxidant activation [124]. N_2O-OCM is advantageous because it is the direct valorization of two greenhouse gases (N_2O and CH_4). In addition, the use of N_2O can be instrumental in investigating the role of different oxygen species and their involvement in selective and unselective pathways [119, 125]. Upscaling N_2O-OCM has the disadvantage of high cost of N_2O and contributes to a more complicated separation of CO and N_2 (formed from N_2O), since their boiling points are similar (-192 °C vs. -196 °C).

OCM with S_2 (S_2-OCM) is less studied as compared to N_2O-OCM. The lower reactions exothermicity could be advantageous for better heat management [124]. The possibility of using sulfur vapor in reaction with methane to produce hydrocarbons was first demonstrated by Anderson et al. in 1993 [126]. The reaction received a renewed attention later when it was reported that it was possible to achieve 33% selectivity to C_2H_4 over Fe_3O_4 at 950 °C (X(CH_4) ca. 5-6%). The catalyst was stable for 48 h. Compared

to O_2-OCM, the C_2H_4/C_2H_6 ratio in S_2-OCM was remarkably high (9-12, while this value is typically around 1 in O_2-OCM). The unselective products are H_2S and CS_2. The latter can be recycled back to S_2, while the formation of the former remains problematic.

1.3. What is known about the promising MnO_x-Na_2WO_4/SiO_2 catalyst?

Among the OCM catalysts developed up to now, a supported catalyst consisting of MnO_x, Na_2WO_4 and SiO_2 as the active species and the support, respectively, should be especially noted. This catalyst was first reported in 1992 [127, 128]. Since then, it and its various derivatives have been developed and investigated to understand the fundamentals of catalyst functioning and product formation, as highlighted in reviews on this topic [129, 130]. In comparison with the best-performing catalysts based on non-reducible metal oxides, the MnO_x-Na_2WO_4/SiO_2 catalyst demonstrates higher selectivity to the desired products at methane conversion degrees between 10 and 40% [98]. Moreover, this material is also attractive due to its high thermostability; a stable performance has been confirmed for hundreds of hours on reaction stream [131-133]. Several studies proved a synergy between all components (MnO_x, Na_2WO_4 and SiO_2) to achieve high selectivity to hydrocarbons. MnO_x-free Na_2WO_4/SiO_2 is also known to be selective in the OCM reaction. The presence of MnO_x increases overall catalyst activity without any significant improvements in the selectivity to the desired products [134-136]. It should, however, be mentioned that the fundamentals behind the role of each catalyst component in activity and product selectivity are not well understood and are still under debate, as described in the following sections.

1.3.1. Preparation methods/phase composition of MnO_x-Na_2WO_4/SiO_2

The most employed method for MnO_x-Na_2WO_4/SiO_2 preparation is incipient wetness impregnation (IWI). Some previous studies directly compared the catalysts prepared by IWI and sol-gel (SG) methods. The performance of the catalysts prepared by SG was inferior to that of the catalysts prepared by IWI [133], [137]. The application of aqueous solutions of active components to the support material in the IWI preparation method results in their higher enrichment on the surface or subsurface, resulting in improved catalyst performance. MnO_x-Na_2WO_4/SiO_2 can also be successfully prepared by a fluidized-bed method, in which silica particles are uniformly covered with dispersed Mn_2O_3 and Na_2WO_4 in a fluidized bed. This method is suitable for the preparation of large catalyst amounts that can be particularly important for industrial implementation [138].

The phase composition of the prepared catalysts has been mainly determined by ex situ XRD, XPS or Raman spectroscopy [130]. However, from a few published results of in situ/operando characterization,

it is known that the phase composition of MnO_x-Na_2WO_4/SiO_2 is very dynamic under reaction conditions. For example, it was shown that the crystalline Na_2WO_4 phase disappears at temperatures above 700 °C due to melting [135, 139-143]. Moreover, the often reported α-cristobalite is also not present under reaction conditions and transforms into β-modification at elevated temperatures, that was confirmed by several studies using Raman spectroscopy [144], differential thermal analysis [138], differential scanning calorimetry [145] or XRD/XRD-CT [135, 139, 140, 142-145]. Therefore, it is essential to apply in situ/operando techniques.

1.3.2. Role of SiO_2 phase in MnO_x-Na_2WO_4/SiO_2

Apart from many unanswered questions regarding the nature of active sites, the role of the SiO_2 support also remains unclear. SiO_2 alone is an unselective material in the OCM reaction. To date, there are several hypotheses regarding its role. It is known that due to the presence of Na^+ in the catalyst composition, the originally amorphous SiO_2 undergoes a low-temperature phase transformation (below 800 °C, whereas the typical temperature in the absence of alkali metal ion is 1500 °C) from the amorphous to the cristobalite (α or β modifications) during catalyst preparation, i.e., calcination at high temperature. Palermo et al. [146] established a correlation between the presence of the α-cristobalite phase and catalyst activity and C_2-hydrocarbons selectivity.

Recent in situ studies have shown that the α-cristobalite transforms into the β-modification under reaction conditions [135, 138-140, 142-145]. In [147], the use of SBA-15 as a support for MnO_x-Na_2WO_4 was reported to result in a catalyst that outperforms the classically prepared MnO_x-Na_2WO_4/SiO_2. In [148], different silica sources such as dealuminated β-zeolite, mesoporous SBA-15, and microporous fumed silica were used as supports to investigate the effects of surface morphology and surface composition on catalyst performance. The catalyst based on SBA-15 showed the lowest performance, which was explained by the closed porosity of this material. It was concluded that the critical parameters for the design of active and selective MnO_x-Na_2WO_4/SiO_2 catalysts are the morphology (porosity) of the support, the dispersion of Mn_2O_3 and the size of Na_2WO_4 species. It should be noted that it is not clear whether the crystalline size of Na_2WO_4 can be directly correlated with the observed activity, since this phase does not possess a crystalline structure under reaction conditions. In another attempt to investigate the role of support, 12 different supports as well as based on them materials containing MnO_x, WO_x, Na_2WO_4, and MnO_x-Na_2WO_4 were tested [149]. It was confirmed that SiO_2-supported trimetallic catalyst was the best performed among catalysts studied. It was emphasized that the catalysts based on TiO_2, SiC,

Fe_2O_3, or Fe_3O_4 supports have promising OCM performance. Though the exact reasons of the observed differences in the catalysts' performance were not explained.

1.3.3. Enhancing effect of water on catalyst activity and product selectivity

Another distinctive feature of the MnO_x-Na_2WO_4/SiO_2 catalysts is the positive effect of co-fed water. The effect was first discovered by Takanabe et al. [96, 97] and was explained by a new mechanistic pathway, i.e., abstraction of H from CH_4 by OH radicals. A rigorous kinetic analysis in the absence of water revealed that methane conversion rate is first-order in methane partial pressure ($p(CH_4)$) and 0.5-order in oxygen partial pressure ($p(O_2)$). The addition of water is proposed to lead to the additional H_2O-mediated pathway. In this pathway, methane conversion was calculated to be first-order in $p(CH_4)$, 0.25-order in $p(O_2)$, and 0.5-order in $p(H_2O)$. The origin of OH radicals over MnO_x-Na_2WO_4/SiO_2 or $(Na, K)_2WO_4/SiO_2$ was explained by the presence of the peroxide species (due to the presence of alkali metals, which can form peroxides in the presence of O_2). These peroxo species readily react with added water forming H_2O_2 that further decomposes yielding two OH radicals, which can activate CH_4 (Scheme 2) [150, 151]. The authors supported their assumption by previously detected OH radicals over La_2O_3 catalyst [152-154]. It should be noted that the addition of water has no or even a negative effect on activity and selectivity of La-containing catalysts [155, 156].

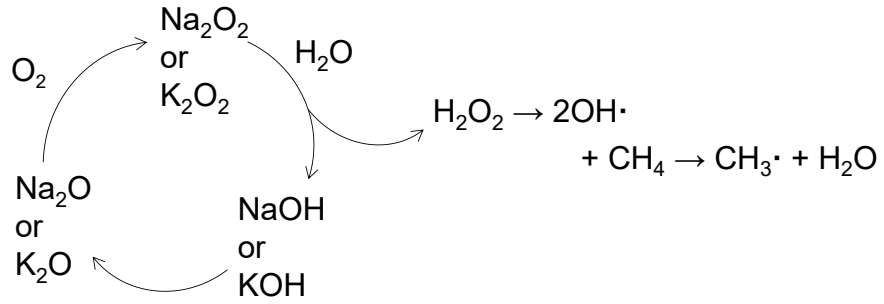

Scheme 2. Proposed role of H_2O and peroxides in OCM by Takanabe et al. [150, 151].

Further mechanistic studies of the effect of water showed that water accelerates the formation rates of all products, but to a different extent [156]. Moreover, the water effect was observed even under conditions, where gas-phase reactions do not occur. Thus, the water effect must be (at least partially) of a heterogeneous nature. The observed suppression of CO_2 formation through co-fed water was explained by water-assisted transformation of unselective biatomic species into selective monoatomic ones with a simultaneous formation of OH radicals (Scheme 3).

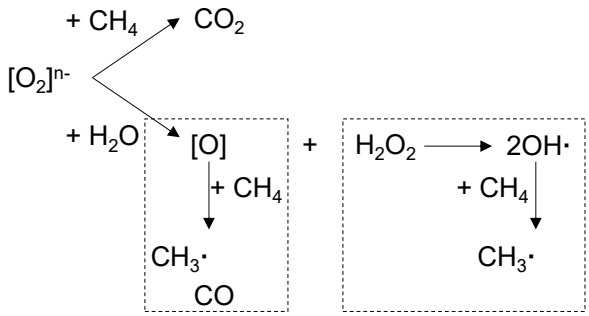

Scheme 3. Proposed effect of water in OCM over MnO_x-Na_2WO_4/SiO_2 by Aydin et al [156].

An alternative explanation for the water effect was proposed by Lomonosov et al. [155]. It was suggested that water shifts the equilibrium of hydroxyl group recombination. Higher concentration of formed hydroxy groups leads to a faster formation of active sites [O] (Scheme 4). Thus, water increases the turnover frequency of active sites. However, the effect of water on selectivity remains unclear within the framework of this explanation.

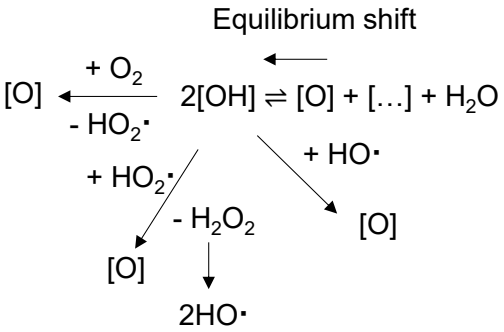

Scheme 4. Proposed positive effect of water on activity by Lomonosov et al [155].

1.3.4. Proposed active phase/species

Jiang et al. [157] have previously suggested that the active species of Na_2WO_4/SiO_2 is tetrahedral [WO_4], which has three bridge oxygen bonds W–O–Si and one double oxygen bond W=O directed upward. It is important to note that in this environment W has an oxidation state +5 but not +6 as in the form of Na_2WO_4 used for catalyst preparation. This conclusion was drawn from ex situ characterization of the catalyst by XRD and Raman spectroscopy. The importance of the tetrahedral [WO_4] groups was further confirmed in [158]. The authors proposed that the presence of Na^+ facilitates the distortion of [WO_4], providing an optimal W–O bond for the selective CH_4 oxidation to C_2H_6. The importance of these distorted [WO_4] groups was further elaborated by Li et al [159]. Methane activation was proposed to occur on W=O sites of two adjacent [WO_4] groups connected by the common bridge oxygen. Methane was proposed to reduce the initial W^{+6} to W^{+4}, forming an anion vacancy, which would then be reoxidized

by gas-phase oxygen. As evidence for such mechanism, W^{+4} was detected by EPR over Mn_2O_3-Na_2WO_4/SiO_2 after catalyst pretreatment in CH_4 at 800 °C. However, the reference spectrum of W^{+4} is unknown, as noted in [129]. The functions of both Mn_2O_3 and Na_2WO_4 were then studied in [160]. From EPR spectra combined with XANES spectra of Na_2WO_4/SiO_2 and MnO_x-Na_2WO_4/SiO_2 catalysts, it was concluded that methane is activated on the W^{+6} sites, which are reduced to W^{+5}, then due to the fast electron transfer from W^{+5} to Mn^{+3}, the active site for selective methane activation is recovered. Meanwhile, the generated Mn^{+2} is reoxidized to Mn^{+3} by gas-phase oxygen. Thus, the selective conversion of CH_4 occurs on W^{+6} sites over both Na_2WO_4/SiO_2 and MnO_x-Na_2WO_4/SiO_2, and the addition of Mn_2O_3 leads to a faster reoxidation of active sites. According to the authors, this is why the MnO_x-Na_2WO_4/SiO_2 composition is 3 times more active and as selective as Na_2WO_4/SiO_2. It is important to highlight that all mentioned explanations are based on ex-situ characterization studies that do not always reflect the accurate chemical composition that is present under reaction conditions.

Regarding the kind of oxygen species involved in the OCM reaction over MnO_x-Na_2WO_4/SiO_2, a concept of weakly and strongly adsorbed oxygen was proposed. Using interval pulses in the TAP reactor, it was found that the formation of CO_2 depends on the time delay between the O_2 and CH_4 pulses, while the formation of C_2H_6 does not [161]. Weakly adsorbed oxygen (which concentration depends on the time delay between the pulses) was ascribed as unselective species, while strongly adsorbed oxygen species was suggested to be selective. Differently bound oxygen species were also defined in [137]. Oxygen removed by H_2 or CH_4 was referred as strongly bound, and oxygen detected during the O_2-TPD experiment was denoted as weakly adsorbed. This less bound oxygen was assigned as responsible for catalytic activity. Adsorbed (not catalyst lattice oxygen) oxygen species were not considered. From the H_2-TPR, O_2-TPR and TPSR experiments used over MnO_x-Na_2WO_4/SiO_2, it was proposed that adsorbed oxygen in the form of $[O_2]_{ads}$ is unselective species involved in the formation of deep-oxidation products, while [O] of a more nucleophilic nature is responsible for the selective methane activation [162].

The most recent discussion about the kind of oxygen species/active phases is based on redox reactions shown in equations 17 or 18 [140, 163]. According to [140], the interaction of the Mn-phase with Na_2WO_4 results in the formation of Na_2O, which is responsible for the high performance in OCM. Low partial pressure of oxygen is required to stabilize these Na_2O sites and prevent their sublimation under OCM conditions. The stabilization of these sites was explained by the existence of the molten Na_2WO_4 phase and the occurrence of the redox reaction (eq. 17). Meanwhile, Si et al. [163] also insisted on the importance of the $Mn^{+3} \rightarrow Mn^{+2}$ redox cycle, but when MnO_x reacts with SiO_2 (eq. 18). The role of Na_2WO_4 was not identified.

$$Mn_7SiO_{12} + 7Na_2WO_4 \rightleftharpoons 7MnWO_4 + 7Na_2O + SiO_2 + 1.5O_2 \quad (17)$$

$$Mn_7SiO_{12} + 6SiO_2 \rightleftharpoons 7MnSiO_2 + 5O_2 \quad (18)$$

Contrarily to all above proposals, Kiani et al. [164] claimed that MnO_x sites play a spectator role and they are not necessary for OCM. The active sites were reported to be non-stochiometric Na-WO_x sites [144, 164]. Regarding oxygen species involved, it was further proposed that lattice oxygen of such surface non-stoichiometric Na-WO_x species is selective, while the molecular oxygen dissolved in Na_2WO_4 is responsible for the formation of CO_2. [165, 166]. However, the role of MnO_x was suggested as a promoter to the previously defined Na_2WO_4 and Na-WO_x sites in the most recent study by the same group [167].

In summary, many discussions of synergy/active phases/species/sites in the OCM reaction over MnO_x-Na_2WO_4/SiO_2 point to the presence of the molten phase of Na_2WO_4 as of paramount importance. However, this suggestion lacks the solid evidence, as the reciprocal fact (that the presence of crystalline phase would result in poorer activity/selectivity) has never been presented. Moreover, there is no consensus on oxygen species involved in selective and unselective pathways. The highly dynamic nature of active phases/sites of MnO_x-Na_2WO_4/SiO_2 under reaction conditions needs to be investigated under relevant reaction conditions, which will allow to better understand the mechanism and, most importantly, to elucidate the means how to maximize the selective production of the desired products.

2. Objectives and outline

2.1. Objectives

Highly demanded ethylene is produced nowadays through energy-intensive steam or fluid catalytic cracking of different oil fractions, which, along with the production of the desired products, results in high emissions of CO_2. With increasing oil price, the oxidative coupling of methane to C_2H_6/C_2H_4 may compete with or even replace the conventional methods to produce ethylene in the near future. Such shift from oil-based technologies to those utilizing CH_4 can contribute substantially to making the petrochemical industry more sustainable, as biogas can be a feedstock for OCM and the oxygen needed for this reaction can be produced through electrolysis of water using renewable energy. This provides an opportunity to control CO_2 emissions. MnO_x-Na_2WO_4/SiO_2 is a promising catalyst for the OCM reaction. Despite numerous relevant studies, many fundamental aspects such as reaction mechanism/kinetics, nature of active sites/phases, etc. are still unclear. However, in order to further improve its performance through catalyst design and/or optimizing reaction conditions/mode of operation, it is important to elucidate fundamentals of catalyst functioning.

In view of this, the main objective of the present study was to identify factors that determine activity and selectivity in the OCM reaction over (MnO_x)-M_2WO_4/SiO_2 (M=Na, K, Rb, or Cs). To achieve this, sophisticated kinetic measurements in a broad range of CH_4 conversion degrees were complemented by time-resolved in situ/operando catalyst characterization using XRD and UV-vis spectroscopy, as well as by transient kinetic analyses (temporal analysis of products with submillisecond resolution, oxygen isotopic exchange, steady-state isotopic transient kinetic analysis) using isotopic tracers.

In general, the specific objectives can be formulated as follows:

1. To investigate the effect of the oxidant (O_2 vs. N_2O) in OCM over MnO_x-Na_2WO_4/SiO_2 on the product formation scheme including the effect of co-fed water in N_2O-OCM.
2. To study activity and selectivity of lattice and adsorbed oxygen species over M_2WO_4/SiO_2 and MnO_x-M_2WO_4/SiO_2 (M=Na, K, Rb, or Cs).
3. To study the role of alkali metal in (MnO_x)-M_2WO_4/SiO_2 (M=Na, K, Rb, or Cs) in OCM and, in particular, whether the presence of the molten Na_2WO_4 phase is essential for activity and selectivity.
4. To elucidate the role of MnO_x in MnO_x-M_2WO_4/SiO_2 (M=Na, K, Rb, or Cs).

2.2. Outline

The strategies implemented in this work to address the abovementioned objectives are discussed below. In Section 3.1, the effects of oxidant (O_2 vs. N_2O) and co-fed H_2O on activity and C_2-hydrocarbons selectivity over MnO_x-Na_2WO_4/SiO_2 were investigated. The presence of biatomic oxygen species formed from gas-phase oxygen was confirmed by EPR spectroscopy and oxygen isotopic exchange tests. Catalytic tests were conducted in a wide range of methane conversion degrees to determine how the oxidant affects the overall pathways leading to the desired hydrocarbons and carbon oxides. They were complemented by in situ/operando UV-vis spectroscopy measurements to investigate changes in the oxidation state of Mn and W in MnO_x/SiO_2, Na_2WO_4/SiO_2, and MnO_x-Na_2WO_4/SiO_2 under different conditions (O_2/N_2, H_2/N_2, O_2-OCM, or N_2O-OCM).

Section 3.2 deals with the study of the M_2WO_4/SiO_2 (M=Na, K, Rb, or Cs) catalysts to elucidate (i) the origin and the role of oxygen species participating in methane activation and product formation, (ii) whether the phase(s) of MnO_x or molten Na_2WO_4 are necessary to achieve high selectivity to C_2-hydrocarbons. Other tungstates M_2WO_4 do not melt under reaction conditions. The state of the M_2WO_4 phase and the oxidation state of W under reaction conditions were investigated by in situ XRD and operando UV-vis spectroscopy measurements, respectively. The involvement of lattice and adsorbed oxygen species (that come from gas-phase oxygen) was studied by pulse experiments at ambient pressure as well as in high vacuum in the TAP reactor. The results of oxygen isotopic exchange tests combined with steady-state kinetic analysis allowed to establish the role of alkali metal in M_2WO_4/SiO_2 (M=Na, K, Rb, or Cs) on methane conversion activity and product formation pathways.

In Section 3.3, the trimetallic MnO_x-M_2WO_4/SiO_2 (M=Na, K, Rb, or Cs) catalysts were compared to their bimetallic MnO_x-free counterparts (M_2WO_4/SiO_2 (M=Na, K, Rb, or Cs)) to unravel the nature and the origin of oxygen species involved in product formation and the role of MnO_x and alkali metal in MnO_x-M_2WO_4/SiO_2 (M=Na, K, Rb, or Cs). O_2-TPD and oxygen isotopic exchange tests were conducted to study the ability of the catalysts to release lattice and to activate gas-phase oxygen. In situ XRD and UV-vis tests were used to identify the phase composition and the oxidation state of Mn and W, respectively. The characterization studies were complemented by sophisticated kinetic tests. The lifetime and the concentration of intermediates leading to H_2O and CO_2 were derived from steady-state isotopic transient kinetic analysis.

The results obtained in this work are summarized in Section 4. Directions and suggestions for further works are given in Section 5.

3. Results

3.1. Effects of N_2O and water on activity and selectivity in the oxidative coupling of methane over MnO_x-Na_2WO_4/SiO_2: role of oxygen species.

When N_2O was used as oxidant instead of O_2 in the OCM reaction over MnO_x-Na_2WO_4/SiO_2, a noticeably higher selectivity to C_2-hydrocarbons was observed at different methane conversion degrees (Figure 3.1 (a)). The positive effect of N_2O was due to the different origins of CO_2 in O_2-OCM and N_2O-OCM (Figure 3.1 (b)). The non-zero CO_2 selectivity obtained at zero CH_4 conversion in O_2-OCM indicates that this product is formed directly from CH_4. While it is a secondary product when N_2O is used, as seen from the near-to-zero value of the extrapolated to zero CH_4 conversion CO_2 selectivity in N_2O-OCM (Figure 3.1 (g)). The observed improvement in the selectivity to C_2-hydrocarbons in N_2O-OCM can be explained by the involvement of biatomic oxygen species into CO_2 formation as previously proposed [156]. Since N_2O decomposes predominantly with the formation of monoatomic oxygen species (eq. 19), the direct CH_4 oxidation to CO_2 was strongly hindered in N_2O-OCM thus resulting in higher selectivity to C_2-hydrocarbons in comparison with O_2-OCM, where biatomic oxygen species can be formed from gas-phase oxygen. Performing N_2O-OCM with co-fed H_2O results in a further improvement in C_2-hydrocarbons selectivity up to ca. 87% at about 6-8% CH_4 conversion (Figure 3.1 (d)). This enhancement was due to an additional hindering of CO_2 formation (Figure 3.1 (e)). The absence of biatomic species in N_2O-OCM cannot be completely ruled out, as they can be formed either by the recombination of two monoatomic oxygen species (which were formed during N_2O decomposition (eq. 19, 20)) or by the further N_2O decomposition on the monoatomic oxygen species (eq. 21). Since no effect of the kind of oxidant (N_2O vs. O_2) on CO formation was observed (Figure 3.1 (c)), the oxidant used should generate the same oxygen species on the catalyst surface. Co-fed water should not affect the formation of such species, as there was no effect of water on CO formation (Figure 3.1 (f)). Thus, the observed improvement in C_2-hydrocarbons selectivity when N_2O was used as an oxidant should be related to the lower concentration of unselective biatomic oxygen species. The positive effect of water on C_2-hydrocarbons selectivity in N_2O-OCM is likely of the same nature as it is in O_2-OCM [156], i.e., water-accelerated transformation of biatomic species responsible for the direct conversion of CH_4 into CO_2 to the selective monoatomic ones.

$$N_2O + * \rightarrow O^* + N_2 \quad (19)$$

$$O^* + O^* \rightleftharpoons O_2^* + * \rightleftharpoons O_2 + 2^* \quad (20)$$

$$N_2O + O^* \rightarrow N_2 + O_2^* \rightleftharpoons N_2 + O_2 + * \quad (21)$$

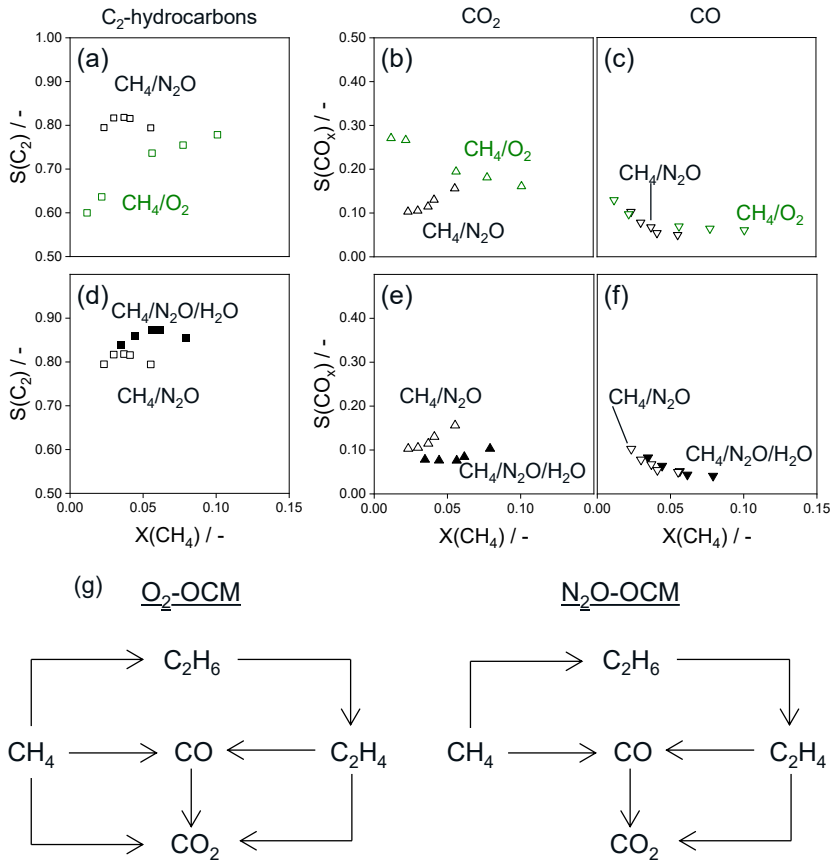

Figure 3.1. Selectivity-conversion relationships for (a) C_2-hydrocarbons, (b) CO_2 and (c) CO in O_2-OCM (green) vs. N_2O-OCM (black); Selectivity-conversion relationships for (d) C_2-hydrocarbons, (e) CO_2 and (f) CO in N_2O-OCM (open symbols) and N_2O-H_2O-OCM (filled symbols) over MnO_x-Na_2WO_4/SiO_2 at 800 °C; (g) Scheme of product formation in O_2-OCM and N_2O-OCM.

Oxygen isotopic exchange (OIE) experiments using a feed with 1vol% $^{18}O_2$ in Ar were carried out in a temperature-programmed mode to derive mechanistic insights into the interactions of gas-phase oxygen with catalyst lattice oxygen. The obtained responses of differently labeled oxygen molecules in the gas-phase are shown in Figure 3.2 (a). The formation of nonlabeled $^{16}O_2$ started at 450 °C, that is ~80 °C lower than the starting formation temperature of $^{16}O^{18}O$. Importantly, the concentration of the latter passes a maximum with rising temperatures, while the concentration of $^{16}O_2$ has a minimum. According to the established mechanisms of OIE [168-170], the formation of $^{16}O^{18}O$ can occur via the interaction of gas-phase $^{18}O_2$ with one lattice (^{16}O) oxygen atom or via the co-called "homoexchange", when adsorbed oxygen $^{16}O_2$ and $^{18}O_2$ react with each other on the surface (R_1 or R_0 mechanisms, accordingly, Figure 3.2 (b)). If the exchange proceeded in our experiments through the R_1 mechanism, it would not be possible to explain the delayed appearance of $^{16}O^{18}O$ in comparison with $^{16}O_2$, since both R_1 and R_2 mechanisms proceed with the involvement of the same lattice oxygen (Figure 3.2 (b)). Thus, $^{16}O^{18}O$ must be formed via the R_0 mechanism with the participation of adsorbed species. The presence of adsorbed

biatomic oxygen species on the surface of Na_2WO_4/SiO_2 was also proved by EPR spectroscopy (Figure 3.2 (c)). The simulated EPR spectrum of the superoxide-DMPO adduct corresponds well to the experimental one. Thus, the presence of biatomic oxygen was confirmed by the OIE test and EPR spectroscopy.

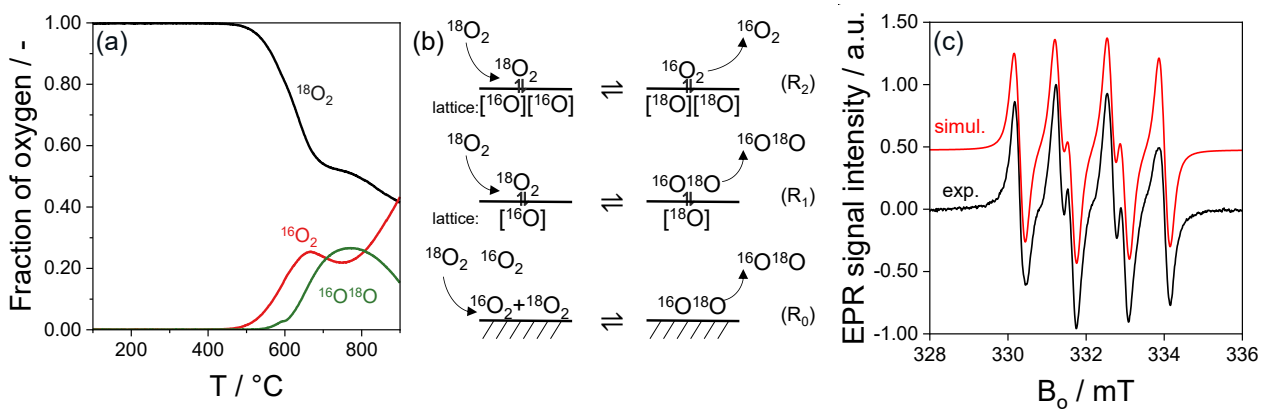

Figure 3.2. (a) Transient responses of $^{16}O_2$ (red) and $^{16}O^{18}O$ (green) recorded in temperature-programmed oxygen isotopic exchange tests over MnO_x-Na_2WO_4/SiO_2; (b) Scheme of three mechanisms of oxygen isotopic exchange; (c) EPR spectrum of DMPO-O_2^- (black line) detected over Na_2WO_4/SiO_2 exposed to O_2 at 20 °C after catalyst treatment in vacuum at 700 °C. The simulated spectrum of DMPO-O_2^- (red line) obtained using the easy spin program.

O_2-TPD tests revealed that Na_2WO_4/SiO_2 catalyst does not desorb any oxygen in the temperature range of 300-900 °C, while lattice oxygen of MnO_x/SiO_2 and MnO_x-Na_2WO_4/SiO_2 can be released at high temperatures (Figure 3.3 (a)). The amount of oxygen desorbed from MnO_x/SiO_2 was lower than that from MnO_x-Na_2WO_4/SiO_2. In addition, oxygen desorption from MnO_x/SiO_2 starts at ca. 680 °C, the starting desorption temperature of MnO_x-Na_2WO_4/SiO_2 is 80 °C lower (Figure 3.3 (b)). Thus, there is a synergistic interaction between MnO_x and Na_2WO_4 in terms of oxygen desorption.

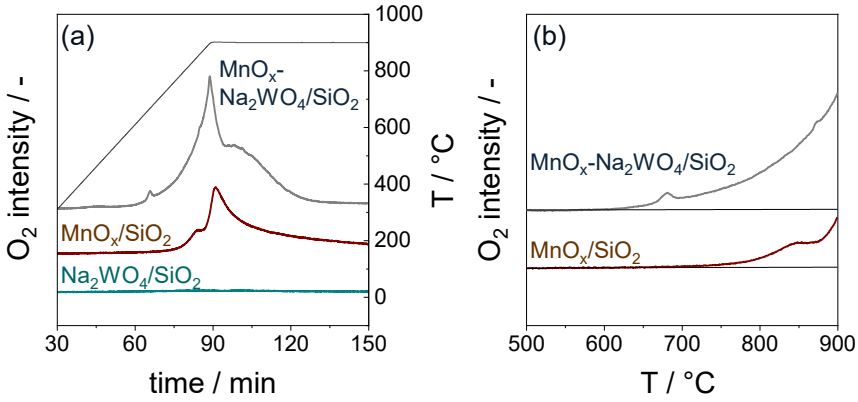

Figure 3.3. O_2 signal for Na_2WO_4/SiO_2, MnO_x/SiO_2 and MnO_x-Na_2WO_4/SiO_2 vs. (a) time and (b) temperature in O_2-TPD tests.

In situ/operando UV-vis spectroscopy was used to analyze the oxidation state of manganese and tungsten under OCM reaction conditions and to check if there is any relationship with catalyst performance. First, the spectra of MnO_x/SiO_2, Na_2WO_4/SiO_2 as well as MnO_x-Na_2WO_4/SiO_2 in fully oxidized state were recorded in O_2/N_2 at 750 °C. When MnO_x/SiO_2 was treated in H_2/N_2, the intensity of the obtained spectrum decreased in the whole range of wavelengths compared to the intensity of the spectra recorded in O_2/N_2 (Figure 3.4 (b)). In contrast, the intensity of the spectra of the reduced Na_2WO_4/SiO_2 was higher relatively to the intensity of the oxidized sample (Figure 3.4 (c)). These spectral changes should be due to the reduction of Mn^{+3} to Mn^{+2} and W^{+6} to $W^{+(6-n)}$ caused by the removal of lattice oxygen by H_2 in the form of water. Due to the thermal radiation at this high temperature, which is more pronounced at higher wavelengths (about λ>500 nm), the individual bands in the detected spectra are not discussed.

How fast the H_2-induced changes occurred over MnO_x/SiO_2, Na_2WO_4/SiO_2 and MnO_x-Na_2WO_4/SiO_2 are shown in Figure 3.4 (a). As can be seen, the relative Kubelka-Munk function (eq. 22) at 420 nm (the most pronounced changes in the spectra of MnO_x-Na_2WO_4/SiO_2 below 500 nm) in the spectrum of MnO_x/SiO_2 rapidly decreased after 1 minute in H_2/N_2. These changes are significantly slower for Na_2WO_4/SiO_2 than the changes in the spectrum of MnO_x/SiO_2. In other words, the reduction of Mn^{+3} is meaningfully faster than that of W^{+6}. Due to its higher reducibility, MnO_x is reduced rapidly in MnO_x-Na_2WO_4/SiO_2, followed by a slower reduction of Na_2WO_4 (Figure 3.4 (a)).

$$F(R)_{rel} = \frac{F(R)_{H2}}{F(R)_{O2}} \tag{22}$$

The operando UV-vis tests showed that the oxidation state of manganese and tungsten in MnO_x/SiO_2, Na_2WO_4/SiO_2 and MnO_x-Na_2WO_4/SiO_2 tested in O_2-OCM fully corresponds to that in O_2/N_2 (completely oxidized) (Figure 3.4 (b, c, d)). However, a slightly reduced state of MnO_x-Na_2WO_4/SiO_2 was observed under N_2O-OCM conditions (Figure 3.4 (d)). This was due to a partial reduction of MnO_x as the spectra of Na_2WO_4/SiO_2 did not change for 90 min on CH_4/N_2O stream, while some changes in the spectra of MnO_x/SiO_2 and MnO_x-Na_2WO_4/SiO_2 became visible under this condition. This can be explained by the lower ability of N_2O to reoxidize reduced MnO_x sites in comparison with O_2. As a result, the density of lattice oxygen species is lower when N_2O is used as an oxidant that is favorable to the formation of methyl radical, since only one lattice oxygen is required for this. The recombination of two methyl radicals yields ethane without further oxygen consumption. The formation of CO or CO_2 requires three or four lattice oxygen atoms. Therefore, their formation is suppressed when the density of oxygen species lowers.

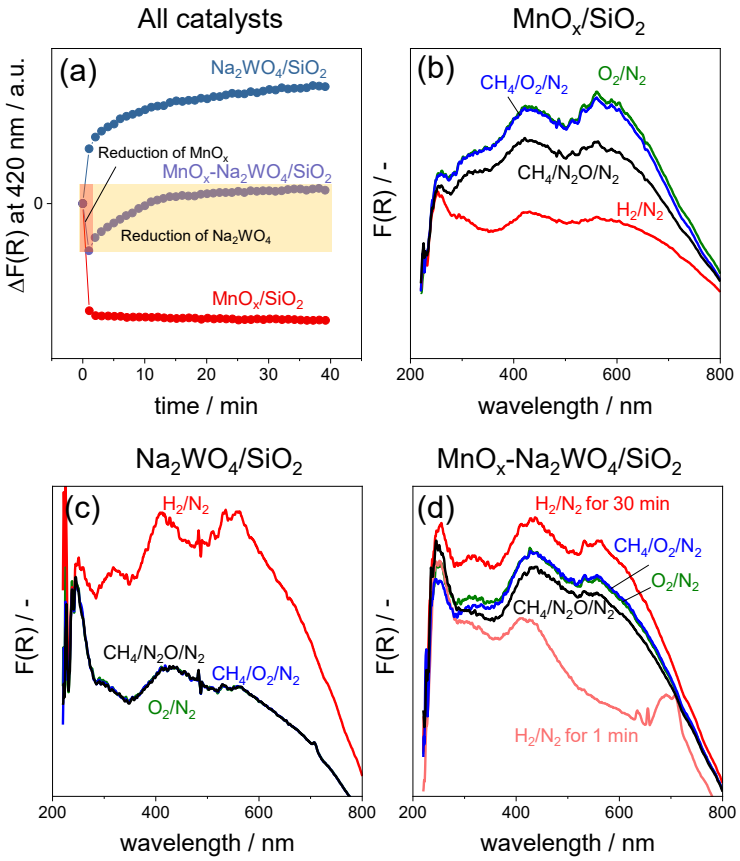

Figure 3.4. (a) Time-resolved relative Kubelka-Munk function at 420 nm for MnO_x/SiO_2, Na_2WO_4/SiO_2 and MnO_x-Na_2WO_4/SiO_2 upon reduction in H_2/N_2 at 750 °C; Spectra in O_2/N_2, $CH_4/O_2/N_2$; $CH_4/N_2O/N_2$ and H_2/N_2 flows at 750 °C of (b) MnO_x/SiO_2; (c) Na_2WO_4/SiO_2; (d) MnO_x-Na_2WO_4/SiO_2.

In summary, there are two types of oxygen species present over MnO_x-Na_2WO_4/SiO_2, namely mono- and biatomic. The former are responsible for C_2-hydrocarbons and CO formation, while the latter directly convert CH_4 into CO_2. The selectivity to C_2-hydrocarbons can be improved by the addition of water that transforms unselective biatomic species into selective monoatomic ones, and/or using N_2O as oxidant, which decomposes with the predominant formation of monoatomic oxygen species as compared to O_2. In addition, N_2O has lower ability to reoxidize reduced MnO_x sites, resulting in an increase in the reduction degree of catalyst surface. This is favorable for hindering the oxidation of the desired products and methane. Thus, based on this knowledge, higher C_2-hydrocarbons selectivity could be achieved over materials that can be easily reduced by CH_4 rather than reoxidized by O_2.

3.2. The role of adsorbed and lattice oxygen species in product formation in the oxidative coupling of methane over M_2WO_4/SiO_2 (M=Na, K, Rb, or Cs)

The phase composition of M_2WO_4/SiO_2 was investigated by in situ XRD analysis at 800 °C in air (Figure 3.5 (a)). To increase the signal to noise ratio in XRD patterns at such high temperature, the concentration of M_2WO_4 was 3-times increased. The presence of only SiO_2 phases (β-cristobalite and tridymite) was observed over Na_2WO_4/SiO_2 at 800 °C. The reflections characteristic of crystalline Na_2WO_4 disappeared after 700 °C due to melting of this compound. In contrast to this material, the reflections of crystalline K_2WO_4, Rb_2WO_4, and Cs_2WO_4 phases were detected even at 800 °C.

Furthermore, the oxidation state of W in M_2WO_4 was investigated by in situ/operando UV-vis spectroscopy (Figure 3.5 (b-c)) performed under different conditions, namely, oxidative (under O_2/N_2), reductive (H_2/N_2) and OCM ($CH_4/O_2/N_2$) atmospheres. It was found that the spectra of all samples under oxidative conditions correspond to those under $CH_4/O_2/N_2$ conditions. This indicates that the oxidation state of W must be close to +6. This result is in agreement with previous operando XANES spectroscopic results [142].

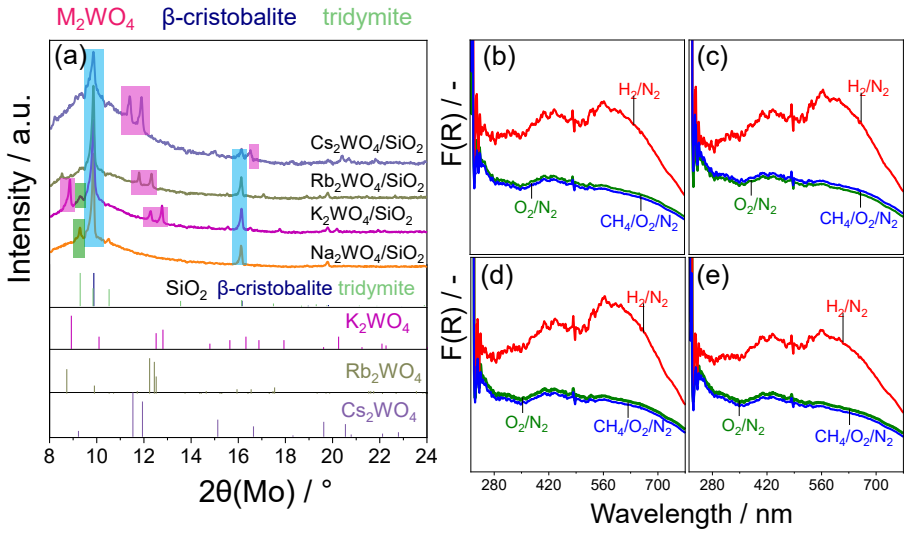

Figure 3.5. (a) In situ XRD patterns of M_2WO_4/SiO_2 at 800 °C in air. Identified phases: SiO_2 cubic (β-cristobalite, dark blue bars, PDF-No. 01-077-8670), SiO_2 hexagonal (tridymite, light green bars, PDF-No. 01-073-0403), K_2WO_4 hexagonal (purple bars, PDF-No. 00-024-0902), Rb_2WO_4 orthorhombic (olive green bars, PDF-No. 00-024-0976), Cs_2WO_4 hexagonal (violet bars, PDF-No. 00-030-0377); In situ UV-vis spectra of (b) Na_2WO_4/SiO_2; (c) K_2WO_4/SiO_2; (d) Rb_2WO_4/SiO_2; (e) Cs_2WO_4/SiO_2 at 750 °C under O_2/N_2 (green), H_2/N_2 (red) and $CH_4/O_2/N_2$ (blue) flows.

To elucidate the effect of alkali metal in M_2WO_4/SiO_2 on activity and selectivity in the OCM reaction in the absence and in the presence of water, segmental rates of products formation were calculated (Figure 3.6). As the selectivity of (MnO_x)-Na_2WO_4/SiO_2 is improved after the first addition of water [156], we

compare the activity and selectivity in the presence of water and in the absence of water after the catalysts had been exposed to a water-containing feed for 6 hours on stream. Though the kind of alkali metal affects the activity, no significant influence of alkali metal on the segmental rate profiles was observed (Figure 3.6 (b-i)). Thus, the intrinsic rate of C_2H_6 ($r_1(C_2H_6)$) (in the first segment, under differential conditions) decreased in the order Na_2WO_4>K_2WO_4>Rb_2WO_4>Cs_2WO_4 in the absence or in the presence of water. The same tendency was observed for the intrinsic rate of CO_2, while no correlation could be found for the rate of CH_4 conversion to CO. In general, the highest rates of CH_4 oxidation to C_2H_6, CO_2 and CO were achieved in the first segment, which decreased along the catalyst bed due to the transition from differential to integral operation and the subsequent conversion of C_2H_6 to C_2H_4. Due to this secondary reaction, the maximum of C_2H_4 rate was reached in the third/fourth segment over Na_2WO_4/SiO_2 and K_2WO_4/SiO_2. The continuous increase of C_2H_4 segmental rate $r_s(C_2H_4)$ was observed for Rb_2WO_4/SiO_2 and Cs_2WO_4/SiO_2, but no obvious maximum was reached under the applied conditions. When water was present in the feed, the initial rates to all products were higher. Moreover, the position of the maximum $r_s(C_2H_4)$ was shifted towards upstream. Thus, it was no longer pronounced for Na_2WO_4/SiO_2 and K_2WO_4/SiO_2, Rb_2WO_4/SiO_2 due to the accelerated by water C_2H_6 dehydrogenation.

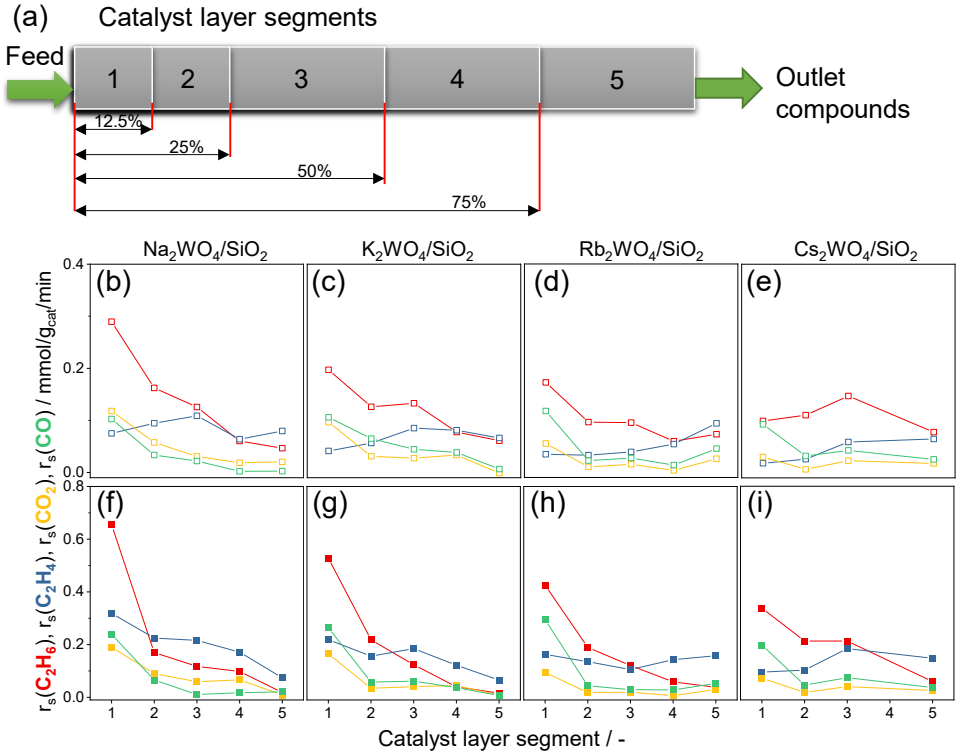

Figure 3.6. (a) Scheme of how the catalysts' segments were defined; (b-i) Segmental rates of C_2H_6, C_2H_4, CO_2 and CO determined at 800 °C using (b-e) $CH_4/O_2/N_2$ 40/5/55 or (f-i) $CH_4/O_2/H_2O/N_2$ 40/5/30/25 over Na_2WO_4/SiO_2 (b, f), K_2WO_4/SiO_2 (c, g), Rb_2WO_4/SiO_2 (d, h), Cs_2WO_4/SiO_2 (e, i); flow 30 ml/min, catalyst amount 25-300 mg.

The reaction scheme of product formation was derived by analyzing selectivity-conversion relationships obtained under steady-state conditions with or without co-fed water (Figure 3.7). Co-fed water was found not to alter the overall scheme of product formation. In general, non-zero selectivity to C_2H_6, CO and CO_2 at zero CH_4 conversion indicated that all these products are formed directly from CH_4. The selectivity to C_2H_4 was close to zero at zero CH_4 conversion, suggesting that this product is not formed directly from CH_4. As can be seen in Figure 3.7 (a-d), the C_2H_6 selectivity decreases with increasing CH_4 conversion due to dehydrogenation to C_2H_4. Since the determined reaction scheme of product formation was the same for all catalysts, the molten state of Na_2WO_4 should not play any significant role. It should be mentioned that the catalysts differ in the primary (at zero CH_4 conversion degree) selectivity to CO in the absence or in the presence of water, which increased in order Na_2WO_4<K_2WO_4<Rb_2WO_4<Cs_2WO_4 (Figure 3.7 (m-p)). A reverse order was established for the primary selectivity to C_2H_6 and CO_2 (Figure 3.7 (a-d, i-l)). The ratio of C_2H_4/C_2H_6 did not depend on the kind of alkali metal, thus we could not confirm that the dissolved oxygen in the molten Na_2WO_4 phase (other tungstates are in their crystalline state under the reaction conditions) can be responsible for the dehydrogenation of C_2H_6 to C_2H_4 as suggested in [165, 166].

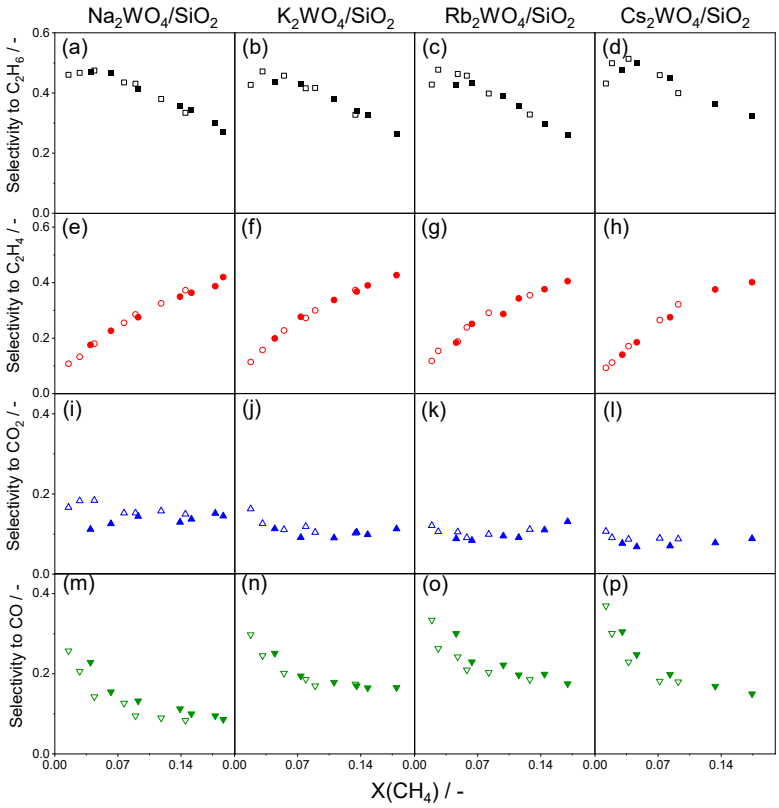

Figure 3.7. Selectivity-conversion relationships to (a-d) C_2H_6, (e-h) C_2H_4, (i-l) CO_2 and (m-p) CO over M_2WO_4/SiO_2 at 800 °C in the absence (open symbols) and in the presence (closed symbols) of water. Feed $CH_4/O_2/N_2$ 40/5/55 or $CH_4/O_2/H_2O/N_2$ 40/5/30/25, flow 30 ml/min, catalyst amount 25-300 mg.

The kind of oxygen species (lattice from the catalysts or adsorbed from gas-phase oxygen) involved in product formation over M_2WO_4/SiO_2 was investigated by CH_4 pulse experiments in the absence and in the presence of gas-phase oxygen (Figure 3.8 (a)). The experiments with only CH_4 revealed that lattice oxygen of M_2WO_4/SiO_2 cannot selectively convert CH_4 into C_2-hydrocarbons, but exclusively forms CO_x products. When CH_4 was pulsed with O_2, the catalyst activity was significantly increased and C_2-hydrocarbons were formed. Thus, it can be concluded that adsorbed oxygen species formed form gas-phase oxygen play an essential role in the course of the OCM reaction over M_2WO_4/SiO_2.

Activation of gas-phase oxygen over M_2WO_4/SiO_2 (M=Na, K, Rb, or Cs) was studied by oxygen isotopic exchange (OIE) tests. For all catalysts, the first appeared oxygen was $^{16}O_2$, which, according to the established mechanisms of OIE (Figure 3.2 (b)), can be formed when gas-phase $^{18}O_2$ interacts with two lattice oxygen atoms (R_2). Importantly, $^{16}O^{18}O$ appeared at ~70-100 °C higher temperatures than $^{16}O_2$ and passed a maximum with increasing temperature (Figure 3.8 (b)). Such pattern can be explained by the homoexchange mechanism, when two adsorbed biatomic oxygen species formed from gas-phase oxygen interact on the surface to form $^{16}O^{18}O$ according to R_0 (Figure 3.2 (b)). Its formation by an exchange reaction of $^{18}O_2$ with one lattice oxygen (R_1 (Figure 3.2 (b)) can be excluded, otherwise it is not possible to explain the delayed appearance of $^{16}O^{18}O$ in comparison with $^{16}O_2$ (nonlabeled lattice oxygen is involved in the formation of both products) and the existence of a maximum concentration of $^{16}O^{18}O$. Thus, the formation of adsorbed oxygen species was indirectly confirmed, and the total amount of these species can be a measure of catalyst effectiveness for oxygen activation.

The overall profiles of differently labeled gas-phase oxygen species were similar for all M_2WO_4/SiO_2 (M=Na, K, Rb, or Cs). However, the kinetics of individual exchange reactions expressed as the starting temperature of $^{16}O_2$ and $^{16}O^{18}O$ formation and the temperature of $^{16}O^{18}O$ maximum was found to be dependent on the kind of alkali metal. All these temperatures increased in the order $Na_2WO_4<K_2WO_4<Rb_2WO_4<Cs_2WO_4$. The amount of formed $^{16}O^{18}O$ increased in the reverse order.

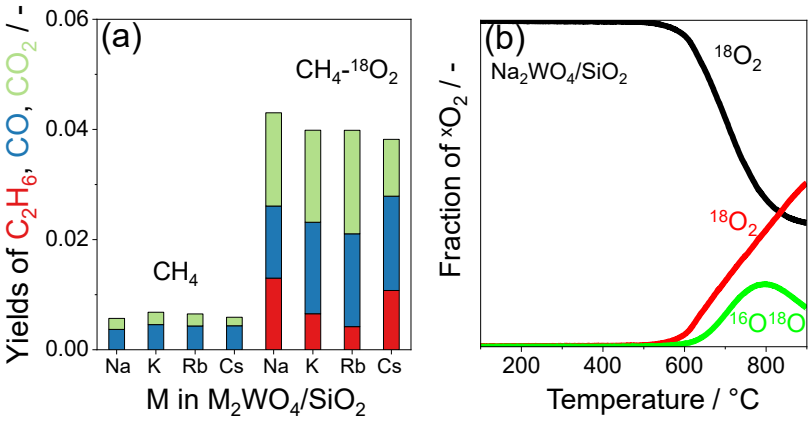

Figure 3.8. a) Yields of C_2H_6, CO and CO_2 in the pulse experiments over M_2WO_4/SiO_2 at 800 °C and ambient pressure pulsing CH_4/Ar or $CH_4/^{18}O_2$/Ar; b) Transient profiles $^{18}O_2$ (black), $^{16}O_2$ (red), $^{16}O^{18}O$ (green) detected in the isotopic exchange test over Na_2WO_4/SiO_2 using a feed with 1vol%$^{18}O_2$ in Ar.

As it was shown by the OIE test, the formation of $^{16}O^{18}O$ occurs through a reaction of two adsorbed oxygen species. The pulse experiments demonstrated that these adsorbed species are required for the CH_4 activation over M_2WO_4/SiO_2 (M=Na, K, Rb, or Cs). Since oxygen activation on the surface of a metal-oxide catalyst is an electron-acceptor process, we put forward that electronic properties of alkali metals must be crucial in this regard. This statement is supported by a correlation between the fraction of $^{16}O^{18}O$ formed in OIE tests and the Allen electronegativity of alkali metals (Figure 3.9 (a)). It was also established that the formation rates of C_2-hydrocarbons and CO_2 are directly dependent on the kind of alkali metal in the presence and in the absence of water, while no such correlation can be seen for the formation rate of CO (Figure 3.9 (b)). This can be explained by the different origins of these products. The C_2-hydrocarbons and CO_2 are formed with the participation of adsorbed oxygen species, while lattice oxygen of M_2WO_4/SiO_2 (M=Na, K, Rb, or Cs) is involved in the CO formation.

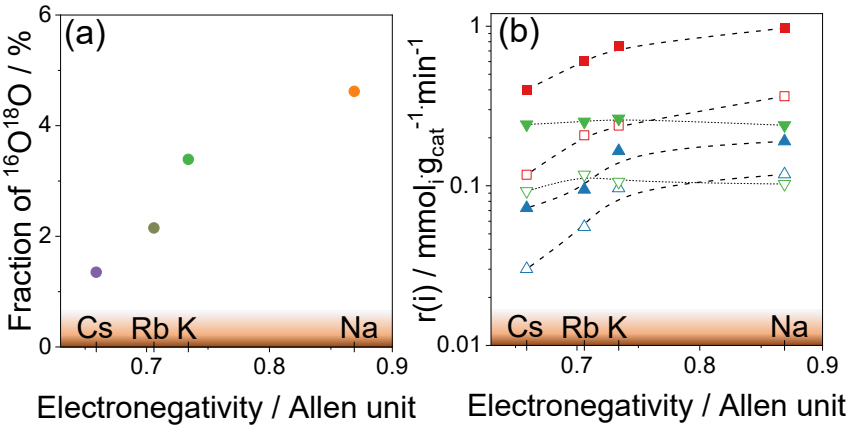

Figure 3.9. (a) Correlation of the fraction of formed $^{16}O^{18}O$ over M_2WO_4/SiO_2 (M=Na, K, Rb, or Cs) in the OIE with the electronegativity of the corresponded alkali metal; (b) Dependence of C_2-hydrocarbons, CO_2 and CO formation rates on the electronegativity of alkali metals in M_2WO_4/SiO_2. OCM reaction conditions: 800 °C, $CH_4/O_2/N_2$ 40/5/55.

To conclude, high selectivity to C_2-hydrocarbons can be achieved over M_2WO_4/SiO_2 materials regardless of the kind of alkali metal. It is also not necessary to have a MnO_x-containing component to selectively oxidize methane. Lattice oxygen of M_2WO_4 was found to be inactive for methyl radical formation. The presence of adsorbed oxygen species is essential for the selective formation of C_2-hydrocarbons over M_2WO_4/SiO_2. Activity of M_2WO_4/SiO_2 was proposed to depend on electronic properties of the catalysts. Higher electronegativity of alkali metals favors the formation of adsorbed oxygen species. Finally, no exceptional role of the molten Na_2WO_4 phase could be verified. This may help in further studies to better understand the working catalysts. For example, the crystalline M_2WO_4 (K, Rb or Cs) phase can be used in the density function theory calculations instead of unformed Na_2WO_4 phase.

3.3. Performance-defining factors of MnO_x-M_2WO_4/SiO_2 (M=Na, K, Rb or Cs) catalysts in oxidative coupling of methane

The ability of MnO_x-M_2WO_4/SiO_2 and M_2WO_4/SiO_2 (M=Na, K, Rb, or Cs) to release lattice oxygen was investigated by O_2-TPD tests. Oxygen desorption from M_2WO_4/SiO_2 catalysts was not observed in the temperature range of 100-900 °C, while their trimetallic counterparts desorbed oxygen starting from 610-680 °C. In the absence of alkali metals (MnO_x/SiO_2, MnO_x-WO_x/SiO_2), the desorption begins at 760 °C. The amount of oxygen desorbed from the trimetallic catalysts depends on the kind of alkali metal in the tungstate phase. The highest amount of oxygen was desorbed by MnO_x-Na_2WO_4/SiO_2 and the lowest amount was found for MnO_x-Cs_2WO_4/SiO_2. Further insights into the interaction of lattice oxygen of the bimetallic and trimetallic catalysts with gas-phase oxygen were obtained from OIE tests. Parameters such as temperature of onset formation of $^{16}O_2$ and $^{16}O^{18}O$, the temperature of maximum concentration of $^{16}O^{18}O$, and the amount of $^{16}O^{18}O$ were found to depend on the kind of alkali metal present in M_2WO_4/SiO_2 but no dependence could be established in the case of MnO_x-M_2WO_4/SiO_2 (Figure 3.10).

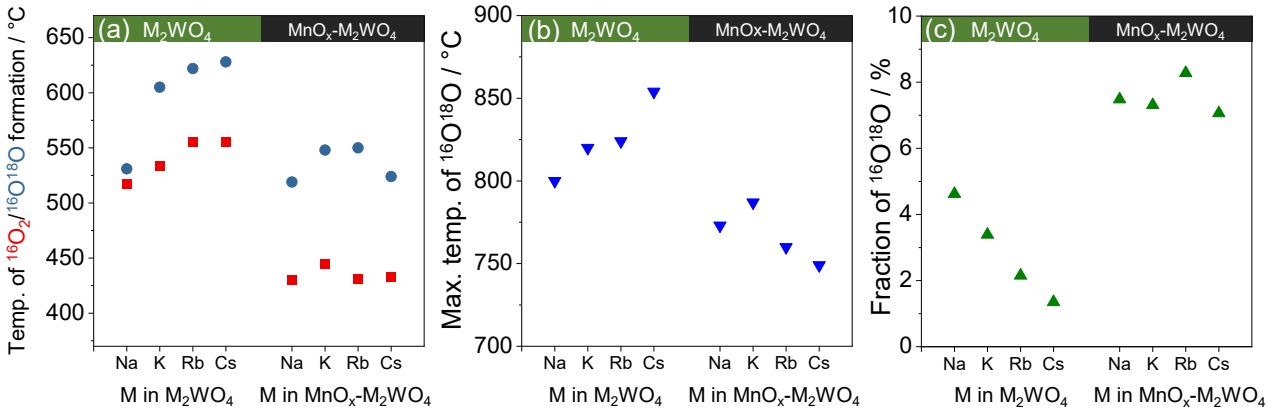

Figure 3.10. (a) Starting temperature of $^{16}O_2$ (■) and $^{16}O^{18}O$ (●) formation in oxygen isotopic exchange test; (b) Temperature of the maximal concentration of $^{16}O^{18}O$ (▼); (c) Amount of $^{16}O^{18}O$ (▲) calculated by integration of the corresponding profiles obtained in oxygen isotopic exchange tests over (MnO_x)-M_2WO_4/SiO_2 (M=Na, K, Rb, or Cs) using a feed with 1vol%$^{18}O_2$ in Ar.

Pulse experiments with CH_4 and CH_4/O_2 were performed to investigate the participation of lattice and adsorbed oxygen in product formation over M_2WO_4/SiO_2 and MnO_x-M_2WO_4/SiO_2. Compared to the MnO_x-free catalysts, which did not form hydrocarbons upon pulsing of CH_4 without gas-phase oxygen (Figure 3.11 (a)), their MnO_x-containing counterparts showed higher activity, which was dependent on the kind of alkali metal (Figure 3.11 (b)). In addition, lattice oxygen of MnO_x-M_2WO_4/SiO_2 was able to form C_2-hydrocarbons. The activity of all catalysts was improved when gas-phase O_2 was co-pulsed with CH_4. Thus, it can be concluded that the formation of C_2H_6 over M_2WO_4/SiO_2 (M=Na, K, Rb, or Cs) occurs solely with the participation of adsorbed oxygen species, whereas both lattice and adsorbed oxygen species contribute to the formation of this hydrocarbon over the trimetallic catalysts.

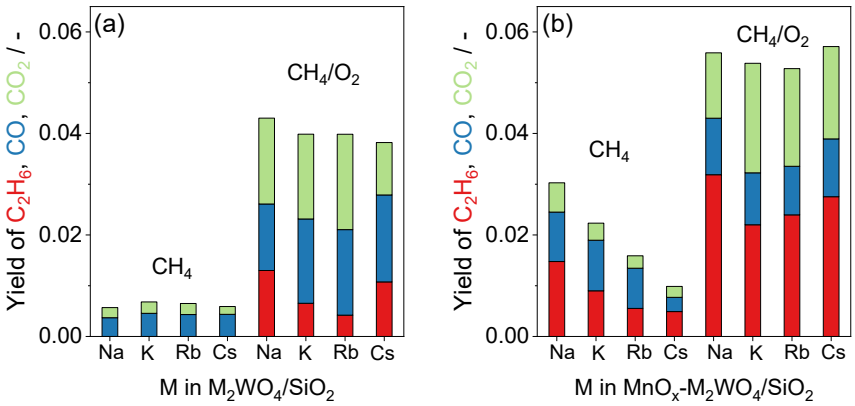

Figure 3.11. Yields of C_2H_6, CO and CO_2 determined in the pulse experiments with CH_4 or $CH_4/^{18}O_2$ at 800 °C over (a) M_2WO_4/SiO_2 and (b) MnO_x-M_2WO_4/SiO_2 (M=Na, K, Rb, or Cs).

Steady-state catalytic tests showed a similar methane conversion rate over the trimetallic catalysts at 800 °C (Figure 3.12 (a)). This rate, however, depends on the kind of alkali metal in the bimetallic

catalysts. The presence of MnO_x resulted in a 2-3 times higher CH_4 conversion rate compared to the MnO_x-free counterparts. The selectivity to C_2-hydrocarbons was in the range of ~70-80% for all catalysts at the maximal conversion of O_2 achieved under applied conditions (Figure 3.12 (b)). Thus, neither MnO_x nor the kind of alkali metal should play a decisive role for achieving high selectivity to the desired products.

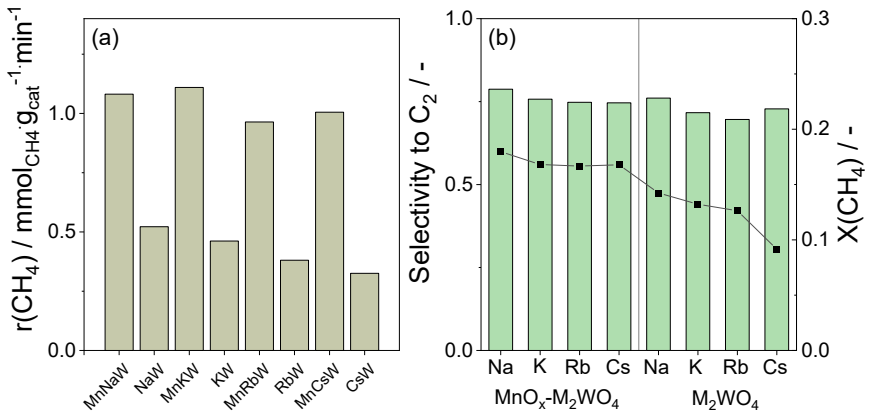

Figure 3.12. (a) The methane conversion rate (after 6 h tos) over (MnO_x)-M_2WO_4 at 800 °C, $CH_4/O_2/N_2$ 40/5/55 flow 30 ml/min, cat. amount 10 or 25 mg; (b) C_2-hydrocarbons selectivity and CH_4 conversion at maximal conversion of O_2 at 800 °C, $CH_4/O_2/N_2$ 40/5/55, flow 30 ml/min, cat. amount 100 or 300 mg.

Unlike M_2WO_4/SiO_2, lattice oxygen of the trimetallic catalysts is active and can convert CH_4 into C_2H_6. However, the amount of desorbed oxygen detected in the O_2-TPD test does not correlate with the CH_4 conversion rate obtained in steady-state catalytic tests. In contrast, it can be correlated with the activity established by the pulse experiments in the absence of gas-phase oxygen (Figure 3.13 (a)). Based on these results, we can propose that adsorbed oxygen species are essential for both bimetallic and trimetallic catalysts. Since $^{16}O^{18}O$ detected in the OIE tests must be formed from adsorbed oxygen species, its amount can be a measure of how effectively a catalyst can generate such species from gas-phase oxygen. As can be seen in Figure 3.13 (b), the kind of alkali metal is decisive for activity of M_2WO_4/SiO_2 (M=Na, K, Rb, or Cs), while no such effect can be confirmed for their MnO_x-containing counterparts.

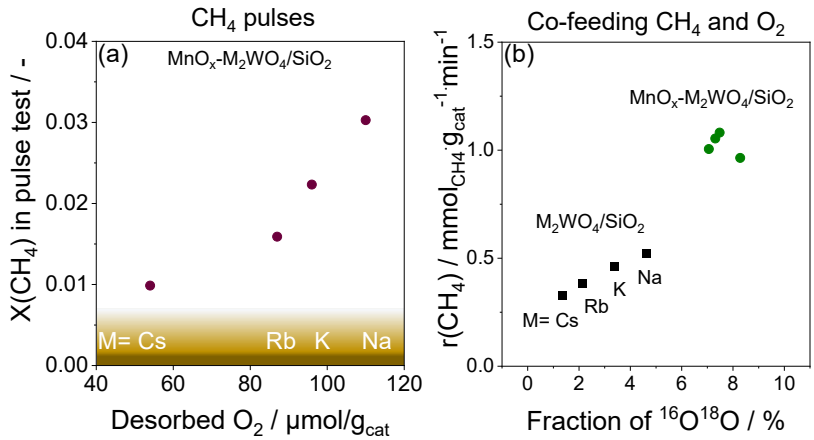

Figure 3.13. (a) Correlation of CH_4 conversion in the anaerobic pulse tests with the amount of desorbed oxygen in O_2-TPD tests detected over MnO_x-M_2WO_4/SiO_2; (b) Dependence between the CH_4 conversion rate and the amount of formed $^{16}O^{18}O$ in OIE tests over (MnO_x)-M_2WO_4/SiO_2 (M=Na, K, Rb, or Cs).

The reason for the higher activity of the MnO_x-M_2WO_4/SiO_2 catalysts in comparison with their MnO_x-free counterparts might be due to either (i) higher concentration of active sites or (ii) higher reactivity (turnover) of active sites. To verify these possibilities, steady-state isotopic transient kinetic analysis (SSITKA) was performed using (MnO_x)-M_2WO_4/SiO_2 M=Na or K. The experiments were conducted as follows: first, a steady-state operation was achieved using the nonlabeled $CH_4/^{16}O_2$ mixture. Hereafter, this feed was switched to the $CH_4/^{18}O_2$/Ar feed. The small amount of Ar was used to determine the hold-up time. The lifetime (τ(i)) of intermediates leading to the formation of H_2O and CO_2 was calculated through integrating the profiles of Ar and the formed labeled products under consideration of the SSITKA theory [171, 172]. The concentration of the intermediates was calculated according to the eq. 23. The lifetime (τ(i)) of surface intermediates leading to H_2O or CO_2 was 2-3 times higher for the trimetallic catalysts (Figure 3.14 (c, d)). However, the concentration of H_2O intermediates (N(H_2O)) was practically independent of the presence of MnO_x (Figure 3.14 (c)). The same conclusions about the role of MnO_x are also valid for τ(CO_2) and N(CO_2) of (MnO_x)-K_2WO_4/SiO_2 (Figure 3.14 (d)). Thus, the presence of MnO_x does not result in a higher concentration of intermediates leading to the formation of all products, but rather increases their reactivity.

$$N_i = \tau_i r_i \qquad (23)$$

Importantly, τ(H_2O) is higher than τ(CO_2) for all catalysts. CO_2 is formed directly from CH_4, what requires the breakage of C–H bonds and the formation of C=O bonds. If the abstraction of H from CH_4 was a step-limiting step, τ(CO_2) would be higher than τ(H_2O). The opposite result was obtained in this work, suggesting that H_2O removal/formation controls the rate of CH_4 conversion. The previously observed kinetic isotope effect (KIE) over Li/MgO or MnO_x-Na_2WO_4/SiO_2 with CH_4 and CD_4 was used

as evidence that methyl radical formation is the rate-limiting step in the OCM reaction [97, 173, 174]. However, the observed KIE cannot unambiguously indicate whether it is due to the C–H/C–D bond cleavage or recombination of formed OH/OD groups. Thus, as it was shown in this work, the rate-limiting step in the OCM reaction over (MnO_x)-M_2WO_4/SiO_2 does not seem to be the breakage of C–H bond, i.e., the formation of methyl radical, but the formation of H_2O.

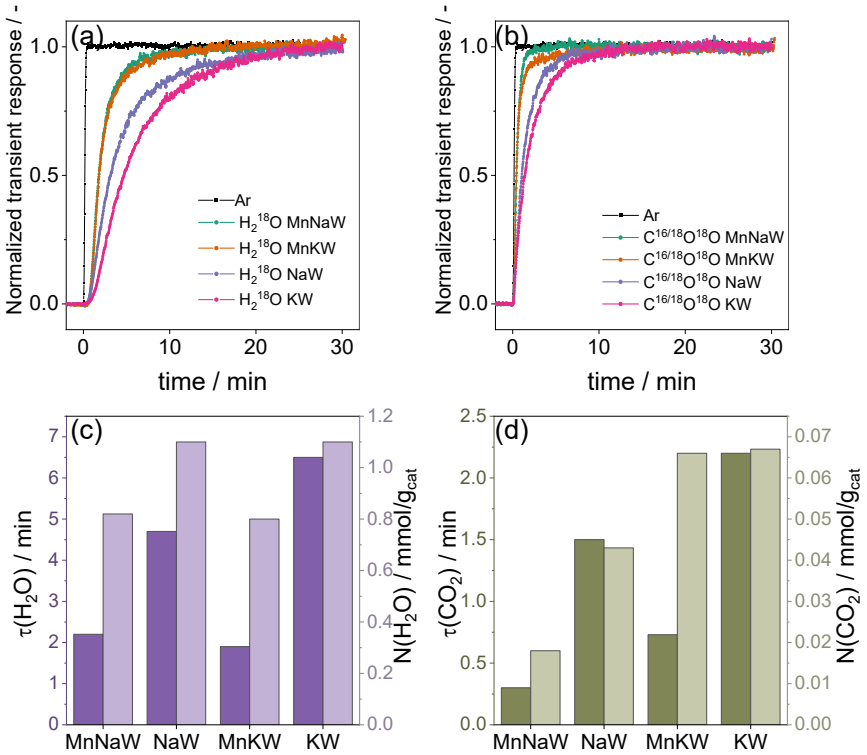

Figure 3.14. Transient responses of (a) $H_2{}^{18}O$ and (b) $C^{16}O^{18}O+C^{18}O_2$ recorded in SSITKA tests over (MnO_x)-M_2WO_4/SiO_2 (M=Na or K) at 775 °C upon switching from $CH_4/{}^{16}O_2$ to $CH_4/{}^{18}O_2$/Ar; The lifetime and the concentration of surface intermediates of (c) H_2O and (d) CO_2. These characteristics were calculated from the corresponding transients according to [171, 172].

In conclusion, high selectivity to C_2-hydrocarbons in the OCM reaction over (MnO_x)-M_2WO_4/SiO_2 can be achieved whether M_2WO_4 is present as the molten Na_2WO_4 phase or as crystalline M_2WO_4 (M=K, Rb, or Cs). Lattice oxygen of MnO_x-M_2WO_4/SiO_2 is more active than that of M_2WO_4/SiO_2 and can form C_2-hyrocarbons. Nevertheless, for both systems, adsorbed oxygen species seems to be more active compared to lattice oxygen. The kind of alkali metal in MnO_x-M_2WO_4/SiO_2 affects the strength of the Mn–O and/or W–O bonds that is decisive for the catalyst activity under anaerobic conditions. However, under aerobic conditions, unlike M_2WO_4/SiO_2, the OCM activity of MnO_x-M_2WO_4/SiO_2 does not depend on the kind of alkali metal. The role of MnO_x was established to increase the turnover of active sites without changing their number.

4. Conclusions

The present work provides new fundamentals affecting activity and product selectivity of (MnO_x)-M_2WO_4/SiO_2 (M=Na, K, Rb, or Cs) materials, which are promising for the oxidative coupling of methane to C_2-hydrocarbons (C_2H_6 and C_2H_4). It was shown that the use of N_2O instead of O_2 significantly improves the selectivity to these products. This was explained by the lower ability of N_2O to generate biatomic adsorbed oxygen species, which are formed in larger amounts from gas-phase oxygen and are involved in the direct conversion of CH_4 into undesired CO_2. The selectivity to C_2-hydrocarbons can be further improved by adding H_2O to the N_2O-OCM feed. H_2O is responsible for the transformation of biatomic adsorbed oxygen species into monoatomic ones, which are selective for methane oxidation into the desired C_2-hydrocarbons. In addition to the hindered ability of N_2O to generate biatomic oxygen species, this oxidant also has a lower ability to reoxidize reduced MnO_x species in comparison with O_2. As a result, the coverage of easily removable lattice oxygen species decreases that is favorable for the selective conversion of methane into C_2-hydrocarbons.

The study of MnO_x-free M_2WO_4/SiO_2 (M=Na, K, Rb, or Cs) revealed that the MnO_x or molten Na_2WO_4 phase(s) do not play an important role in the selective formation of C_2-hydrocarbons. Lattice oxygen species of M_2WO_4/SiO_2 were found to be inactive and unselective. Adsorbed oxygen species formed from gas-phase oxygen are essential for the formation of methyl radicals that couple to C_2H_6 in the gas phase. Electronic properties of alkali metals were proposed to determine the effectiveness of M_2WO_4/SiO_2 to form adsorbed oxygen species and consequently define the overall OCM activity. In addition, it was found that C_2-hydrocarbons and CO_2 are formed with the participation of adsorbed oxygen species, while lattice oxygen is involved in the formation of CO.

In the comparative study of trimetallic MnO_x-M_2WO_4/SiO_2 and bimetallic M_2WO_4/SiO_2 (M=Na, K, Rb, or Cs), the previously proposed importance of the molten Na_2WO_4 phase or its ability to release lattice oxygen for catalyst activity or C_2-hydrocarbons selectivity was not confirmed. All materials tested, i.e., bimetallic and trimetallic, were selective to these products. While lattice oxygen of M_2WO_4/SiO_2 is not active towards selective conversion of methane, lattice oxygen of MnO_x-M_2WO_4/SiO_2 was found to be able to produce C_2-hydrocarbons. Nevertheless, the involvement of adsorbed species is decisive for activity of both bimetallic and trimetallic catalysts. MnO_x was found to play the role of a promoter, increasing the reactivity of active sites but not changing their concertation. In contrast to M_2WO_4/SiO_2, no effect of alkali metal on catalyst activity was found over MnO_x-M_2WO_4/SiO_2.

5. Outlook

As it was shown in this work, the selectivity to C_2-hydrocarbons can be improved by the controlled formation of monoatomic oxygen species over MnO_x-Na_2WO_4/SiO_2. One way to form these species is to add water in the feed. The same high concentration of monoatomic oxygen species as when N_2O is used can be achieved by reactor design, namely by using a membrane reactor. In this concept, the uniform distribution of monoatomic oxygen could be realized. In addition, it was found in this work that the slightly reduced oxidation state of the MnO_x-Na_2WO_4/SiO_2 catalyst leads to more isolated lattice oxygen species. This favors the selective conversion of methane into C_2-hydrocarbons. Such isolation of oxygen sites can be achieved through a purposeful catalyst design of materials that can provide an optimal mismatch between the rates of CH_4 reduction and reoxidation by O_2.

Recent discussion in the literature regarding active phases over MnO_x-Na_2WO_4/SiO_2 or Na_2WO_4/SiO_2 includes the importance of molten Na_2WO_4 under reaction conditions. The presence of this molten Na_2WO_4 phase complicates comprehensible theoretical calculations of the multiphase MnO_x-Na_2WO_4/SiO_2. However, as shown in this work, the crystalline phase of M_2WO_4 (K, Rb, or Cs) can be used instead of this ill-defined phase. These calculations could provide new insights into oxygen species involved, structure of active sites, and synergistic interaction between MnO_x and M_2WO_4. Theoretical findings need to be further complemented by in situ/operando studies.

Apart from a catalyst material design, the problems of heat management and product separation need to be addressed for future upscaling of the OCM process. The former is related to the exothermic nature of the OCM reactions, particularly the oxidation to the undesired CO_x products. Temperature control is therefore necessary to avoid the formation of hot spots, which can lead to a significant increase in temperature, adversely affecting the selectivity and long-term catalyst stability. This problem can be solved by optimizing the mode of operation, e.g., by using a chemical looping regime or a membrane reactor. Alternatively, the OCM reaction can be combined with an endothermic process to compensate for the heat generated during OCM. For example, integrating OCM with ethane dehydrogenation reaction may offer two advantages: (i) some level of autothermal operation and (ii) an increase in the yield of target ethylene. Regarding product separation, the conventional method of hydrocarbon separation is cryogenic distillation, which significantly increases operating costs. The solution to this problem could be the use of other technologies, such as adsorptive or membrane-based separation.

6. References

[1] BP, bp Statistical Review of World Energy 2021, 2021.
[2] M. Melikoglu, Shale gas: Analysis of its role in the global energy market, Renew. Sust. Energ. Rev., 37 (2014) 460-468.
[3] J. Zhang, M. Shi, D. Wang, Z. Tong, X. Hou, J. Niu, X. Li, Z. Li, P. Zhang, Y. Huang, Fields and directions for shale gas exploration in China, Nat. Gas Ind. B, 9 (2022) 20-32.
[4] Y.F. Makogon, S.A. Holditch, T.Y. Makogon, Natural gas-hydrates — A potential energy source for the 21st Century, J. Pet. Sci. Eng., 56 (2007) 14-31.
[5] G.J. Moridis, T.S. Collett, R. Boswell, M. Kurihara, M.T. Reagan, C. Koh, E.D. Sloan, Toward Production From Gas Hydrates: Current Status, Assessment of Resources, and Simulation-Based Evaluation of Technology and Potential, SPE Reservoir Evaluation & Engineering, 12 (2009) 745-771.
[6] The World Bank, Global Gas Flaring Reduction Partnership (GGFR): What is Gas Flaring? https://www.worldbank.org/en/programs/gasflaringreduction/gas-flaring-explained, (last access 12.2022).
[7] V.R. Choudhary, A.M. Rajput, B. Prabhakar, Energy efficient methane-to-syngas conversion with low H_2/CO ratio by simultaneous catalytic reactions of methane with carbon dioxide and oxygen, Catal. Lett., 32 (1995) 391-396.
[8] J.P. Van Hook, Methane-Steam Reforming, Catal. Rev., 21 (1980) 1-51.
[9] J.R. Rostrupnielsen, J.H.B. Hansen, CO_2-Reforming of Methane over Transition Metals, J. Catal., 144 (1993) 38-49.
[10] I. Wender, Reactions of synthesis gas, Fuel Proc. Techn., 48 (1996) 189-297.
[11] H.T. Luk, C. Mondelli, D.C. Ferré, J.A. Stewart, J. Pérez-Ramírez, Status and prospects in higher alcohols synthesis from syngas, Chem. Soc. Rev., 46 (2017) 1358-1426.
[12] M.R. Gogate, Methanol-to-olefins process technology: current status and future prospects, Pet. Sci. Technol., 37 (2019) 559-565.
[13] I. Amghizar, L.A. Vandewalle, K.M. Van Geem, G.B. Marin, New Trends in Olefin Production, Engineering, 3 (2017) 171-178.
[14] I.-T. Trotuş, T. Zimmermann, F. Schüth, Catalytic Reactions of Acetylene: A Feedstock for the Chemical Industry Revisited, Chem. Rev., 114 (2014) 1761-1782.
[15] E. Bartholomé, The BASF-process for production of acetylene by partial oxidation of gaseous hydrocarbons, Chem. Eng. Sci., 3 (1954) 94-104.
[16] P. Pässler, W. Hefner, K. Buckl, H. Meinass, A. Meiswinkel, H.J. Wernicke, G. Ebersberg, R. Müller, J. Bässler, H. Behringer, Acetylene, Ullmann's Encyclopedia of Industrial Chemistry, (2000).
[17] H. Schobert, Production of Acetylene and Acetylene-based Chemicals from Coal, Chem. Rev., 114 (2014) 1743-1760.
[18] V. Paunović, J. Pérez-Ramírez, Catalytic halogenation of methane: a dream reaction with practical scope?, Catal. Sci. Tech., 9 (2019) 4515-4530.
[19] M. Rossberg, W. Lendle, G. Pfleiderer, A. Tögel, E.-L. Dreher, E. Langer, H. Rassaerts, P. Kleinschmidt, H. Strack, R. Cook, Chlorinated hydrocarbons, Ullmann's encyclopedia of industrial chemistry, (2006) 1-186.
[20] Z. Liu, L. Huang, W.S. Li, F. Yang, C.T. Au, X.P. Zhou, Higher hydrocarbons from methane condensation mediated by HBr, J. Mol. Catal. A, 273 (2007) 14-20.
[21] J. Bao, G. Yang, Y. Yoneyama, N. Tsubaki, Significant Advances in C1 Catalysis: Highly Efficient Catalysts and Catalytic Reactions, ACS Catal., 9 (2019) 3026-3053.
[22] R. Lin, A.P. Amrute, J. Pérez-Ramírez, Halogen-Mediated Conversion of Hydrocarbons to Commodities, Chem. Rev., 117 (2017) 4182-4247.

[23] R. Horn, R. Schlögl, Methane Activation by Heterogeneous Catalysis, Catal. Lett., 145 (2015) 23-39.
[24] B.Y.K. Pan, Characteristics of Pt-Rh gauze catalyst and kinetics of the HCN synthesis, J. Catal., 21 (1971) 27-38.
[25] S. Delagrange, Y. Schuurman, HCN synthesis from methane and ammonia over platinum, Catal. Today, 121 (2007) 204-209.
[26] V.A. Kondratenko, Mechanistic aspects of the Andrussow process over Pt–Rh gauzes. Pathways of formation and consumption of HCN, Appl. Catal. A, 381 (2010) 74-82.
[27] T. Ren, M.K. Patel, K. Blok, Steam cracking and methane to olefins: Energy use, CO_2 emissions and production costs, Energy, 33 (2008) 817-833.
[28] I. Amghizar, J.N. Dedeyne, D.J. Brown, G.B. Marin, K.M. Van Geem, Sustainable innovations in steam cracking: CO_2 neutral olefin production, Reaction Chemistry & Engineering, 5 (2020) 239-257.
[29] E.V. Kondratenko, T. Peppel, D. Seeburg, V.A. Kondratenko, N. Kalevaru, A. Martin, S. Wohlrab, Methane conversion into different hydrocarbons or oxygenates: current status and future perspectives in catalyst development and reactor operation, Catal. Sci. Tech., 7 (2017) 366-381.
[30] N. Kosinov, E.J.M. Hensen, Reactivity, Selectivity, and Stability of Zeolite-Based Catalysts for Methane Dehydroaromatization, Adv. Mater., 32 (2020) 2002565.
[31] W. Taifan, J. Baltrusaitis, CH_4 conversion to value added products: Potential, limitations and extensions of a single step heterogeneous catalysis, Appl. Catal. B, 198 (2016) 525-547.
[32] J.-P. Lange, Economics of Alkane Conversion, in: E.G. Derouane, V. Parmon, F. Lemos, F. Ramôa Ribeiro (Eds.) Sustainable Strategies for the Upgrading of Natural Gas: Fundamentals, Challenges, and Opportunities, Springer Netherlands, Dordrecht, 2005, pp. 51-83.
[33] C. Díaz-Urrutia, T. Ott, Activation of methane: A selective industrial route to methanesulfonic acid, Science, 363 (2019) 1326-1329.
[34] https://www.basf.com/global/de/media/news-releases/2020/01/p-20-115.html, (last access 12.2022).
[35] C. Karakaya, R.J. Kee, Progress in the direct catalytic conversion of methane to fuels and chemicals, Prog. Energ. Combust., 55 (2016) 60-97.
[36] T. Koerts, M.J. Deelen, R.A. Van Santen, Hydrocarbon formation from methane by a low-temperature two-step reaction sequence, J. Catal., 138 (1992) 101-114.
[37] M.C. Wu, P. Lenz-Solomun, D.W. Goodman, Two-step, oxygen-free route to higher hydrocarbons from methane over ruthenium catalysts, Journal of Vacuum Science & Technology A, 12 (1994) 2205-2209.
[38] L. Guczi, K. Sarma, L. Borkó, Non-oxidative methane coupling over Co-Pt/NaY bimetallic catalysts, Catal. Lett., 39 (1996) 43-47.
[39] A. Amariglio, M. Belgued, P. Paréja, H. Amariglio, Oxygen-free Conversion of Methane to Higher Hydrocarbons through a Dual-Temperature Two-Step Reaction Sequence on Platinum and Ruthenium: 1. Chemisorption of CH_4 at a Fixed Temperature, J. Catal., 177 (1998) 113-120.
[40] Y. Xiao, A. Varma, Highly Selective Nonoxidative Coupling of Methane over Pt-Bi Bimetallic Catalysts, ACS Catal., 8 (2018) 2735-2740.
[41] X. Guo, G. Fang, G. Li, H. Ma, H. Fan, L. Yu, C. Ma, X. Wu, D. Deng, M. Wei, D. Tan, R. Si, S. Zhang, J. Li, L. Sun, Z. Tang, X. Pan, X. Bao, Direct, Nonoxidative Conversion of Methane to Ethylene, Aromatics, and Hydrogen, Science, 344 (2014) 616-619.
[42] S.J. Han, S.W. Lee, H.W. Kim, S.K. Kim, Y.T. Kim, Nonoxidative Direct Conversion of Methane on Silica-Based Iron Catalysts: Effect of Catalytic Surface, ACS Catal., 9 (2019) 7984-7997.
[43] R.S. Postma, L. Lefferts, Influence of Axial Temperature Profiles on Fe/SiO_2 Catalyzed Non-oxidative Coupling of Methane, ChemCatChem, 13 (2021) 1157-1160.

[44] R.S. Postma, P.S.F. Mendes, L. Pirro, A. Banerjee, J.W. Thybaut, L. Lefferts, Modelling of the catalytic initiation of methane coupling under non-oxidative conditions, Chem. Eng. J., 454 (2023) 140273.
[45] G.E. Keller, M.M. Bhasin, Synthesis of ethylene via oxidative coupling of methane: I. Determination of active catalysts, J. Catal., 73 (1982) 9-19.
[46] V. Spallina, I.C. Velarde, J.A.M. Jimenez, H.R. Godini, F. Gallucci, M. Van Sint Annaland, Techno-economic assessment of different routes for olefins production through the oxidative coupling of methane (OCM): Advances in benchmark technologies, Energy Convers. Manag., 154 (2017) 244-261.
[47] https://www.penpet.com/news/news-ethylene-october-2021.html, (last access 12.2022).
[48] A. Cruellas, J.J. Bakker, M. van Sint Annaland, J.A. Medrano, F. Gallucci, Techno-economic analysis of oxidative coupling of methane: Current state of the art and future perspectives, Energy Convers. Manag., 198 (2019) 111789.
[49] T. Degnan, Siluria and OCM – close to full scale commercializaton?, Focus on Catalysts, 2016 (2016) 1-2.
[50] G. Radaelli, G. Chachra, D. Jonnavittula, Low-Energy, Low-Cost Production of Ethylene by Low-Temperature Oxidative Coupling of Methane, Siluria Technologies, Inc., San Francisco, CA (United States), 2017.
[51] B. Pyrmak, Low-Energy, Low-Cost Ethylene Production by Low-Temperature Oxidative Coupling of Methane, EERE Publication and Product Library, Washington, DC (United States), 2019.
[52] E.C.S. Fabio R. Zucher, Joel M. Cizeron, Wayne P. Schammel, Alex Tkachenko, Joel Gamoras, Dmitry Karshtedt, Greg Nyce, Anja Rumplecker, Jarod McCormick, Anna Merzlyak, Marian Alcid, Daniel Rosenberg, Erik-Jan Ras, Nanowire catalysts and methods for their use and preparation, U.S., 2015.
[53] J.M.C. Erik C. Scher, Wayne P. Schammel, Alex Tkachenko, Joel Gamoras, Dmitry Karshtedt, Greg Nyce, Fabio R. Zurcher, Method for the oxidative coupling of methane in the presence of a nanowire catalyst, in: S.T. Inc (Ed.), 2015.
[54] Y.S. Su, J.Y. Ying, W.H. Green, Upper bound on the yield for oxidative coupling of methane, J. Catal., 218 (2003) 321-333.
[55] V. Fleischer, P. Littlewood, S. Parishan, R. Schomäcker, Chemical looping as reactor concept for the oxidative coupling of methane over a $Na_2WO_4/Mn/SiO_2$ catalyst, Chem. Eng. J., 306 (2016) 646-654.
[56] S. Parishan, P. Littlewood, A. Arinchtein, V. Fleischer, R. Schomäcker, Chemical looping as a reactor concept for the oxidative coupling of methane over the Mn_xO_y-Na_2WO_4/SiO_2 catalyst, benefits and limitation, Catal. Today, 311 (2018) 40-47.
[57] N.H. Othman, Z. Wu, K. Li, An oxygen permeable membrane microreactor with an in-situ deposited $Bi_{1.5}Y_{0.3}Sm_{0.2}O_{3-\delta}$ catalyst for oxidative coupling of methane, J. Membr. Sci., 488 (2015) 182-193.
[58] W. Yang, H. Wang, X. Zhu, L. Lin, Development and Application of Oxygen Permeable Membrane in Selective Oxidation of Light Alkanes, Topics Catal., 35 (2005) 155-167.
[59] D. Matras, A. Vamvakeros, S.D. Jacques, V. Middelkoop, G. Vaughan, M.A. Aran, R.J. Cernik, A.M. Beale, In situ X-ray diffraction computed tomography studies examining the thermal and chemical stabilities of working $Ba_{0.5}Sr_{0.5}Co_{0.8}Fe_{0.2}O_{3-\delta}$ membranes during oxidative coupling of methane, PCCP, 22 (2020) 18964-18975.
[60] H. Wang, Y. Cong, W. Yang, Oxidative coupling of methane in $Ba_{0.5}Sr_{0.5}Co_{0.8}Fe_{0.2}O_{3-\delta}$ tubular membrane reactors, Catal. Today, 104 (2005) 160-167.
[61] N.H. Othman, Z. Wu, K. Li, A micro-structured $La_{0.6}Sr_{0.4}Co_{0.2}Fe_{0.8}O_{3-\delta}$ hollow fibre membrane reactor for oxidative coupling of methane, J. Membr. Sci., 468 (2014) 31-41.
[62] X. Tan, Z. Pang, Z. Gu, S. Liu, Catalytic perovskite hollow fibre membrane reactors for methane oxidative coupling, J. Membr. Sci., 302 (2007) 109-114.

[63] V.O. Igenegbai, R.J. Meyer, S. Linic, In search of membrane-catalyst materials for oxidative coupling of methane: Performance and phase stability studies of gadolinium-doped barium cerate and the impact of Zr doping, Appl. Catal. B, 230 (2018) 29-35.
[64] G. Dimitrakopoulos, B. Koo, B. Yildiz, A.F. Ghoniem, Highly durable C_2 hydrocarbon production via the oxidative coupling of methane using a $BaFe_{0.9}Zr_{0.1}O_{3-\delta}$ mixed ionic and electronic conducting membrane and La_2O_3 catalyst, ACS Catal., 11 (2021) 3638-3661.
[65] B.L. Farrell, S. Linic, Oxidative coupling of methane over mixed oxide catalysts designed for solid oxide membrane reactors, Catal. Sci. Tech., 6 (2016) 4370-4376.
[66] M. Baerns, E.V. Kondratenko, Oxidative coupling of methane, Handbook of heterogeneous catalysis, Wiley-VCH, 2008, pp. 3010-3023.
[67] K. Otsuka, T. Komatsu, Active catalysts in oxidative coupling of methane, J. Chem. Soc., Chem. Commun., (1987) 388-389.
[68] N. Hiyoshi, T. Ikeda, Oxidative coupling of methane over alkali chloride–Mn–Na_2WO_4/SiO_2 catalysts: Promoting effect of molten alkali chloride, Fuel Proc. Techn., 133 (2015) 29-34.
[69] K. Otsuka, M. Hatano, T. Komatsu, Synthesis of C_2H_4 by Partial Oxidation of CH_4 Over Transition Metal Oxides With Alkali-Chlorides, in: D.M. Bibby, C.D. Chang, R.F. Howe, S. Yurchak (Eds.) Stud. Surf. Sci. Catal., Elsevier, 1988, pp. 383-387.
[70] T. Ito, J.H. Lunsford, Synthesis of ethylene and ethane by partial oxidation of methane over lithium-doped magnesium oxide, Nature, 314 (1985) 721-722.
[71] V.R. Choudhary, V.H. Rane, M.Y. Pandit, Comparison of Alkali Metal Promoted MgO Catalysts for Their Surface Acidity/Basicity and Catalytic Activity/Selectivity in the Oxidative Coupling of Methane, J. Chem. Technol. Biotechnol., 68 (1997) 177-186.
[72] C.H. Lin, T. Ito, J. Wang, J.H. Lunsford, Oxidative dimerization of methane over magnesium and calcium oxide catalysts promoted with group IA ions: The role of $[M^+O^-]$ centers, J. Am. Chem. Soc., 109 (1987) 4808-4810.
[73] S. Arndt, G. Laugel, S. Levchenko, R. Horn, M. Baerns, M. Scheffler, R. Schlögl, R. Schomäcker, A Critical Assessment of Li/MgO-Based Catalysts for the Oxidative Coupling of Methane, Catal. Rev., 53 (2011) 424-514.
[74] D.J. Driscoll, W. Martir, J.X. Wang, J.H. Lunsford, Formation of gas-phase methyl radicals over magnesium oxide, J. Am. Chem. Soc., 107 (1985) 58-63.
[75] J.X. Wang, J.H. Lunsford, Characterization of [Li+ O] centers in lithium-doped magnesium oxide catalysts, The Journal of Physical Chemistry, 90 (1986) 5883-5887.
[76] J.H. Lunsford, The Catalytic Oxidative Coupling of Methane, Angew. Chem., Int. Ed., 34 (1995) 970-980.
[77] J.S.J. Hargreaves, G.J. Hutchings, R.W. Joyner, C.J. Kiely, The relationship between catalyst morphology and performance in the oxidative coupling of methane, J. Catal., 135 (1992) 576-595.
[78] M.C. Wu, C.M. Truong, K. Coulter, D.W. Goodman, Investigations of Active Sites for Methane Activation in the Oxidative Coupling Reaction over Pure and Li-Promoted MgO Catalysts, J. Catal., 140 (1993) 344-352.
[79] U. Zavyalova, G. Weinberg, W. Frandsen, F. Girgsdies, T. Risse, K.P. Dinse, R. Schloegl, R. Horn, Lithium as a Modifier for Morphology and Defect Structure of Porous Magnesium Oxide Materials Prepared by Gel Combustion Synthesis, ChemCatChem, 3 (2011) 1779-1788.
[80] L. Luo, Y. Jin, H. Pan, X. Zheng, L. Wu, R. You, W. Huang, Distribution and role of Li in Li-doped MgO catalysts for oxidative coupling of methane, J. Catal., 346 (2017) 57-61.
[81] K. Qian, R. You, Y. Guan, W. Wen, Y. Tian, Y. Pan, W. Huang, Single-Site Catalysis of Li-MgO Catalysts for Oxidative Coupling of Methane Reaction, ACS Catal., 10 (2020) 15142-15148.
[82] J.M. DeBoy, R.F. Hicks, The oxidative coupling of methane over alkali, alkaline earth, and rare earth oxides, Ind. Eng. Chem. Res., 27 (1988) 1577-1582.

[83] P. Huang, Y. Zhao, J. Zhang, Y. Zhu, Y. Sun, Exploiting shape effects of La_2O_3 nanocatalysts for oxidative coupling of methane reaction, Nanoscale, 5 (2013) 10844-10848.
[84] T. Jiang, J. Song, M. Huo, N. Yang, J. Liu, J. Zhang, Y. Sun, Y. Zhu, La_2O_3 catalysts with diverse spatial dimensionality for oxidative coupling of methane to produce ethylene and ethane, RSC Adv., 6 (2016) 34872-34876.
[85] E.Y. Chung, W.K. Wang, S.G. Nadgouda, D.S. Baser, J.A. Sofranko, L.-S. Fan, Catalytic Oxygen Carriers and Process Systems for Oxidative Coupling of Methane Using the Chemical Looping Technology, Ind. Eng. Chem. Res., 55 (2016) 12750-12764.
[86] V. Fleischer, U. Simon, S. Parishan, M.G. Colmenares, O. Görke, A. Gurlo, W. Riedel, L. Thum, J. Schmidt, T. Risse, K.-P. Dinse, R. Schomäcker, Investigation of the role of the $Na_2WO_4/Mn/SiO_2$ catalyst composition in the oxidative coupling of methane by chemical looping experiments, J. Catal., 360 (2018) 102-117.
[87] W. Sun, G. Zhao, Y. Gao, J. Si, Y. Liu, Y. Lu, An oxygen carrier catalyst toward efficient chemical looping-oxidative coupling of methane, Appl. Catal. B, 304 (2022) 120948.
[88] J. Huang, K. Zhao, S. Jiang, S. Kang, Y. Lin, Z. Huang, A. Zheng, Z. Zhao, Heteroatom-doping regulated Mg_6MnO_8 for improving C_{2+} hydrocarbons during chemical looping oxidative coupling of methane, Fuel Proc. Techn., 235 (2022) 107352.
[89] K. Zhao, J. Huang, Z. Huang, Y. Lin, M. Zheng, D. Song, A. Liu, X. Wang, A. Zheng, Z. Zhao, Tungstate promoted $CaMnO_3$-based core-shell redox catalysts for efficient chemical looping oxidative coupling of methane, J. Energy Inst., 105 (2022) 273-281.
[90] D. Zeng, C. Wang, T. Liu, W. Ou, R. Xiao, Enhanced performance of chemical looping methane oxidative coupling by the synergistic effect of TiO_2 doped $Na_2WO_4/Mn_2O_3/SiO_2$ oxygen carriers, Fuel Proc. Techn., 234 (2022) 107320.
[91] P.F. Nelson, C.A. Lukey, N.W. Cant, Isotopic evidence for direct methyl coupling and ethane to ethylene conversion during partial oxidation of methane over lithium/magnesium oxide, The Journal of Physical Chemistry, 92 (1988) 6176-6179.
[92] D.J. Driscoll, J.H. Lunsford, Gas-phase radical formation during the reactions of methane, ethane, ethylene, and propylene over selected oxide catalysts, The Journal of Physical Chemistry, 89 (1985) 4415-4418.
[93] H. Schwarz, Chemistry with Methane: Concepts Rather than Recipes, Angew. Chem., Int. Ed., 50 (2011) 10096-10115.
[94] C.H. Lin, K.D. Campbell, J.X. Wang, J.H. Lunsford, Oxidative dimerization of methane over lanthanum oxide, The Journal of Physical Chemistry, 90 (1986) 534-537.
[95] J.H. Lunsford, The role of surface-generated gas-phase radicals in catalysis, Langmuir, 5 (1989) 12-16.
[96] K. Takanabe, E. Iglesia, Rate and Selectivity Enhancements Mediated by OH Radicals in the Oxidative Coupling of Methane Catalyzed by $Mn/Na_2WO_4/SiO_2$, Angew. Chem., Int. Ed., 47 (2008) 7689-7693.
[97] K. Takanabe, E. Iglesia, Mechanistic Aspects and Reaction Pathways for Oxidative Coupling of Methane on $Mn/Na_2WO_4/SiO_2$ Catalysts, J. Phys. Chem. C, 113 (2009) 10131-10145.
[98] K. Takanabe, Catalytic conversion of methane: carbon dioxide reforming and oxidative coupling, J. Japan Pet. Inst., 55 (2012) 1-12.
[99] P. Schwach, X.L. Pan, X.H. Bao, Direct Conversion of Methane to Value-Added Chemicals over Heterogeneous Catalysts: Challenges and Prospects, Chem. Rev., 117 (2017) 8497-8520.
[100] D. Dissanayake, J.H. Lunsford, M.P. Rosynek, Site Differentiation in Homolytic vs. Heterolytic Activation of Methane over Ba/MgO Catalysts, J. Catal., 146 (1994) 613-615.

[101] M.Y. Sinev, L.Y. Margolis, V.Y. Bychkov, V.N. Korchak, Free radicals as intermediates in oxidative transformations of lower alkanes, in: R.K. Grasselli, S.T. Oyama, A.M. Gaffney, J.E. Lyons (Eds.) Stud. Surf. Sci. Catal., Elsevier, 1997, pp. 327-335.
[102] Z. Kalenik, E.E. Wolf, Transient and isotopic studies of the oxygen transport and exchange during oxidative coupling of methane on Sr promoted La_2O_3, Catal. Lett., 9 (1991) 441-449.
[103] A. Bielanski, J. Haber, Oxygen in catalysis, CRC Press1990.
[104] H. Borchert, M. Baerns, The Effect of Oxygen-Anion Conductivity of Metal–Oxide Doped Lanthanum Oxide Catalysts on Hydrocarbon Selectivity in the Oxidative Coupling of Methane, J. Catal., 168 (1997) 315-320.
[105] Y. Osada, S. Koike, T. Fukushima, S. Ogasawara, T. Shikada, T. Ikariya, Oxidative coupling of methane over Y_2O_3CaO catalysts, Appl. Catal., 59 (1990) 59-74.
[106] T.L. Yang, L.B. Feng, S.K. Shen, Oxygen Species on the Surface of La_2O_3/CaO and Its Role in the Oxidative Coupling of Methane, J. Catal., 145 (1994) 384-389.
[107] K. Otsuka, K. Jinno, Kinetic studies on partial oxidation of methane over samarium oxides, Inorg. Chim. Acta, 121 (1986) 237-241.
[108] O. Kiyoshi, S.A. A., J. Kiyotaka, K. Takayuki, Peroxide Anions as Possible Active Species in Oxidative Coupling of Methane, Chem. Lett., 16 (1987) 77-80.
[109] K.C. Kharas, J.H. Lunsford, Catalytic partial oxidation of methane over barium metaplumbate $BaPbO_3$: possible involvement of peroxide ion, J. Am. Chem. Soc., 111 (1989) 2336-2337.
[110] H. Yamashita, Y. Machida, A. Tomita, Oxidative coupling of methane with peroxide ions over barium-lanthanum-oxygen mixed oxide, Appl. Catal. A, 79 (1991) 203-214.
[111] M.S. Palmer, M. Neurock, M.M. Olken, Periodic density functional theory study of methane activation over La_2O_3: activity of O^{2-}, O^-, O_2^{2-}, oxygen point defect, and Sr^{2+}-doped surface sites, J. Am. Chem. Soc., 124 (2002) 8452-8461.
[112] M.S. Palmer, M. Neurock, M.M. Olken, Periodic Density Functional Theory Study of the Dissociative Adsorption of Molecular Oxygen over La_2O_3, J. Phys. Chem. B, 106 (2002) 6543-6547.
[113] C. Chu, Y. Zhao, S. Li, Y. Sun, Role of Peroxides on La_2O_3 Catalysts in Oxidative Coupling of Methane, J. Phys. Chem. C, 118 (2014) 27954-27960.
[114] Y. Lei, C. Chu, S. Li, Y. Sun, Methane Activations by Lanthanum Oxide Clusters, J. Phys. Chem. C, 118 (2014) 7932-7945.
[115] D. Wolf, M. Slinko, E. Kurkina, Baerns, Kinetic simulations of surface processes of the oxidative coupling of methane over a basic oxide catalyst, Appl. Catal. A, 166 (1998) 47-54.
[116] E.V. Kondratenko, D. Wolf, M. Baerns, Influence of electronic properties of Na_2O/CaO catalysts on their catalytic characteristics for the oxidative coupling of methane, Catal. Lett., 58 (1999) 217-223.
[117] E.V. Kondratenko, O.V. Buyevskaya, M. Soick, M. Baerns, Transient kinetics and mechanism of oxygen adsorption over oxide catalysts from the TAP-reactor system, Catal. Lett., 63 (1999) 153-159.
[118] E.V. Kondratenko, O. Buyevskaya, M. Baerns, Mechanistic insights in the activation of oxygen on oxide catalysts for the oxidative dehydrogenation of ethane from pulse experiments and contact potential difference measurements, J. Mol. Catal. A, 158 (2000) 199-208.
[119] E. Kondratenko, N. Maksimov, G. Selyutin, A. Anshits, Oxidative coupling of methane over oxides of alkali earth metals using N_2O as oxidant, Catal. Today, 24 (1995) 273-275.
[120] H. Yamamoto, H.Y. Chu, M.T. Xu, C.L. Shi, J.H. Lunsford, Oxidative Coupling of Methane over a Li^+/MgO Catalyst Using N_2O as an Oxidant, J. Catal., 142 (1993) 325-336.
[121] G.J. Hutchings, M.S. Scurrell, J.R. Woodhouse, Partial oxidation of methane over samarium and lanthanum oxides: a study of the reaction mechanism, Catal. Today, 4 (1989) 371-381.
[122] H. Özdemir, M.A.F. Öksüzömer, M. Ali Gürkaynak, Studies on oxidative coupling of methane using Sm_2O_3-based catalysts, Chem. Eng. Commun., 206 (2019) 48-60.

[123] K. Langfeld, B. Frank, V.E. Strempel, C. Berger-Karin, G. Weinberg, E.V. Kondratenko, R. Schomäcker, Comparison of oxidizing agents for the oxidative coupling of methane over state-of-the-art catalysts, Appl. Catal. A, 417-418 (2012) 145-152.
[124] A.M. Arinaga, M.C. Ziegelski, T.J. Marks, Alternative Oxidants for the Catalytic Oxidative Coupling of Methane, Angew. Chem., Int. Ed., 60 (2021) 10502-10515.
[125] A.G. Anshits, E.V. Kondratenko, E.N. Voskresenskaya, L.I. Kurteeva, N.I. Pavlenko, The influence of O_2 on oxidative coupling of methane over oxide catalysts using N_2O as oxidant, Catal. Today, 46 (1998) 211-216.
[126] J.R. Anderson, Y.F. Chang, K.C. Pratt, K. Foger, Reaction of methane and sulfur: Oxidative coupling and carbon disulfide formation, React. Kinet. Catal. Lett., 49 (1993) 261-269.
[127] X. Fang, S. Li, J. Lin, Y. Chu, Oxidative coupling of methane on W-Mn catalysts, J. Mol. Catal, 6 (1992) 427-433.
[128] X. Fang, S. Li, J. Gu, D. Yang, Preparation and characterization of W-Mn catalyst for oxidative coupling of methane, J. Mol. Catal, 6 (1992) 255-261.
[129] S. Arndt, T. Otremba, U. Simon, M. Yildiz, H. Schubert, R. Schomäcker, Mn–Na_2WO_4/SiO_2 as catalyst for the oxidative coupling of methane. What is really known?, Appl. Catal. A, 425-426 (2012) 53-61.
[130] D. Kiani, S. Sourav, J. Baltrusaitis, I.E. Wachs, Oxidative Coupling of Methane (OCM) by SiO_2-Supported Tungsten Oxide Catalysts Promoted with Mn and Na, ACS Catal., 9 (2019) 5912-5928.
[131] H. Liu, X. Wang, D. Yang, R. Gao, Z. Wang, J. Yang, Scale up and stability test for oxidative coupling of methane over Na_2WO_4-Mn/SiO_2 catalyst in a 200 ml fixed-bed reactor, J. Nat. Gas Chem., 17 (2008) 59-63.
[132] S.B. Li, Oxidative Coupling of Methane over W-Mn/SiO_2 Catalyst, Chinese Journal of Chemistry, 19 (2001) 16-21.
[133] J. Wang, L. Chou, B. Zhang, H. Song, J. Zhao, J. Yang, S. Li, Comparative study on oxidation of methane to ethane and ethylene over Na_2WO_4–Mn/SiO_2 catalysts prepared by different methods, J. Mol. Catal. A, 245 (2006) 272-277.
[134] S.-f. Ji, T.-c. Xiao, S.-b. Li, C.-z. Xu, R.-l. Hou, K.S. Coleman, M.L.H. Green, The relationship between the structure and the performance of Na-W-Mn/SiO_2 catalysts for the oxidative coupling of methane, Appl. Catal. A, 225 (2002) 271-284.
[135] S. Hou, Y. Cao, W. Xiong, H. Liu, Y. Kou, Site Requirements for the Oxidative Coupling of Methane on SiO_2-Supported Mn Catalysts, Ind. Eng. Chem. Res., 45 (2006) 7077-7083.
[136] A. Malekzadeh, A.K. Dalai, A. Khodadadi, Y. Mortazavi, Structural features of Na_2WO_4–MO_x/SiO_2 catalysts in oxidative coupling of methane reaction, Catal.Commun., 9 (2008) 960-965.
[137] Y. Gordienko, T. Usmanov, V. Bychkov, V. Lomonosov, Z. Fattakhova, Y. Tulenin, D. Shashkin, M. Sinev, Oxygen availability and catalytic performance of NaWMn/SiO_2 mixed oxide and its components in oxidative coupling of methane, Catal. Today, 278 (2016) 127-134.
[138] U. Simon, O. Görke, A. Berthold, S. Arndt, R. Schomäcker, H. Schubert, Fluidized bed processing of sodium tungsten manganese catalysts for the oxidative coupling of methane, Chem. Eng. J., 168 (2011) 1352-1359.
[139] A. Vamvakeros, S. Jacques, V. Middelkoop, M. Di Michiel, C. Egan, I. Ismagilov, G. Vaughan, F. Gallucci, M. van Sint Annaland, P. Shearing, Real time chemical imaging of a working catalytic membrane reactor during oxidative coupling of methane, Chem.Commun., 51 (2015) 12752-12755.
[140] M.J. Werny, Y. Wang, F. Girgsdies, R. Schlögl, A. Trunschke, Fluctuating Storage of the Active Phase in a Mn-Na_2WO_4/SiO_2 Catalyst for the Oxidative Coupling of Methane, Angew. Chem., Int. Ed., 59 (2020) 14921-14926.

[141] D. Matras, A. Vamvakeros, S.D.M. Jacques, N. Grosjean, B. Rollins, S. Poulston, G.B.G. Stenning, H.R. Godini, J. Drnec, R.J. Cernik, A.M. Beale, Effect of thermal treatment on the stability of Na–Mn–W/SiO_2 catalyst for the oxidative coupling of methane, Faraday Discuss., 229 (2021) 176-196.
[142] C.A. Ortiz-Bravo, S.J. Figueroa, R. Portela, C.A. Chagas, M.A. Bañares, F.S. Toniolo, Elucidating the structure of the W and Mn sites on the Mn-Na_2WO_4/SiO_2 catalyst for the oxidative coupling of methane (OCM) at real reaction temperatures, J. Catal., 408 (2022) 423-435.
[143] A. Vamvakeros, D. Matras, S.D. Jacques, M. di Michiel, S.W. Price, P. Senecal, M.A. Aran, V. Middelkoop, G.B. Stenning, J.F.W. Mosselmans, Real-time multi-length scale chemical tomography of fixed bed reactors during the oxidative coupling of methane reaction, J. Catal., 386 (2020) 39-52.
[144] D. Kiani, S. Sourav, I.E. Wachs, J. Baltrusaitis, Synthesis and molecular structure of model silica-supported tungsten oxide catalysts for oxidative coupling of methane (OCM), Catal. Sci. Tech., 10 (2020) 3334-3345.
[145] S. Sadjadi, S. Jašo, H. Godini, S. Arndt, M. Wollgarten, R. Blume, O. Görke, R. Schomäcker, G. Wozny, U. Simon, Feasibility study of the Mn–Na_2WO_4/SiO_2 catalytic system for the oxidative coupling of methane in a fluidized-bed reactor, Catal. Sci. Tech., 5 (2015) 942-952.
[146] A. Palermo, J.P. Holgado Vazquez, A.F. Lee, M.S. Tikhov, R.M. Lambert, Critical influence of the amorphous silica-to-cristobalite phase transition on the performance of Mn/Na_2WO_4/SiO_2 catalysts for the oxidative coupling of methane, J. Catal., 177 (1998) 259-266.
[147] M. Yildiz, Y. Aksu, U. Simon, K. Kailasam, O. Goerke, F. Rosowski, R. Schomäcker, A. Thomas, S. Arndt, Enhanced catalytic performance of Mn_xO_y–Na_2WO_4/SiO_2 for the oxidative coupling of methane using an ordered mesoporous silica support, Chem.Commun., 50 (2014) 14440-14442.
[148] N.S. Hayek, N.S. Lucas, C. Warwar Damouny, O.M. Gazit, Critical Surface Parameters for the Oxidative Coupling of Methane over the Mn–Na–W/SiO_2 Catalyst, ACS Appl. Mat. Interf., 9 (2017) 40404-40411.
[149] M. Yildiz, U. Simon, T. Otremba, Y. Aksu, K. Kailasam, A. Thomas, R. Schomäcker, S. Arndt, Support material variation for the Mn_xO_y-Na_2WO_4/SiO_2 catalyst, Catal. Today, 228 (2014) 5-14.
[150] K. Takanabe, A.M. Khan, Y. Tang, L. Nguyen, A. Ziani, B.W. Jacobs, A.M. Elbaz, S.M. Sarathy, F. Tao, Integrated In Situ Characterization of a Molten Salt Catalyst Surface: Evidence of Sodium Peroxide and Hydroxyl Radical Formation, Angew. Chem., Int. Ed., 56 (2017) 10403-10407.
[151] D. Li, S. Yoshida, B. Siritanaratkul, A.T. Garcia-Esparza, D. Sokaras, H. Ogasawara, K. Takanabe, Transient Potassium Peroxide Species in Highly Selective Oxidative Coupling of Methane over an Unmolten K_2WO_4/SiO_2 Catalyst Revealed by In Situ Characterization, ACS Catal., 11 (2021) 14237-14248.
[152] L.C. Anderson, M. Xu, C.E. Mooney, M.P. Rosynek, J.H. Lunsford, Hydroxyl radical formation during the reaction of oxygen with methane or water over basic lanthanide oxide catalysts, J. Am. Chem. Soc., 115 (1993) 6322-6326.
[153] K.B. Hewett, L.C. Anderson, M.P. Rosynek, J.H. Lunsford, Formation of hydroxyl radicals from the reaction of water and oxygen over basic metal oxides, J. Am. Chem. Soc., 118 (1996) 6992-6997.
[154] K.B. Hewett, M.P. Rosynek, J.H. Lunsford, Effect of CH_4 and CO_2 on the catalytic formation of OH· radicals over La_2O_3, Catal. Lett., 45 (1997) 125-128.
[155] V. Lomonosov, Y. Gordienko, M. Sinev, Effect of Water on Methane and Ethane Oxidation in the Conditions of Oxidative Coupling of Methane Over Model Catalysts, Topics Catal., 56 (2013) 1858-1866.
[156] Z. Aydin, V.A. Kondratenko, H. Lund, S. Bartling, C.R. Kreyenschulte, D. Linke, E.V. Kondratenko, Revisiting Activity- and Selectivity-Enhancing Effects of Water in the Oxidative Coupling of Methane over MnO_x-Na_2WO_4/SiO_2 and Proving for Other Materials, ACS Catal., 10 (2020) 8751-8764.

[157] Z.C. Jiang, C.J. Yu, X.P. Fang, S.B. Li, H.L. Wang, Oxide/support interaction and surface reconstruction in the sodium tungstate(Na_2WO_4)/silica system, The Journal of Physical Chemistry, 97 (1993) 12870-12875.
[158] J. Wu, S. Li, The Role of Distorted WO_4 in the Oxidative Coupling of Methane on Supported Tungsten Oxide Catalysts, The Journal of Physical Chemistry, 99 (1995) 4566-4568.
[159] J. Wu, S. Li, J. Niu, X. Fang, Mechanistic study of oxidative coupling of methane over Mn_2O_3・$Na_2WO_4SiO_2$ catalyst, Appl. Catal. A, 124 (1995) 9-18.
[160] Z.-C. Jiang, H. Gong, S.-b. Li, Methane activation over Mn_2O_3-Na_2WO_4/SiO_2 catalyst and oxygen spillover, Stud. Surf. Sci. Catal., Elsevier, 1997, pp. 481-490.
[161] B. Beck, V. Fleischer, S. Arndt, M.G. Hevia, A. Urakawa, P. Hugo, R. Schomäcker, Oxidative coupling of methane—A complex surface/gas phase mechanism with strong impact on the reaction engineering, Catal. Today, 228 (2014) 212-218.
[162] V. Fleischer, R. Steuer, S. Parishan, R. Schomäcker, Investigation of the surface reaction network of the oxidative coupling of methane over $Na_2WO_4/Mn/SiO_2$ catalyst by temperature programmed and dynamic experiments, J. Catal., 341 (2016) 91-103.
[163] J. Si, G. Zhao, W. Sun, J. Liu, C. Guan, Y. Yang, X.-R. Shi, Y. Lu, Oxidative Coupling of Methane: Examining the Inactivity of the MnO_x-Na_2WO_4/SiO_2 Catalyst at Low Temperature, Angew. Chem., Int. Ed., 61 (2022) e202117201.
[164] D. Kiani, S. Sourav, J. Baltrusaitis, I.E. Wachs, Elucidating the Effects of Mn Promotion on SiO_2-Supported Na-Promoted Tungsten Oxide Catalysts for Oxidative Coupling of Methane (OCM), ACS Catal., 11 (2021) 10131-10137.
[165] S. Sourav, Y. Wang, D. Kiani, J. Baltrusaitis, R.R. Fushimi, I.E. Wachs, New Mechanistic and Reaction Pathway Insights for Oxidative Coupling of Methane (OCM) over Supported Na_2WO_4/SiO_2 Catalysts, Angew. Chem., Int. Ed., 60 (2021) 21502-21511.
[166] S. Sourav, Y. Wang, D. Kiani, J. Baltrusaitis, R.R. Fushimi, I.E. Wachs, Resolving the Types and Origin of Active Oxygen Species Present in Supported Mn-Na_2WO_4/SiO_2 Catalysts for Oxidative Coupling of Methane, ACS Catal., 11 (2021) 10288-10293.
[167] S. Sourav, D. Kiani, Y. Wang, J. Baltrusaitis, R.R. Fushimi, I.E. Wachs, Molecular structure and catalytic promotional effect of Mn on supported Na_2WO_4/SiO_2 catalysts for oxidative coupling of methane (OCM) reaction, Catal. Today, (2022) https://doi.org/10.1016/j.cattod.2022.1007.1005.
[168] K. Klier, J. Nováková, P. Jíru, Exchange reactions of oxygen between oxygen molecules and solid oxides, J. Catal., 2 (1963) 479-484.
[169] G.K. Boreskov, The Catalysis of Isotopic Exchange in Molecular Oxygen, in: D.D. Eley, H. Pines, P.B. Weisz (Eds.) Adv. Catal., Academic Press, 1965, pp. 285-339.
[170] E. Winter, Exchange reactions of oxides. Part IX, Journal of the Chemical Society A: Inorganic, Physical, Theoretical, (1968) 2889-2902.
[171] S.L. Shannon, J.G. Goodwin, Jr., Characterization of Catalytic Surfaces by Isotopic-Transient Kinetics during Steady-State Reaction, Chem. Rev., 95 (1995) 677-695.
[172] C. Ledesma, J. Yang, D. Chen, A. Holmen, Recent Approaches in Mechanistic and Kinetic Studies of Catalytic Reactions Using SSITKA Technique, ACS Catal., 4 (2014) 4527-4547.
[173] N.W. Cant, C.A. Lukey, P.F. Nelson, R.J. Tyler, The rate controlling step in the oxidative coupling of methane over a lithium-promoted magnesium oxide catalyst, J. Chem. Soc., Chem. Commun., (1988) 766-768.
[174] C. Shi, M. Xu, M.P. Rosynek, J.H. Lunsford, Origin of kinetic isotope effects during the oxidative coupling of methane over a lithium (1+)/magnesia catalyst, The Journal of Physical Chemistry, 97 (1993) 216-222.

7. Publications

7.1. Effects of N_2O and Water on Activity and Selectivity in the Oxidative Coupling of Methane over Mn−Na_2WO_4/SiO_2: Role of Oxygen Species

Zeynep Aydin[1,#], Anna Zanina[1,#], Vita A. Kondratenko[1], Jabor Rabeah[1], Jianshu Li[2], Juan Chen[2], Yuming Li[2], Guiyuan Jiang[2,*], Henrik Lund[1], Stephan Bartling[1], David Linke[1], Evgenii V. Kondratenko[1,*]

[#]These authors contributed equally.

[1]Leibniz Institut für Katalyse e.V., Albert-Einstein-Str. 29a, 18059 Rostock, Germany

[2]State Key Laboratory of Heavy Oil Processing, China University of Petroleum Beijing, Beijing 102249, People's Republic of China

ACS Catalysis, 2022, 12, 1298-1309

© 2022 American Chemical Society

Cite this: https://doi.org/10.1021/acscatal.1c04915

Author contribution:

In this paper as second co-author with equal contribution with the first authors, I performed and evaluated O_2-TPD, oxygen isotopic exchange and in situ/operando UV-vis measurements and co-wrote the corresponding parts of the manuscript. My contribution is approximately 30%.

7.2. The Role of Adsorbed and Lattice Oxygen Species in Product Formation in the Oxidative Coupling of Methane over M_2WO_4/SiO_2 (M=Na, K, Rb, Cs)

Anna Zanina[1], Vita A. Kondratenko[1], Henrik Lund[1], Jianshu Li[2], Juan Chen[2], Yuming Li[2], Guiyuan Jiang[2,*], Evgenii V. Kondratenko[1,*]

[1]Leibniz-Institut für Katalyse e.V., Albert-Einstein-Str. 29a, 18059 Rostock, Germany

[2]State Key Laboratory of Heavy Oil Processing, China University of Petroleum Beijing, Beijing 102249, People's Republic of China

ACS Catalysis, 2022, 12, 15361-15372
© 2022 American Chemical Society
Cite this: https://doi.org/10.1021/acscatal.2c04916

Author contribution:

In this paper as the first author, I prepared the catalysts for catalytic tests and for in situ XRD measurements, conducted catalytic tests and CH_4 pulse experiments in fixed-bed reactors, performed in situ UV-vis spectroscopic, O_2-TPD, and oxygen isotopic exchange tests as well as evaluated all tests and wrote the first draft and co-edited the paper. My contribution as the first author is approximately 60%.

7.3. Performance-defining factors of (MnO_x)-M_2WO_4/SiO_2 (M=Na, K, Rb, or Cs) catalysts in oxidative coupling of methane

Anna Zanina[1], Vita A. Kondratenko[1], Henrik Lund[1], Jianshu Li[2], Juan Chen[2], Yuming Li[2], Guiyuan Jiang[2,*], Evgenii V. Kondratenko[1,*]

[1]Leibniz Institut für Katalyse e.V., Albert-Einstein-Str. 29a, 18059 Rostock, Germany

[2]State Key Laboratory of Heavy Oil Processing, China University of Petroleum Beijing, Beijing 102249, People's Republic of China

Journal of Catalysis, 2023, 419, 68-79.

© 2023 Elsevier Inc.

Cite this: https://doi.org/10.1016/j.jcat.2023.02.004

Author contribution:

In this paper as the first author, I prepared the catalysts, performed O_2-TPD and oxygen isotopic exchange tests, conducted pulse and continuous-flow OCM experiments, carried out in situ UV-vis, SSITKA experiments, collected and analyzed the data, wrote the first draft and co-edited the final manuscript. My contribution as the first author is approximately 60%.

ACS Catalysis

pubs.acs.org/acscatalysis Research Article

Effects of N_2O and Water on Activity and Selectivity in the Oxidative Coupling of Methane over Mn−Na_2WO_4/SiO_2: Role of Oxygen Species

Zeynep Aydin,[§] Anna Zanina,[§] Vita A. Kondratenko, Jabor Rabeah, Jianshu Li, Juan Chen, Yuming Li, Guiyuan Jiang,* Henrik Lund, Stephan Bartling, David Linke, and Evgenii V. Kondratenko*

Cite This: *ACS Catal.* 2022, 12, 1298−1309 Read Online

ACCESS | Metrics & More | Article Recommendations | Supporting Information

ABSTRACT: The understanding of the reaction mechanism of product formation in the oxidative coupling of methane (OCM) is the prerequisite for designing catalysts with improved selectivity to the desired products, i.e., C_2H_6 and C_2H_4 (C_2 hydrocarbons). One step in this direction is to understand the kind of oxygen species involved in the selective and nonselective reactions. Against this background, a series of kinetic and mechanistic tests of the OCM reaction with N_2O (N_2O−OCM) were carried out over the Mn−Na_2WO_4/SiO_2 system in the absence and the presence of cofed water. The usage of N_2O instead of O_2 was proven to suppress the direct oxidation of CH_4 to CO_2 in favor of the formation of C_2 hydrocarbons. This inhibition was explained by a lower concentration of surface biatomic oxygen species participating in the formation of CO_2. The formation of such species from O_2 was supported by oxygen isotopic exchange and electron paramagnetic resonance (EPR) tests. As proven by in situ UV−vis tests under various reaction conditions at 750 °C, N_2O−OCM and O_2−OCM mainly proceed through a Mars van Krevelen sequence. As MnO_x is reduced faster than Na_2WO_4, it should be primarily involved in oxidant activation. In comparison with O_2, N_2O was proven to reoxidize reduced catalysts significantly slower. This results in reducing surface density (spatial separation) of lattice oxygen species in N_2O−OCM that is unfavorable for the undesired oxidation reactions leading to carbon oxides. As a result, the selectivity to C_2 hydrocarbons increases. This knowledge is essential for catalyst design through controlling the rates of generation and consumption of oxygen species. A further aspect of this work is the positive effect of H_2O on the rate of methane conversion and the selectivity to C_2 hydrocarbons in N_2O−OCM. The strength of this effect on the activity is lower than in O_2−OCM. The enhancing effect was related to H_2O-mediated transformation of surface biatomic oxygen species into monatomic ones.

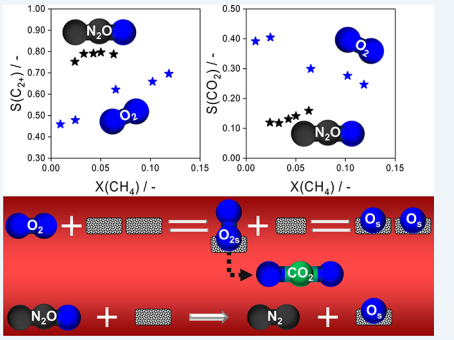

KEYWORDS: *oxidative coupling of methane, N_2O, surface oxygen species, water effect, Mn−Na_2WO_4/SiO_2, MnO_x/SiO_2, Na_2WO_4/SiO_2, C_2 selectivity*

Downloaded via LEIBNIZ INST FOR CATALYSIS (LIKAT) on March 6, 2023 at 08:57:38 (UTC).
See https://pubs.acs.org/sharingguidelines for options on how to legitimately share published articles.

■ INTRODUCTION

The oxidative coupling of methane (OCM) to C_2H_6 and C_2H_4 (C_2 hydrocarbons) is one of the mostly investigated routes of methane valorization.[1−4] It offers the opportunity to utilize the enormous resources of methane from natural gas, renewable biogas, or methane clathrates for the direct production of ethylene that is the most vital building block in the chemical industry.[5−8] This reaction is, however, still not commercialized. The main challenge is to suppress the oxidation of highly reactive C_2 hydrocarbons to carbon oxides at industrially relevant degrees of methane conversion.

The supported Mn−Na_2WO_4/SiO_2 catalyst is one of the most promising candidates for this reaction.[9,10] It shows high activity and long-term stability. Importantly, the selectivity to C_2 hydrocarbons can be enhanced when performing the OCM reaction with cofed water.[11−13] Very recently, we have demonstrated that the selectivity over other catalysts can also be enhanced through cofed water.[14,15] Our mechanistic and kinetic analysis suggests that the improvement should be due to H_2O-assisted decomposition of surface biatomic oxygen species responsible for CO_2 formation.

Resolving the kind and role of surface oxygen species in the OCM reaction over Mn−Na_2WO_4/SiO_2 is an important topic of the ongoing research, because such knowledge may help to improve the catalyst performance.[16−21] For example, Schomäcker and co-workers have analyzed the types of oxygen species by means of temporal analysis of products (TAP) and

Received: October 26, 2021
Revised: December 10, 2021
Published: January 7, 2022

ACS Publications © 2022 American Chemical Society

https://doi.org/10.1021/acscatal.1c04915
ACS Catal. 2022, 12, 1298−1309

Supporting Information

Effects of N_2O and Water on Activity and Selectivity in the Oxidative Coupling of Methane over Mn-Na_2WO_4/SiO_2: Role of Oxygen Species

Zeynep Aydin[1,#], Anna Zanina[1,#], Vita A. Kondratenko[1], Jabor Rabeah[1], Jianshu Li[2], Juan Chen[2], Yuming Li[2], Guiyuan Jiang[2,*], Henrik Lund[1], Stephan Bartling[1], David Linke[1], Evgenii V. Kondratenko[1,*]

[1]Leibniz Institut für Katalyse e.V., Albert-Einstein-Str. 29a, 18059 Rostock, Germany

[2]State Key Laboratory of Heavy Oil Processing, China University of Petroleum Beijing, Beijing 102249, People's Republic of China

*To whom correspondence should be addressed: evgenii.kondratenko@catalysis.de (EVK, primary corresponding author), jianggy@cup.edu.cn (Guiyuan Jiang)

# These authors contributed equally.

Table of content

Figure S1. Setup for the catalytic tests and in situ UV-vis tests.

Figure S2. Determination of the methane conversion rate $r(CH_4)$ from the correlation between the methane conversion $X(CH_4)$ and the contact time τ.

Figure S3. XRD patterns of Mn-Na_2WO_4/SiO_2 before OCM reaction, after O_2-OCM or N_2O-OCM without H_2O or with H_2O.

Figure S4. The selectivity to C_{2+}-hydrocarbons, C_2H_6, C_2H_4, CO_2 and CO as function of methane conversion over Mn-Na_2WO_4/SiO_2 at 775, 800 and 825 °C without and with 30 vol% H_2O in the N_2O-OCM reaction.

Figure S4. The selectivity to C_{2+}-hydrocarbons, C_2H_6, C_2H_4, CO_2 and CO as function of methane conversion over Mn-Na_2WO_4/SiO_2 at 775, 800 and 825 °C without (empty symbols) and with 30 vol% (black symbols) H_2O in the N_2O-OCM reaction. The contact time was varied between 0.09 and 1.3 $g_{cat}\cdot min\cdot mmol^{-1}_{CH4}$.

Figure S5. The selectivity to C_{2+}, C_2H_6, C_2H_4, CO_2 and CO as function of methane conversion over Mn-Na_2WO_4/SiO_2 at 750, 775, 800 and 825 °C without and with 30 vol% H_2O in the O_2-OCM reaction.

Figure S6. The ratio of the rates of methane conversion into C_2-hydrocarbons, CO_2 and CO in O_2-OCM with 30 vol% H_2O to those without H_2O.

Figure S7. Transient response of O_2 detected after pulsing CH_4 over MnO_x/SiO_2, Na_2WO_4/SiO_2 or Mn-Na_2WO_4/SiO_2 at 850 °C.

Figure S8. Oxygen desorption from Mn-Na_2WO_4/SiO_2, MnO_x/SiO_2, Na_2WO_4/SiO_2 in O_2-TPD tests as a function of time or temperature.

Figure S9. EPR spectrum of DMPO-O_2^- detected after adding a mixture of DMPO in cyclohexane to the Na_2WO_4/SiO_2 catalyst exposed to about $4 \cdot 10^{-5}$ mol O_2 at 20°C after reduction in vacuum at 700 °C for 1h.

Figure S10. In situ UV-vis spectra of oxidized and reduced MnO_x/SiO_2, Na_2WO_4/SiO_2 and Mn-Na_2WO_4/SiO_2 at 750 °C.

Figure S11. In situ UV-vis spectra of oxidized MnO_x/SiO_2, Na_2WO_4/SiO_2 and Mn-Na_2WO_4/SiO_2 and after O_2-OCM (CH_4:O_2:N_2 = 40:5:55) or N_2O-OCM (CH_4:N_2O:N_2 = 40:10:50) at 750 °C.

Figure S12. C_2-Selectivity and the ratio of rates of methane conversion to CO_2 to those to CO as function of $p(CH_4)/p(O_2)$ over Mn-Na_2WO_4/SiO_2 at 750, 775 and 800 °C.

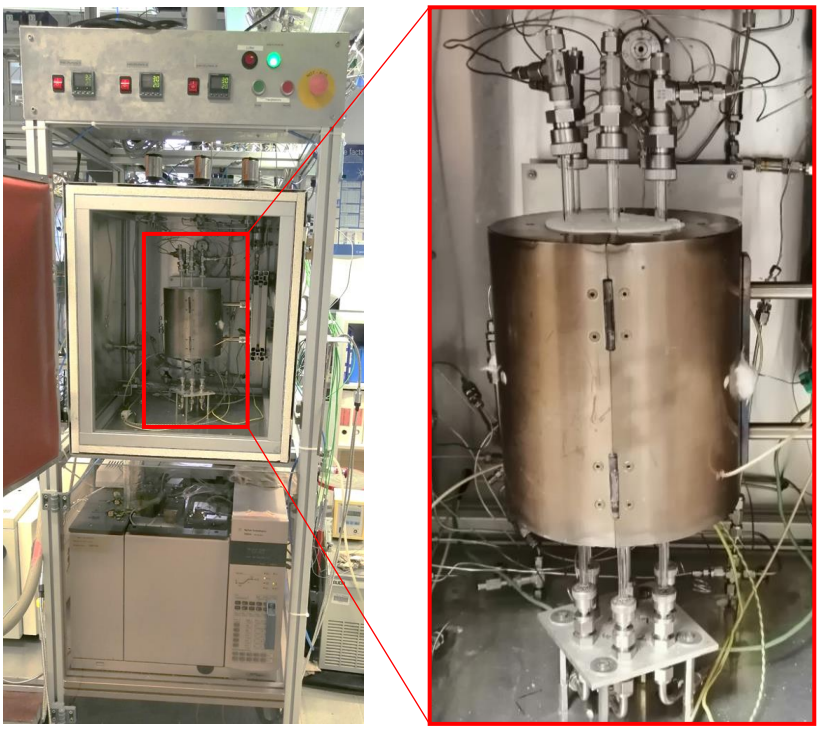

Figure S1. Photos of setup used for catalytic and in situ UV-vis tests.

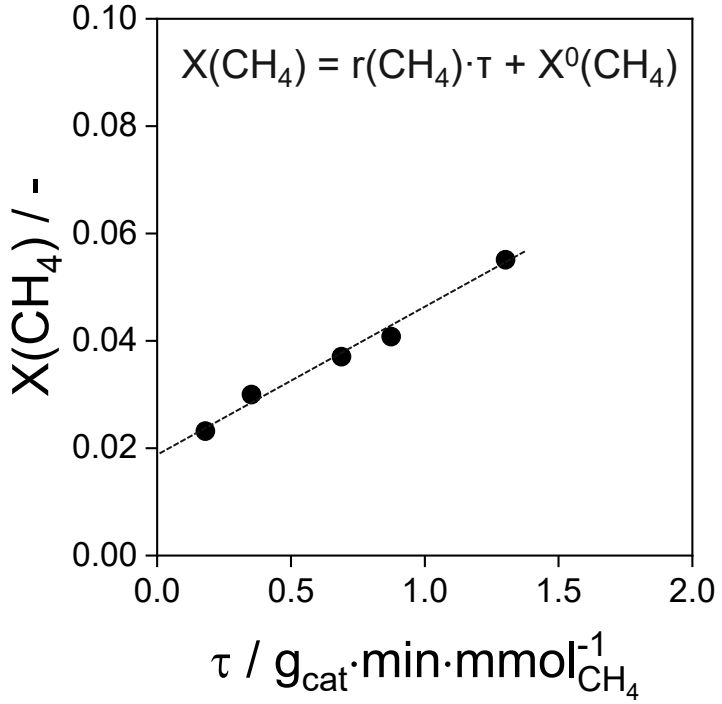

Figure S2. Determination of the methane conversion rate $r(CH_4)$ from the correlation between the methane conversion $X(CH_4)$ and the contact time τ.

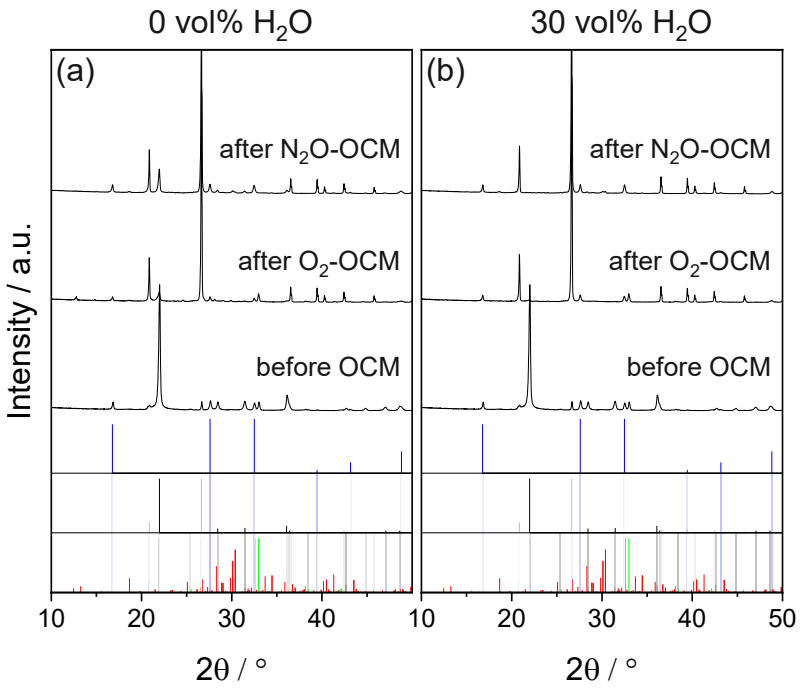

Figure S3. XRD patterns of Mn-Na_2WO_4/SiO_2 before OCM reaction, after O_2-OCM or N_2O-OCM (a) without H_2O or (b) with H_2O. Na_2WO_4 (blue bars) (PDF-No. 01-070-1040), $Mn_7O_8(SiO_4)$ (green bars) (PDF-No. 01-089-5662), $MnSiO_3$ (red bars) (PDF-No. 01-076-0627), hexagonal SiO_2 (grey bars) (PDF-No. 00-033-1161), tetragonal SiO_2 (black bars) (PDF-No. 00-039-1425).

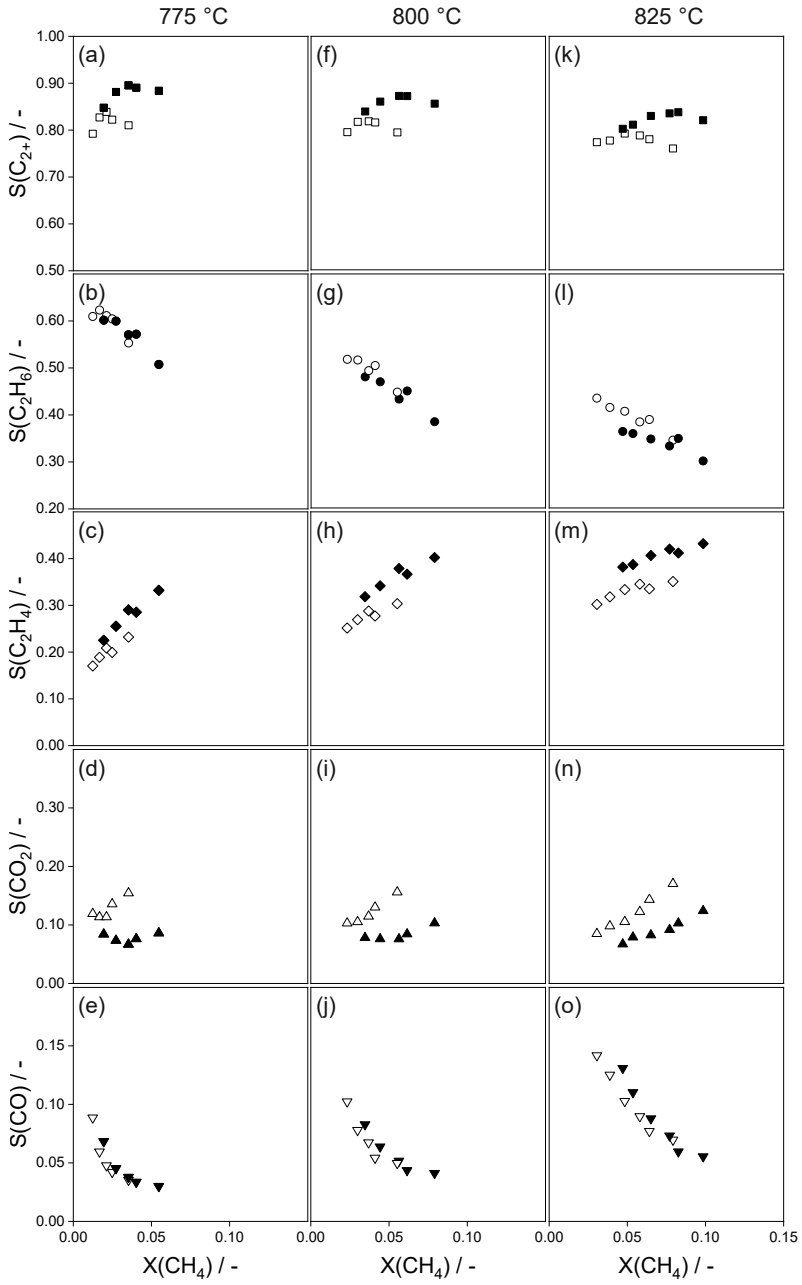

Figure S4. The selectivity to C_{2+}-hydrocarbons, C_2H_6, C_2H_4, CO_2 and CO as function of methane conversion over Mn-Na_2WO_4/SiO_2 at 775, 800 and 825 °C without (empty symbols) and with 30 vol% (black symbols) H_2O in the N_2O-OCM reaction. The contact time was varied between 0.09 and 1.3 $g_{cat}\cdot min\cdot mmol^{-1}_{CH4}$.

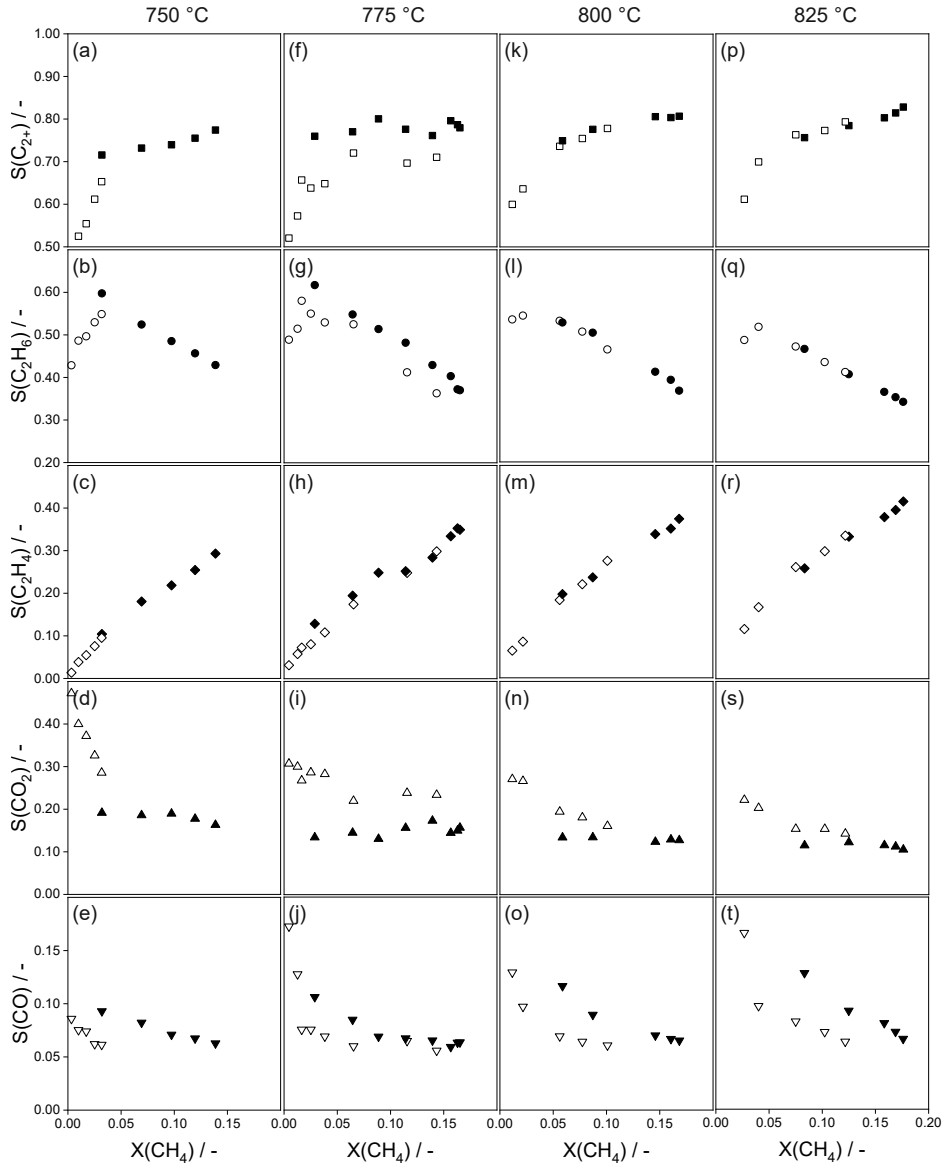

Figure S5. The selectivity to C_{2+}-hydrocarbons, C_2H_6, C_2H_4, CO_2 and CO as function of methane conversion over Mn-Na_2WO_4/SiO_2 at 750, 775, 800 and 825 °C without (empty symbols) and with 30 vol% (black symbols) H_2O in the O_2-OCM reaction. The contact time was varied between 0.013 – 0.47 $g_{cat}\cdot min\cdot mmol^{-1}_{CH4}$.

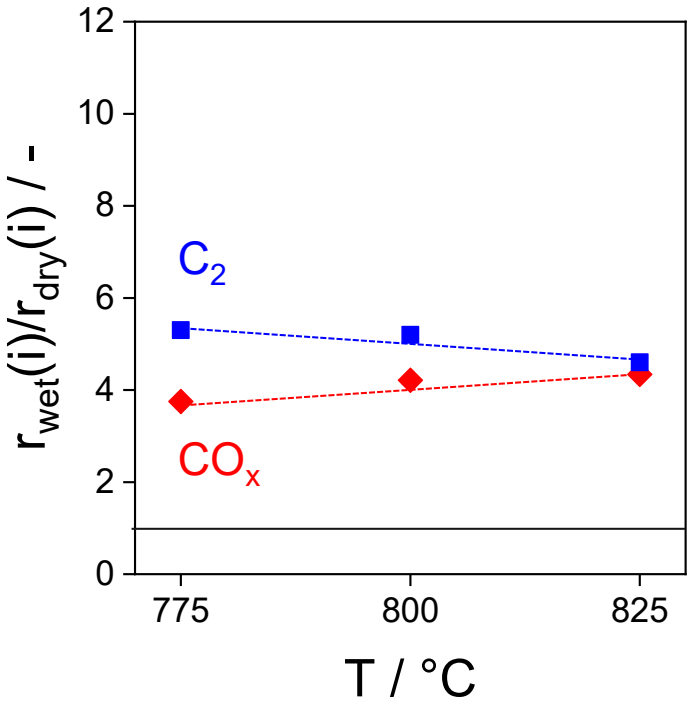

Figure S6. The ratio of the rates ($r_{wet}(i)/r(_{dry}(i))$ of methane conversion into C_2-hydrocarbons (■) and CO_x (◆) in O_2-OCM with 30 vol% H_2O to those without co-fed H_2O. $X(CH_4) = 0.05$.

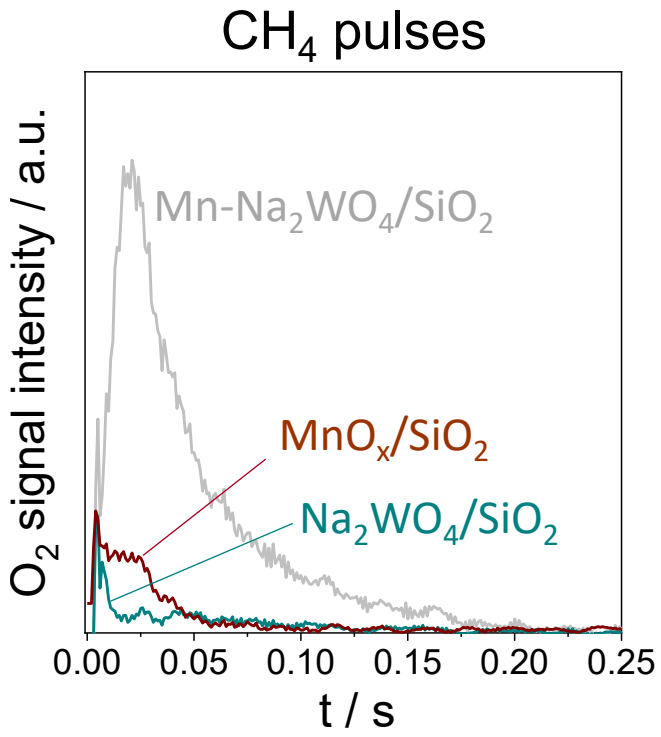

Figure S7. Transient response of O_2 detected after pulsing of CH_4 over MnO_x/SiO_2, Na_2WO_4/SiO_2 or Mn-Na_2WO_4/SiO_2 at 850 °C.

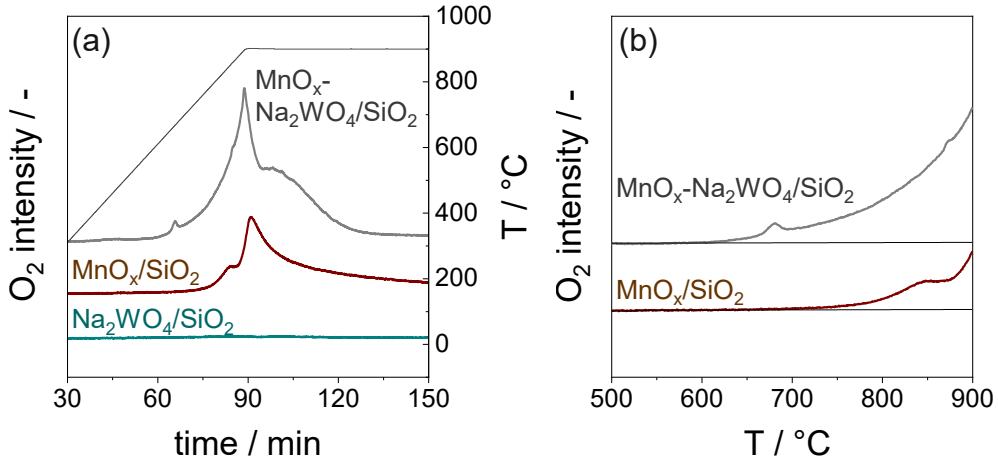

Figure S8. Oxygen desorption from Mn-Na_2WO_4/SiO_2, MnO_x/SiO_2, Na_2WO_4/SiO_2 in O_2-TPD tests as a function of (a) time or (b) temperature.

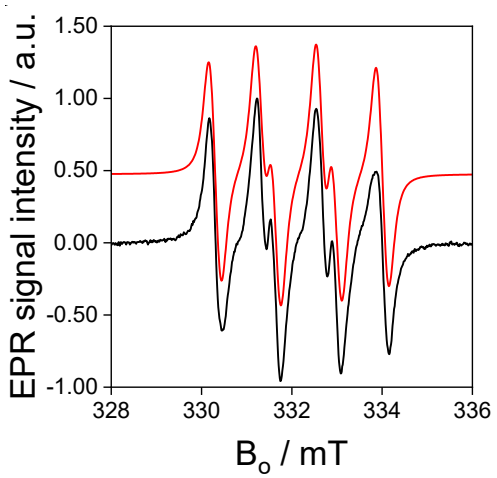

Figure S9. EPR spectrum of DMPO-O_2^- (black line) detected after adding a mixture of DMPO in cyclohexane to the Na_2WO_4/SiO_2 catalyst exposed to about $4 \cdot 10^{-5}$ mol O_2 at 20°C after reduction in vacuum at 700 °C for 1h. Black and red lines stand for experimental and simulated spectra, respectively. The experimental spectrum shows the characteristic signal of the DMPO-O_2^- at g factor of 2.007 with a hyperfine coupling constant a_N = 1.35, a_H^β = 1.04 G, a_H^γ = 0.11 mT as reported in Ref.[1] The simulated spectrum was obtained using easy spin program.[2]

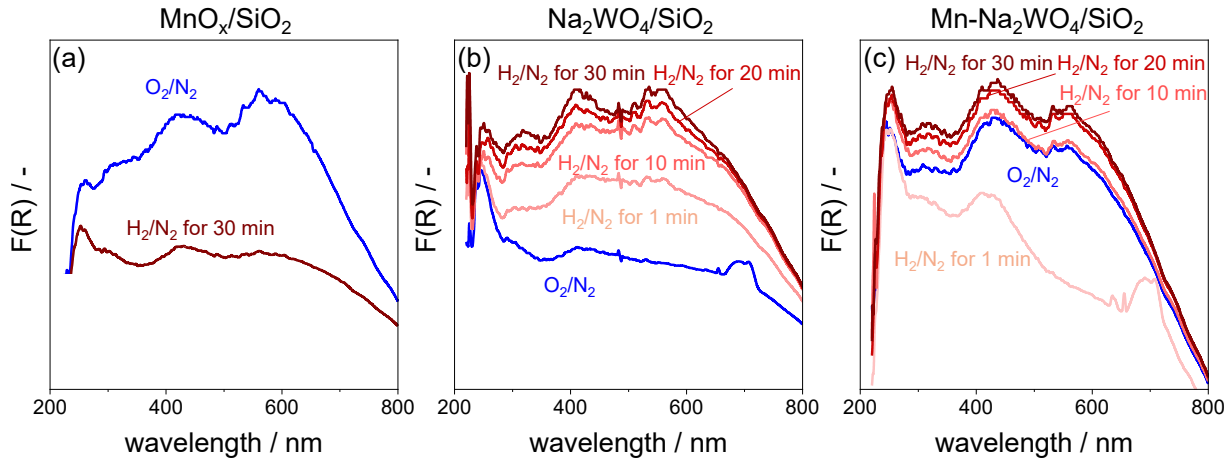

Figure S10. In situ UV-vis spectra of oxidized (O_2/N_2=20/80) and reduced (H_2/N_2=40/60) (a) MnO_x/SiO_2, (b) Na_2WO_4/SiO_2 and (c) Mn-Na_2WO_4/SiO_2 at 750 °C.

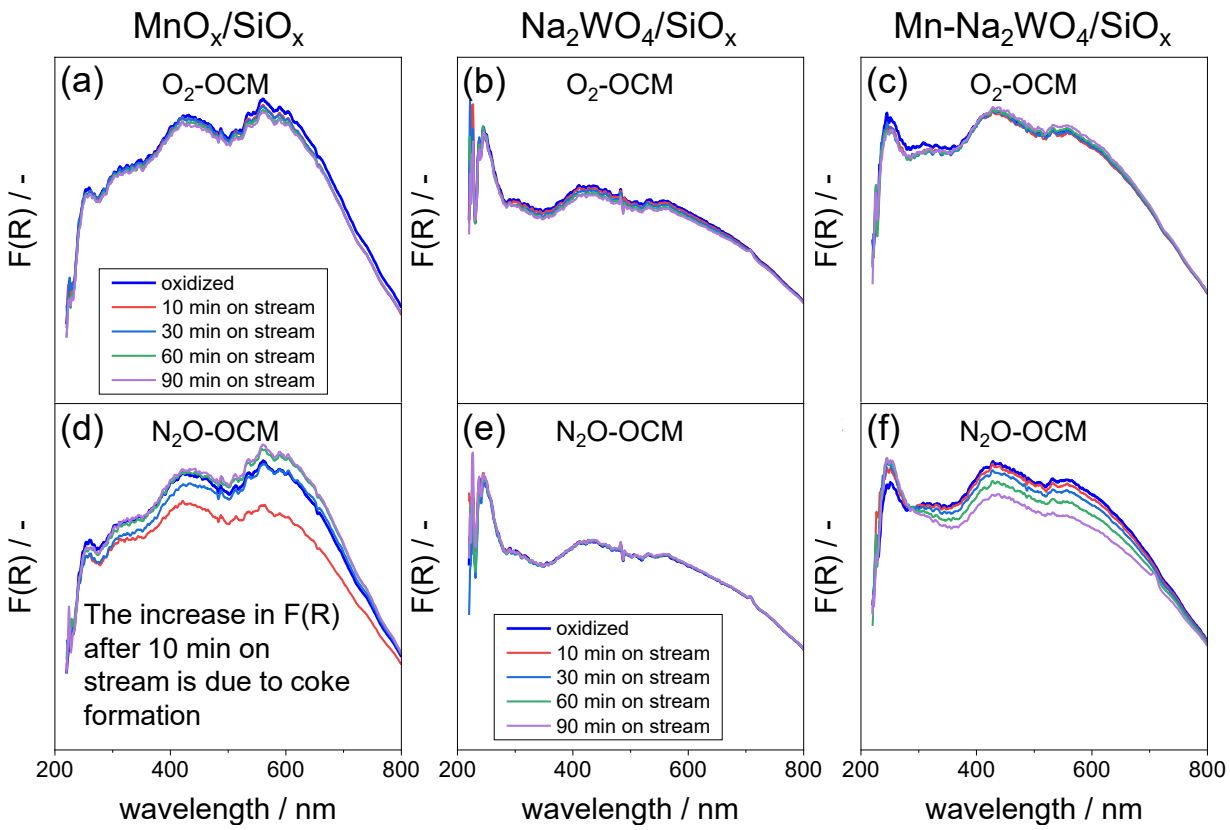

Figure S11. In situ UV-vis spectra of oxidized (O_2/N_2=20/80) MnO_x/SiO_2, Na_2WO_4/SiO_2 and Mn-Na_2WO_4/SiO_2 and after O_2-OCM (CH_4:O_2:N_2 = 40:5:55) or N_2O-OCM (CH_4:N_2O:N_2 = 40:10:50) at 750 °C.

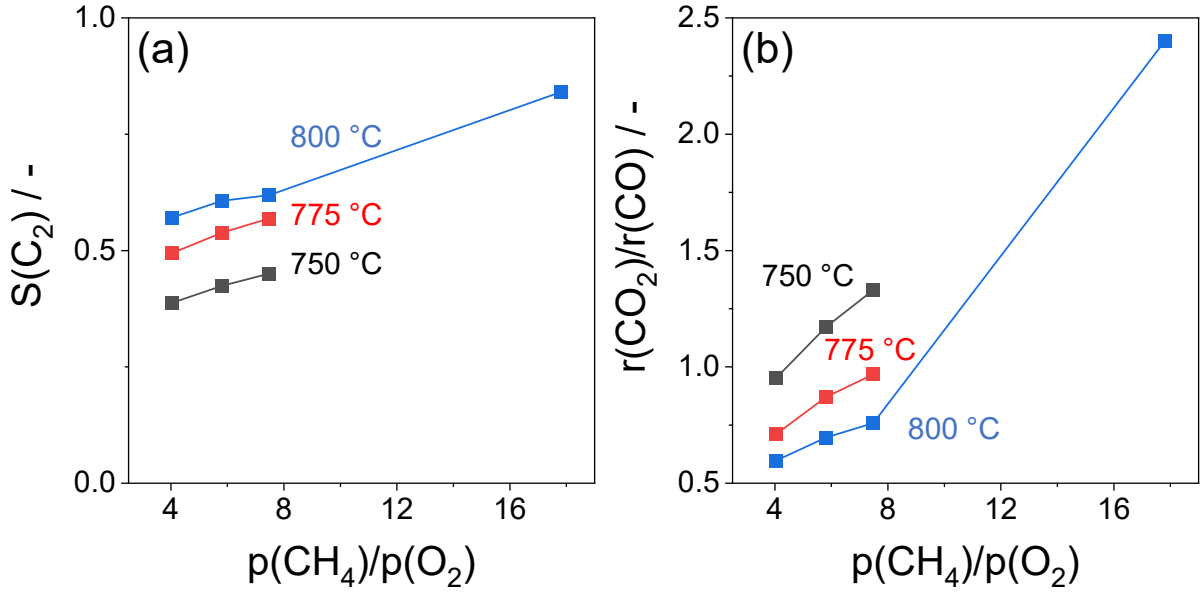

Figure S12. (a) C_2-Selectivity and (b) the ratio of rates of methane conversion to CO_2 to those to CO as function of $p(CH_4)/p(O_2)$ over Mn-Na_2WO_4/SiO_2 at 750, 775 and 800 °C. $X(CH_4)$ is below 5%.

Refeerences

1. Xiao, J.; Rabeah, J.; Yang, J.; Xie, Y.; Cao, H.; Brückner, A. Fast Electron Transfer and •OH Formation: Key Features for High Activity in Visible-Light-Driven Ozonation with C3N4 Catalysts. ACS Catal. 2017, 6198-6206.

2. Stoll, S.; Schweiger, A. EasySpin, a comprehensive software package for spectral simulation and analysis in EPR. J. Magn. Reson. 2006, 178, 42-55.

ACS Catalysis

pubs.acs.org/acscatalysis Research Article

The Role of Adsorbed and Lattice Oxygen Species in Product Formation in the Oxidative Coupling of Methane over M_2WO_4/SiO_2 (M = Na, K, Rb, Cs)

Anna Zanina, Vita A. Kondratenko, Henrik Lund, Jianshu Li, Juan Chen, Yuming Li, Guiyuan Jiang,* and Evgenii V. Kondratenko*

Cite This: *ACS Catal.* 2022, 12, 15361−15372 Read Online

ACCESS | Metrics & More | Article Recommendations | Supporting Information

ABSTRACT: MnO_x−Na_2WO_4/SiO_2 is one of the best-performing catalysts in the oxidative coupling of methane (OCM) to C_2 hydrocarbons (C_2H_6 and C_2H_4). The current mechanistic concepts related to the selectivity to the desired products are based on the involvement of crystalline Mn-containing phases, the molten Na_2WO_4 phase, surface Na−WO_x species, and the associated lattice oxygen. Using in situ X-ray diffraction, operando UV−vis spectroscopy, spatially resolved kinetic analysis of product formation in steady-state OCM tests, and temporal analysis of products with isotopic tracers, we show that these phases/species are not categorically required to ensure high selectivity to the desired products. M_2WO_4/SiO_2 (M = Na, K, Rb, Cs) materials were established to perform similarly to MnO_x−Na_2WO_4/SiO_2 in terms of selectivity−conversion relationships. The unique role of the molten Na_2WO_4 phase could not be confirmed in this regard. Our alternative concept is that the activity of M_2WO_4/SiO_2 and product selectivity are determined by the interplay between the lattice oxygen of M_2WO_4 and adsorbed oxygen species formed from gas-phase O_2. This lattice oxygen cannot convert CH_4 to C_2H_6 but oxidizes CH_4 exclusively to CO and CO_2. Adsorbed monoatomic oxygen species reveal significantly higher reactivity toward overall CH_4 conversion and efficiently generate CH_3 radicals from CH_4. These reactive intermediates couple to C_2H_6 in the gas phase and are oxidized, to a lesser extent, by the lattice oxygen of M_2WO_4 to CO and CO_2. Adsorbed diatomic oxygen is involved in the direct CH_4 oxidation to CO_2. The electronegativity of alkali metal in M_2WO_4 was established to affect the catalyst ability to generate adsorbed oxygen species from O_2. This knowledge opens the possibility to influence product selectivity by controlling the coverage by adsorbed and lattice oxygen via reaction conditions or catalyst design.

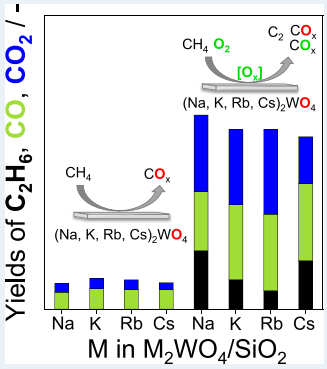

KEYWORDS: *oxidative coupling of methane, methane activation, reaction mechanism, alkali metal, oxygen species*

■ INTRODUCTION

In view of limited oil reserves but higher availability of natural gas or biogas (a mixture of CO_2 and CH_4) and their environmental compatibility, direct conversion of CH_4 into value-added chemicals is becoming increasingly attractive.[1,2] Oxidative coupling of CH_4 (OCM) to C_2H_6/C_2H_4 (C_2 hydrocarbons) is one of the most promising approaches. Although this reaction has been studied for about 40 years, no commercially viable catalyst has been developed. A vital limitation in catalyst development is the insufficient knowledge about the reaction mechanism and the kinetics of product formation and their relationship to the structure of active phases/species/sites. To close such gap, the MnO_x−Na_2WO_4/SiO_2 catalyst, which is one of the best-performing OCM materials, has been intensively investigated.[3,4] Nevertheless, many fundamental questions remain unanswered or are controversially discussed that is detrimental to purposeful catalyst optimization and further development. The most important open queries are (i) the kind of oxygen species responsible for selective and unselective pathways,[5−8] (ii) the role of the molten Na_2WO_4 phase and the crystalline Mn_7SiO_{12} and $MnWO_4$ phases,[9−12] and (iii) the origins of the enhancing water effect on the formation of C_2 hydrocarbons.[13−18]

There is still no consensus on whether methane activation and product formation over the MnO_x−Na_2WO_4/SiO_2 catalyst occur with participation of adsorbed or lattice oxygen.[5,7,10,11,19,20] The origin (which catalyst component provides its lattice oxygen; where gas-phase oxygen is activated) of such species is also not unambiguously understood. Experiments in the chemical looping mode (methane oxidation under anaerobic conditions) showed that lattice oxygen can be active and selective for the conversion of CH_4 into C_2 hydrocarbons.[21] MnO_x was suggested to be the source

Received: October 6, 2022
Revised: November 3, 2022
Published: November 30, 2022

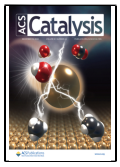

Downloaded via LEIBNIZ INST FOR CATALYSIS (LIKAT) on March 6, 2023 at 08:52:38 (UTC).
See https://pubs.acs.org/sharingguidelines for options on how to legitimately share published articles.

ACS Publications © 2022 American Chemical Society

Supporting Information

The Role of Adsorbed and Lattice Oxygen Species in Product Formation in the Oxidative Coupling of Methane over M_2WO_4/SiO_2 (M=Na, K, Rb, Cs)

Anna Zanina[1], Vita A. Kondratenko[1], Henrik Lund[1], Jianshu Li[2], Juan Chen[2], Yuming Li[2], Guiyuan Jiang[2,], Evgenii V. Kondratenko[1,*]*

[1]Leibniz-Institut für Katalyse e.V., Albert-Einstein-Str. 29a, 18059 Rostock, Germany

[2]State Key Laboratory of Heavy Oil Processing, China University of Petroleum Beijing, Beijing 102249, People's Republic of China

E-mail: evgenii.kondratenko@catalysis.de. Phone: +49(381)1281-290.

E-mail: jianggy@cup.edu.cn.

Table of contents

Mears Criterion for External Heat Transfer Limitations

Table S1. The obtained heat transfer values for M_2WO_4/SiO_2 in the OCM reaction at 800°C without or with cofed water.

Mears Criterion for External Mass Transfer Limitations

Table S2. The obtained mass transport criterion values for M_2WO_4/SiO_2 in the OCM reaction at 800°C without or with cofed water.

Table S3. Elemental composition of fresh and spent (after 36 hours on stream at 800°C using $CH_4/O_2/N_2$=8:1:11 and $CH_4/O_2/H_2O/N_2$=8:1:6:5 feeds) M_2WO_4/SiO_2 (M=Na, K, Rb, Cs) from ICP and AAS (for Cs and Si) analysis.

Table S4. Methane and oxygen conversion in operando UV-vis tests at 750°C with a $CH_4/O_2/N_2$ 8:1:11 feed.

Figure S1. STEM-EDX images of fresh M_2WO_4/SiO_2 catalysts where M = Na (a-d), K (e-h), Rb (i-l), Cs (m-p).

Figure S2. XRD patterns of (a) fresh and (b) spent M_2WO_4/SiO_2 samples. M stands for Na (black), K (blue), Rb (green), Cs (red).

Figure S3. In situ XRD patterns of M_2WO_4/SiO_2 recorded between 30°C and 800°C in air flow. Identified phases: α-cristobalite (ICDD 00-039-1425), β-cristobalite (01-077-8670), α-Na_2WO_4 (PDF 00-012-0772), β-Na_2WO_4 (ICDD 00-020-1163), K_2WO_4 (00-024-0902), Rb_2WO_4 (00-024-0977), $Rb_{1.1}W_{1.65}O_{5.5}$ (00-044-0016), Cs_2WO_4 (00-030-0377).

Figure S4. Ethylene/ethane ratio vs methane conversion over M_2WO_4/SiO_2 M= Na (■), K(■), Rb (■), Cs (■), reaction conditions: 800°C, $CH_4/O_2/N_2$=8:1:11.

Figure S5. Profiles of mass spectrometric signal at m/z of 32 (O_2) during temperature-programmed (30-900°C with a heating rate of 10°C) treatment of M_2WO_4/SiO_2 catalysts in Ar. M stands for Na (black), K (blue), Rb (green), Cs (red).

Figure S6. Profiles of differently labelled oxygen detected during temperature-programmed treatment of M_2WO_4/SiO_2 catalysts in 1 vol% $^{18}O_2$ in Ar. black – $^{18}O_2$, red – $^{16}O_2$, green - $^{16}O^{18}O$.

Figure S7. (a) The responses of $C^{16}O^{18}O$ recorded after pulsing of an CH_4-$^{18}O_2$ mixture over Na_2WO_4 (black) and Cs_2WO_4 (red). (b) the ratio of m/z 46 ($C^{16}O^{18}O$) to 40 for M_2WO_4/SiO_2 M= Na (■), K(■), Rb (■), Cs (■) at 800°C and ambient pressure.

Figure S8. Transient responses of differently labelled carbon monoxide and carbon dioxide formed in CH_4, CH_4-$^{18}O_2$, and CH_4-$^{18}O_2$-H_2O pulse experiments over (a-c) Na_2WO_4/SiO_2, (d-f) K_2WO_4/SiO_2, (g-i) Rb_2WO_4/SiO_2, (j-l) Cs_2WO_4/SiO_2 at 800°C in the TAP reactor.

Figure S9. The dependence of the rates of CH_4 conversion into (a) C_2 hydrocarbons, (b) CO_2, (c) CO over the M_2WO_4/SiO_2 (M=Na (■), K(■), Rb (■), Cs (■)) catalysts at 800°C on oxygen partial pressure.

Figure S10. The dependence of the reciprocal rates of CH_4 conversion into (a) CO_2 or (b) CO on $1/p(O_2)$ over the M_2WO_4/SiO_2 (M=Na (▲, ▼), K(▼, ▲), Rb (▲, ▼), Cs (▼, ▲)) at 800°C

Figure S11. Selectivity-conversion relationships for (a) C_{2+} hydrocarbons, (b) CO_2, and (c) CO over MnO_x-Na_2WO_4/SiO_2 (solid symbols) and Na_2WO_4/SiO_2 (crossed symbols) at 800°C using a $CH_4/O_2/N_2$ 8:1:11 feed.

Figure S12. The dependence of the rate of CH_4 conversion into (a) CO_2, (b) C_2 hydrocarbons, (c) CO over the M_2WO_4/SiO_2 (M=Na (■), K(■), Rb (■), Cs (■)) catalysts at different CH_4/O_2 ratios (circle 12:1, square 8:1, triangle 4:1) at 800°C on the amount of formed $^{16}O^{18}O$ oxygen in the isotopic exchange tests (Figure S6).

Figure S13. The dependence of the rate of CH_4 conversion into (a) CO_2, (b) C_2 hydrocarbons, (c) CO over the M_2WO_4/SiO_2 (M=Na, K, Rb, Cs) catalysts at 800°C using feeds with different CH_4/O_2 ratios (black 12:1, blue 8:1, red 4:1) on the electronegativity of the alkali metal.

Figure S14. The correlation of fraction of $^{16}O^{18}O$ formed during the oxygen isotopic exchange experiment over the M_2WO_4/SiO_2 (M=Na (●), K (●), Rb (●), Cs (●)) catalysts with the electronegativity of the alkali metal.

Mears Criterion for External Heat Transfer Limitations

The Mears criterion was used to evaluate external heat transfer limitations according to Equation S1. The most exothermic reaction, i.e., CH_4 oxidation to CO_2, was considered in the calculations.

$$\frac{r_{obs} \cdot \rho_{catalyst} \cdot R \cdot E_a \cdot \Delta H}{k_g \cdot R_g \cdot T^2} < 0.15 \qquad \text{(S1)}$$

r_{obs} – measured reaction rate, kmol/(kg_{cat}·s)

$\rho_{catalyst}$ – catalyst density, kg/m^3

R – catalyst pellet radius, m

E_a – activation energy, kJ/kmol

ΔH – reaction heat at 1073 K, kJ/mol

k_g – heat transport coefficient, kJ/(m^2·s·K)

R_g – gas constant, kJ/(mol·K)

T – reaction temperature, K

An example of calculations for Na_2WO_4/SiO_2 at 800°C:

$$\frac{r_{obs} \cdot \rho_{catalyst} \cdot R \cdot E_a \cdot \Delta H}{k_g \cdot R_g \cdot T^2} = (9.75 \cdot 10^{-6} \frac{\text{kmol}}{\text{kg·s}} \cdot 496 \frac{\text{kg}}{\text{m}^3} \cdot 3.5 \cdot 10^{-4}\text{m} \cdot 2.1 \cdot 10^5 \frac{\text{kJ}}{\text{kmol}} \cdot 802 \frac{\text{kJ}}{\text{mol}})/$$
$$(167 \frac{\text{kJ}}{\text{m}^2\text{·s·K}} \cdot 8.31 \cdot 10^{-3} \frac{\text{kJ}}{\text{mol·K}} \cdot 1073^2 \text{ K}^2) = \mathbf{1.8 \cdot 10^{-4}} \ll \mathbf{0.15}$$

Table S1. The obtained heat transfer values for M_2WO_4/SiO_2 in the OCM reaction at 800°C without or with cofed water.

Catalyst	Reaction feed	Value for heat criterion
Na_2WO_4/SiO_2	$CH_4/O_2/N_2$=8:1:11	$1.8 \cdot 10^{-4}$
Na_2WO_4/SiO_2	$CH_4/O_2/H_2O/N_2$=8:1:6:5	$2.5 \cdot 10^{-4}$
K_2WO_4/SiO_2	$CH_4/O_2/N_2$=8:1:11	$1.1 \cdot 10^{-4}$
K_2WO_4/SiO_2	$CH_4/O_2/H_2O/N_2$=8:1:6:5	$2.1 \cdot 10^{-4}$
Rb_2WO_4/SiO_2	$CH_4/O_2/N_2$=8:1:11	$0.83 \cdot 10^{-4}$
Rb_2WO_4/SiO_2	$CH_4/O_2/H_2O/N_2$=8:1:6:5	$1.7 \cdot 10^{-4}$
Cs_2WO_4/SiO_2	$CH_4/O_2/N_2$=8:1:11	$0.48 \cdot 10^{-4}$
Cs_2WO_4/SiO_2	$CH_4/O_2/H_2O/N_2$=8:1:6:5	$1.2 \cdot 10^{-4}$

Mears Criterion for External Mass Transfer Limitations

The Mears criterion was used to evaluate external mass transfer limitations according to Equation S2.

$$\frac{r_{obs} \cdot \rho_{catalyst} \cdot R \cdot n}{k_c \cdot C} < 0.15 \qquad \text{(S2)}$$

r_{obs} – measured reaction rate, kmol/(kg_{cat}·s)

$\rho_{catalyst}$ – catalyst density, kg/m^3

R – catalyst pellet radius, m

n – reaction order

k_c – mass transfer coefficient, m/s

C – bulk concentration of reactant, kmol/m^3

The calculation for Na_2WO_4/SiO_2 at 800°C:

$$\frac{r_{obs} \cdot \rho_{catalyst} \cdot R \cdot n}{k_c \cdot C} = (9.75 \cdot 10^{-6} \frac{\text{kmol}}{\text{kg·s}} \cdot 496 \frac{\text{kg}}{\text{m}^3} \cdot 3.5 \cdot 10^{-4} \text{m} \cdot 2)/(0.2 \frac{\text{m}}{\text{s}} \cdot 4.5 \cdot 10^{-3} \frac{\text{kmol}}{m^3}) = \mathbf{3.7 \cdot 10^{-3} \ll 0.15}$$

Table S2. The obtained mass transport criterion values for M_2WO_4/SiO_2 in the OCM reaction at 800°C without or with cofed water.

Catalyst	Reaction feed	Value for mass criterion
Na_2WO_4/SiO_2	$CH_4/O_2/N_2$=8:1:11	$3.7 \cdot 10^{-3}$
Na_2WO_4/SiO_2	$CH_4/O_2/H_2O/N_2$=8:1:6:5	$8.8 \cdot 10^{-3}$
K_2WO_4/SiO_2	$CH_4/O_2/N_2$=8:1:11	$2.8 \cdot 10^{-3}$
K_2WO_4/SiO_2	$CH_4/O_2/H_2O/N_2$=8:1:6:5	$7.5 \cdot 10^{-3}$
Rb_2WO_4/SiO_2	$CH_4/O_2/N_2$=8:1:11	$2.4 \cdot 10^{-3}$
Rb_2WO_4/SiO_2	$CH_4/O_2/H_2O/N_2$=8:1:6:5	$6.0 \cdot 10^{-3}$
Cs_2WO_4/SiO_2	$CH_4/O_2/N_2$=8:1:11	$1.5 \cdot 10^{-3}$
Cs_2WO_4/SiO_2	$CH_4/O_2/H_2O/N_2$=8:1:6:5	$4.4 \cdot 10^{-3}$

Table S3. Elemental composition of fresh and spent (after 36 hours on stream at 800°C using $CH_4/O_2/N_2$=8:1:11 and $CH_4/O_2/H_2O/N_2$=8:1:6:5 feeds) M_2WO_4/SiO_2 (M=Na, K, Rb, Cs) from ICP and AAS (for Cs and Si) analysis.

Catalyst	State	$M_{(ICP/AAS)}$ (wt.%)	$W_{(ICP)}$ (wt. %)	$Si_{(ICP)}$ (wt. %)
Na_2WO_4/SiO_2	fresh	0.7	3.0	38.8
	spent	0.6	2.5	39.5
K_2WO_4/SiO_2	fresh	1.2	3.0	37.8
	spent	1.0	2.3	37.5
Rb_2WO_4/SiO_2	fresh	2.5	3.0	37.1
	spent	2.4	2.7	38.3
Cs_2WO_4/SiO_2	fresh	3.8	2.6	37.2
	spent	3.3	2.0	37.2

Table S4. Methane and oxygen conversion in operando UV-vis tests at 750°C with a $CH_4/O_2/N_2$ 8:1:11 feed.

Catalyst	$X(CH_4)$ / %	$X(O_2)$ / %
Na_2WO_4/SiO_2	1.9	11
K_2WO_4/SiO_2	1.7	16
Rb_2WO_4/SiO_2	1.7	19
Cs_2WO_4/SiO_2	1.4	13

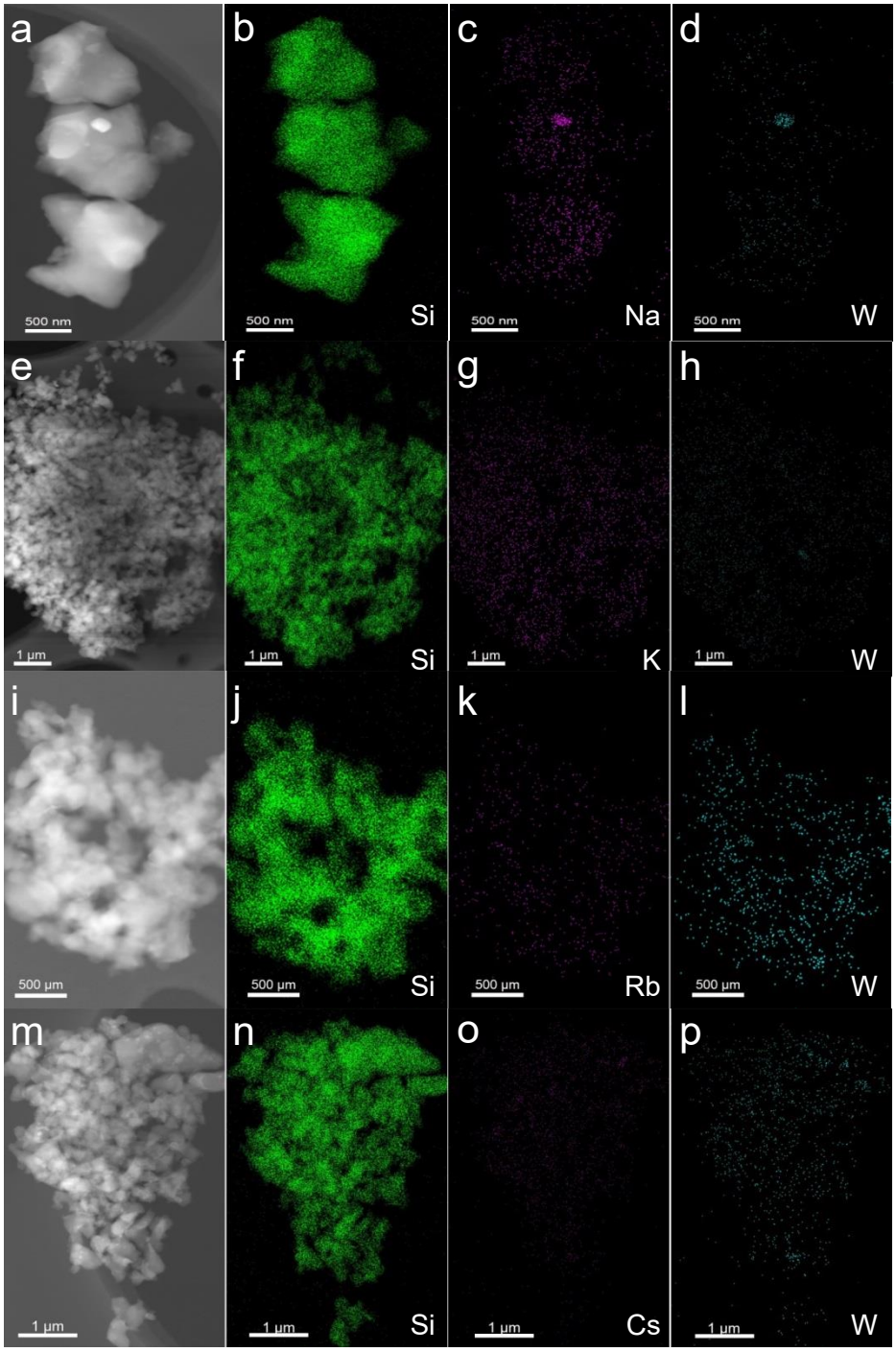

Figure S1. STEM-EDX images of fresh M_2WO_4/SiO_2 catalysts where M = Na (a-d), K (e-h), Rb (i-l), Cs (m-p).

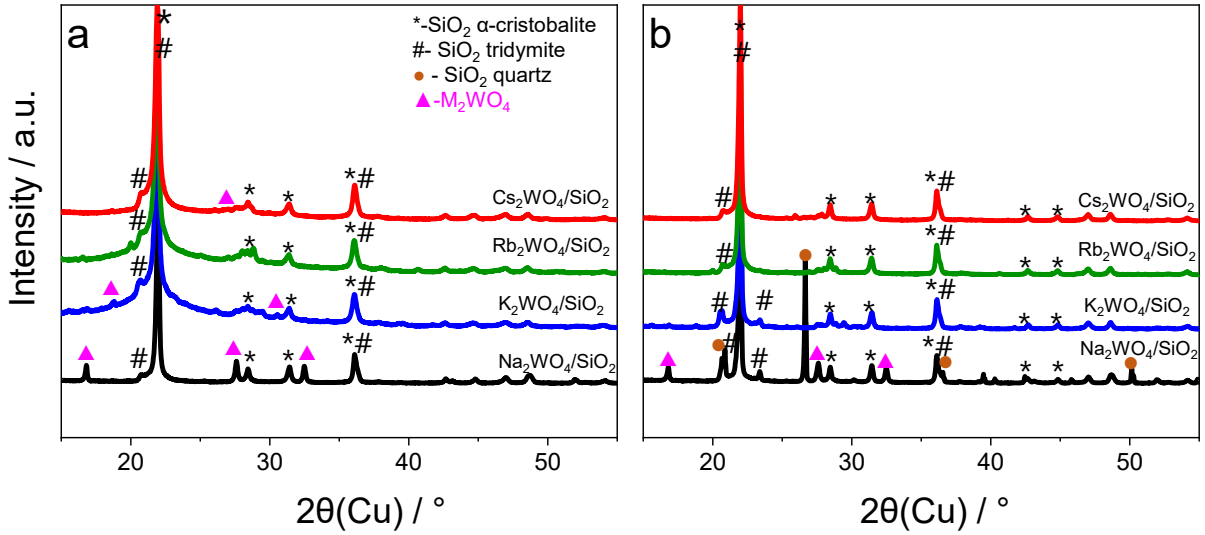

Figure S2. XRD patterns of (a) fresh and (b) spent M_2WO_4/SiO_2 samples. M stands for Na (black), K (blue), Rb (green), Cs (red).

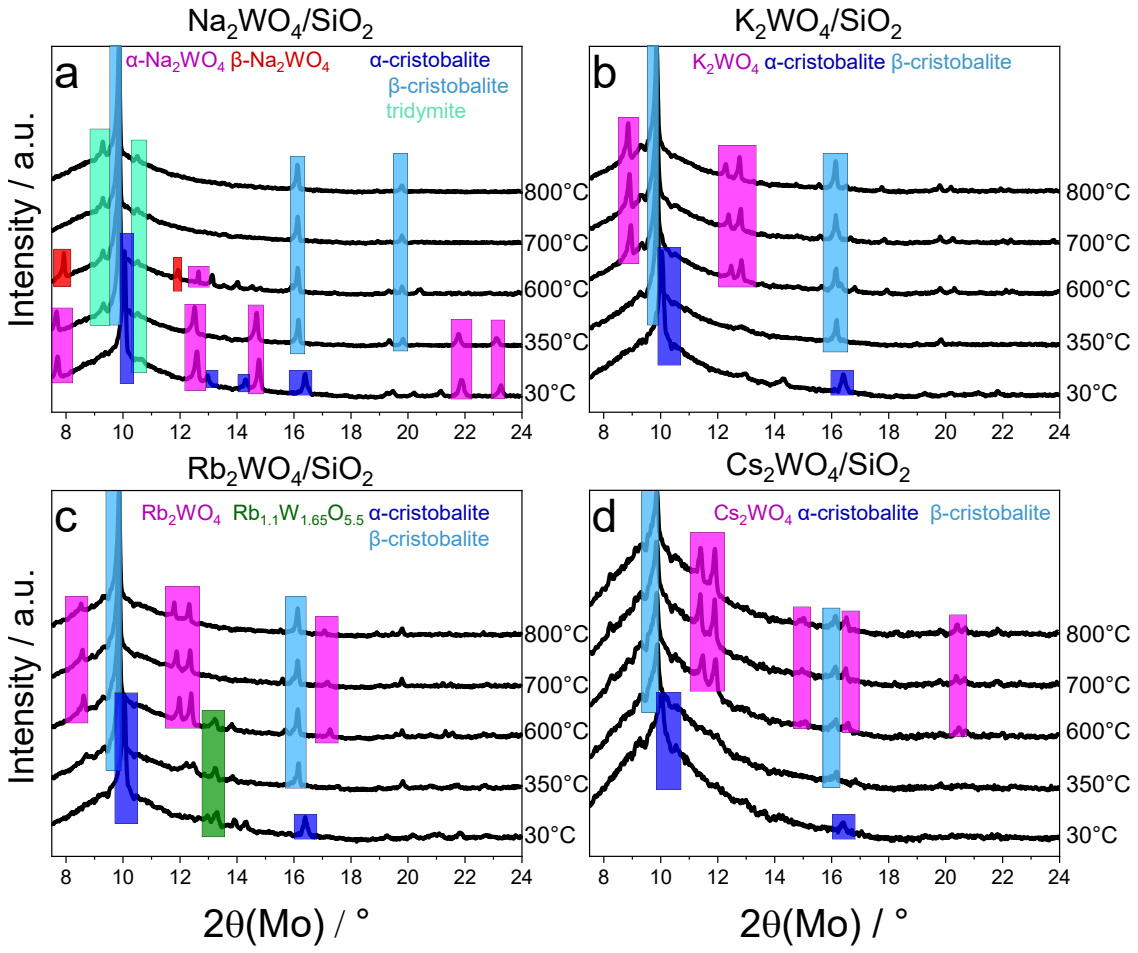

Figure S3. In situ XRD patterns of M_2WO_4/SiO_2 recorded between 30°C and 800°C in air flow. Identified phases: α-cristobalite (ICDD 00-039-1425), β-cristobalite (01-077-8670), α-Na_2WO_4 (PDF 00-012-0772), β-Na_2WO_4 (ICDD 00-020-1163), K_2WO_4 (00-024-0902), Rb_2WO_4 (00-024-0977), $Rb_{1.1}W_{1.65}O_{5.5}$ (00-044-0016), Cs_2WO_4 (00-030-0377).

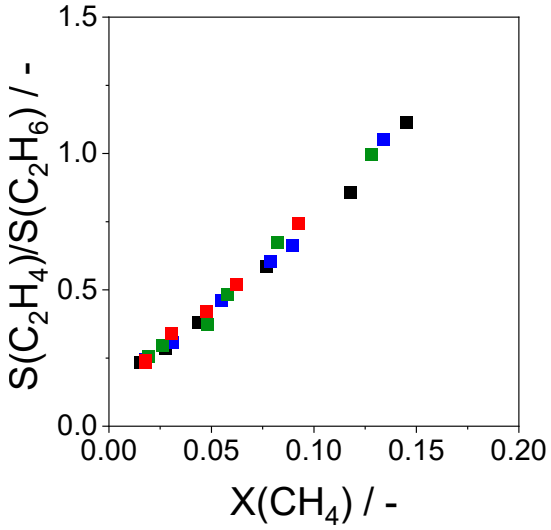

Figure S4. Ethylene/ethane ratio vs methane conversion over M_2WO_4/SiO_2 M= Na (■), K(■), Rb (■), Cs (■), reaction conditions: 800°C, $CH_4/O_2/N_2$=8:1:11.

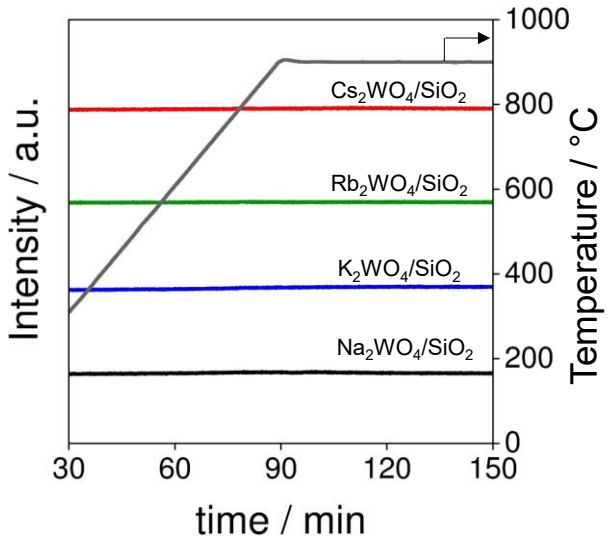

Figure S5. Profiles of mass spectrometric signal at m/z of 32 (O_2) during temperature-programmed (30-900°C with a heating rate of 10°C) treatment of M_2WO_4/SiO_2 catalysts in Ar. M stands for Na (black), K (blue), Rb (green), Cs (red).

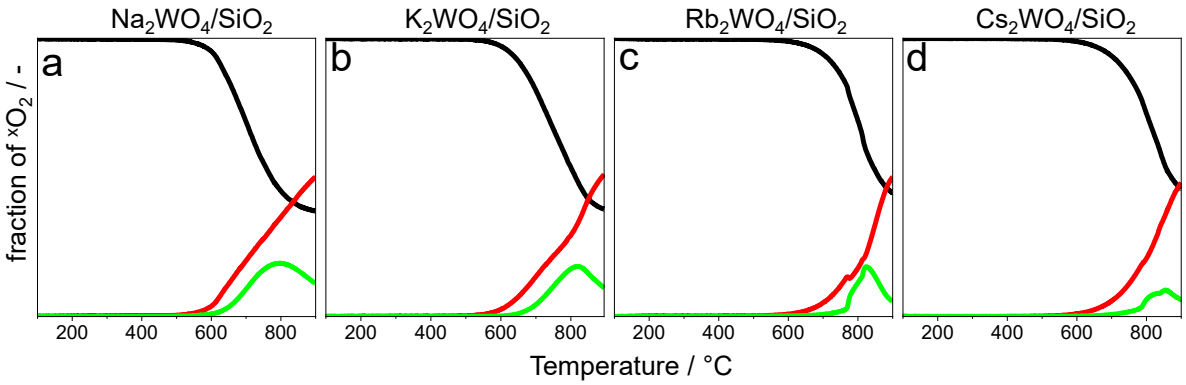

Figure S6. Profiles of differently labelled oxygen detected during temperature-programmed treatment of M_2WO_4/SiO_2 catalysts in 1 vol% $^{18}O_2$ in Ar. black – $^{18}O_2$, red – $^{16}O_2$, green - $^{16}O^{18}O$.

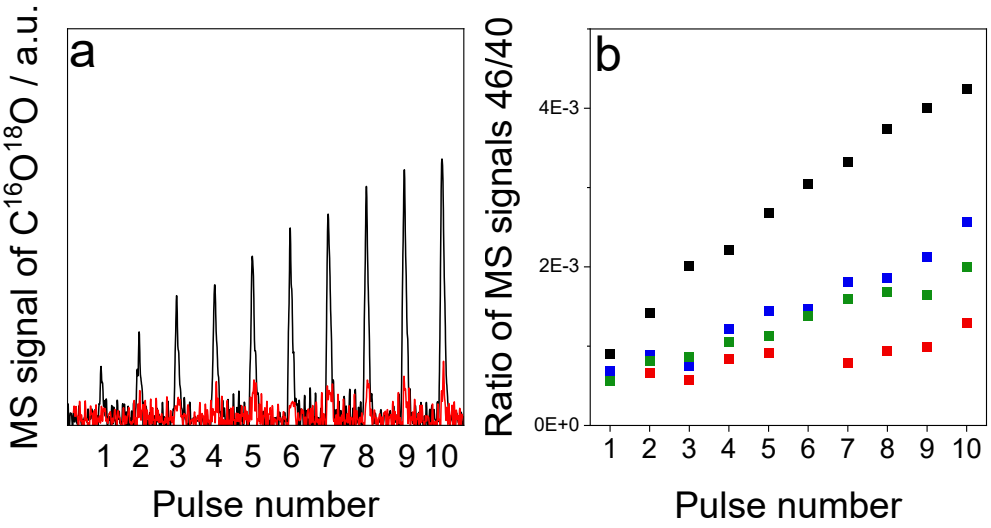

Figure S7. (a) The responses of $C^{16}O^{18}O$ recorded after pulsing of an CH_4-$^{18}O_2$ mixture over Na_2WO_4 (black) and Cs_2WO_4 (red). (b) the ratio of m/z 46 ($C^{16}O^{18}O$) to 40 for M_2WO_4/SiO_2 M= Na (■), K(■), Rb (■), Cs (■) at 800°C and ambient pressure.

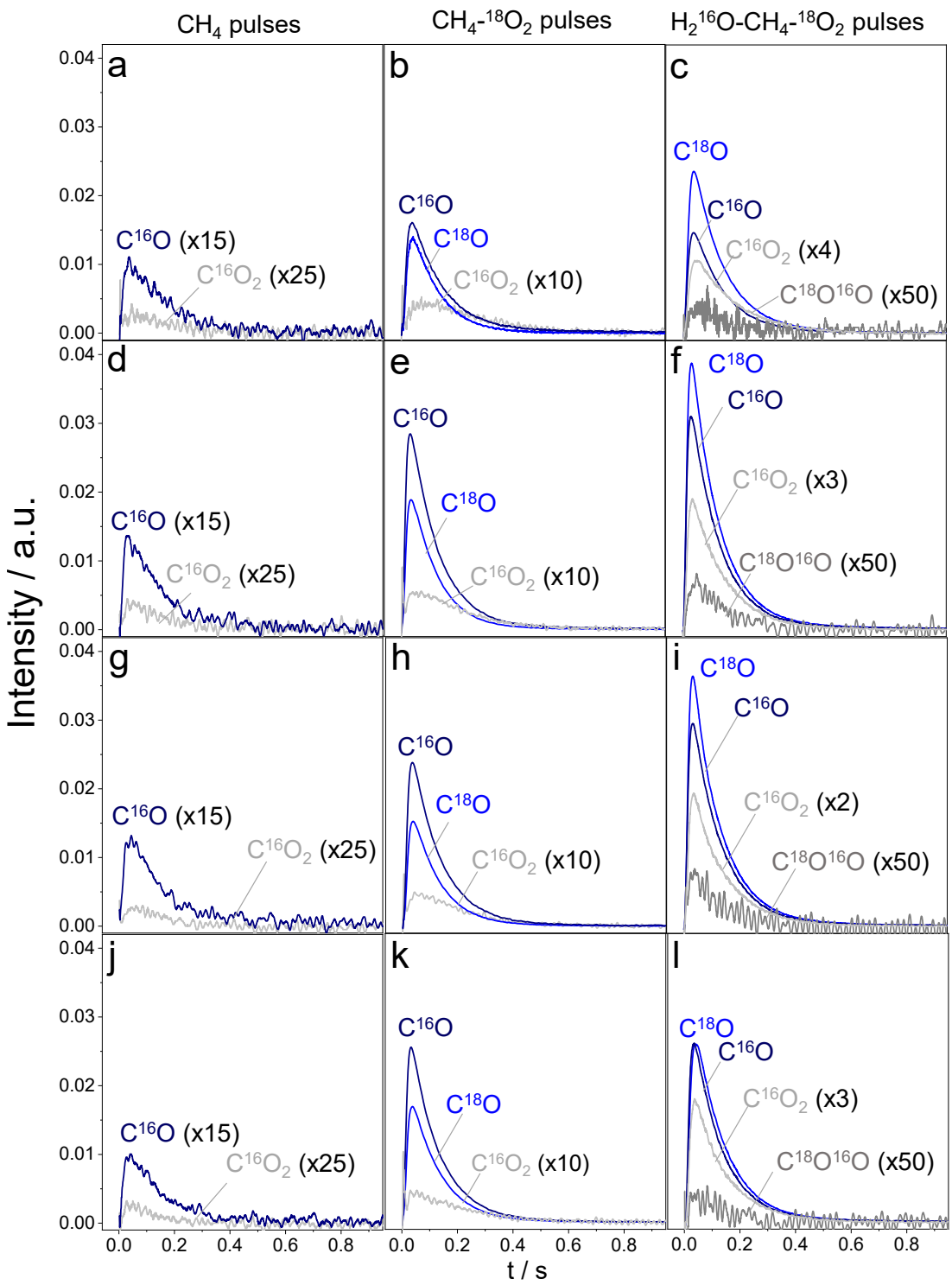

Figure S8. Transient responses of differently labelled carbon monoxide and carbon dioxide formed in CH_4, CH_4-$^{18}O_2$, and CH_4-$^{18}O_2$-H_2O pulse experiments over (a-c) Na_2WO_4/SiO_2, (d-f) K_2WO_4/SiO_2, (g-i) Rb_2WO_4/SiO_2, (j-l) Cs_2WO_4/SiO_2 at 800°C in the TAP reactor.

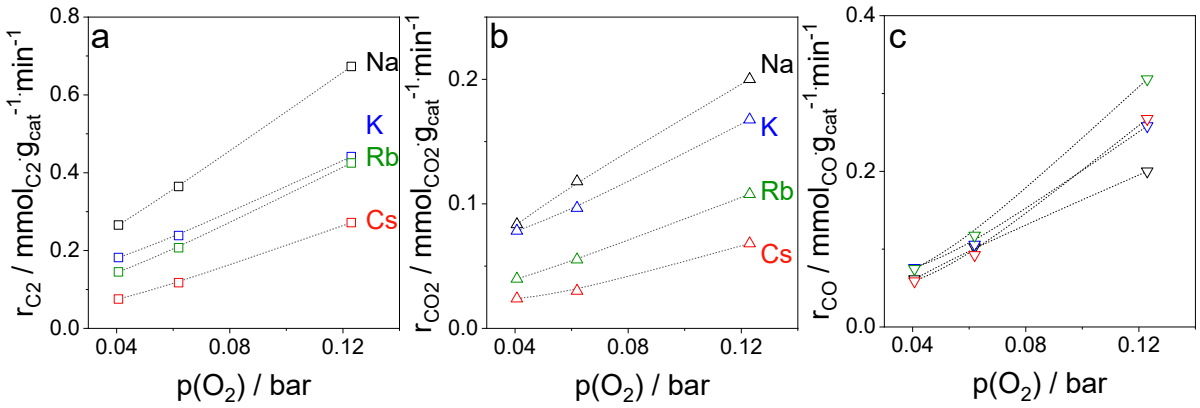

Figure S9. The dependence of the rates of CH_4 conversion into (a) C_2 hydrocarbons, (b) CO_2, (c) CO over the M_2WO_4/SiO_2 (M=Na (■), K(■), Rb (■), Cs (■)) catalysts at 800°C on oxygen partial pressure.

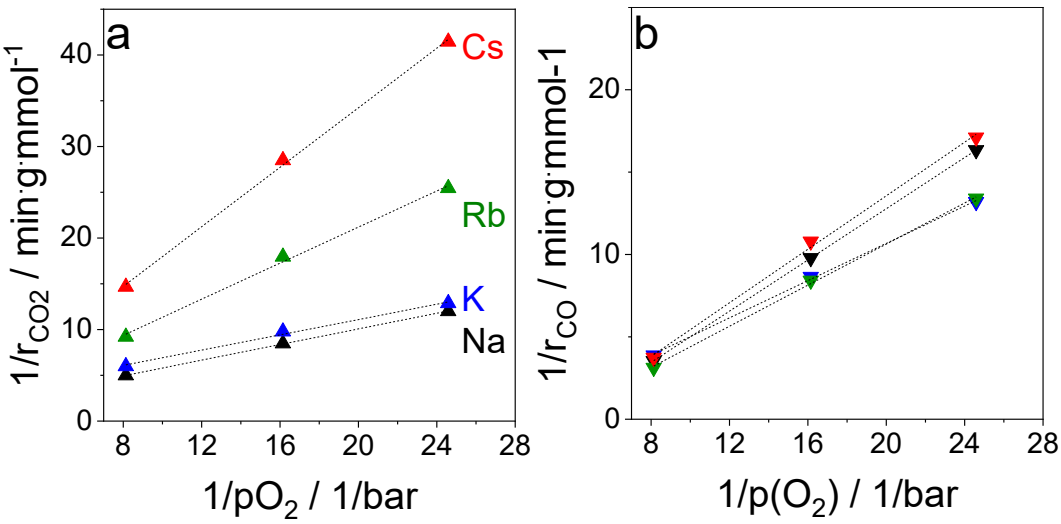

Figure S10. The dependence of the reciprocal rates of CH_4 conversion into (a) CO_2 or (b) CO on $1/p(O_2)$ over the M_2WO_4/SiO_2 (M=Na (▲, ▼), K(▼, ▲), Rb (▲, ▼), Cs (▼, ▲)) at 800°C

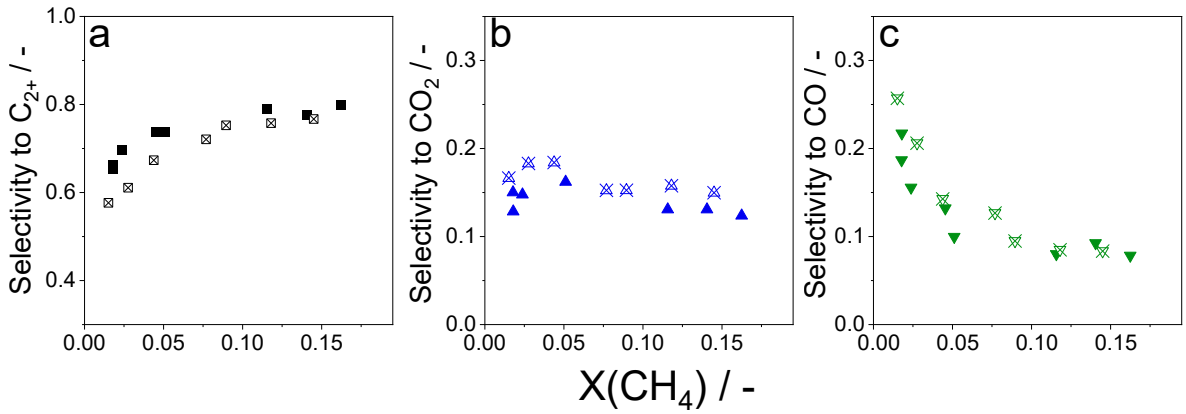

Figure S11. Selectivity-conversion relationships for (a) C_{2+} hydrocarbons, (b) CO_2, and (c) CO over MnO_x-Na_2WO_4/SiO_2 (solid symbols) and Na_2WO_4/SiO_2 (crossed symbols) at 800°C using a $CH_4/O_2/N_2$ 8:1:11 feed.

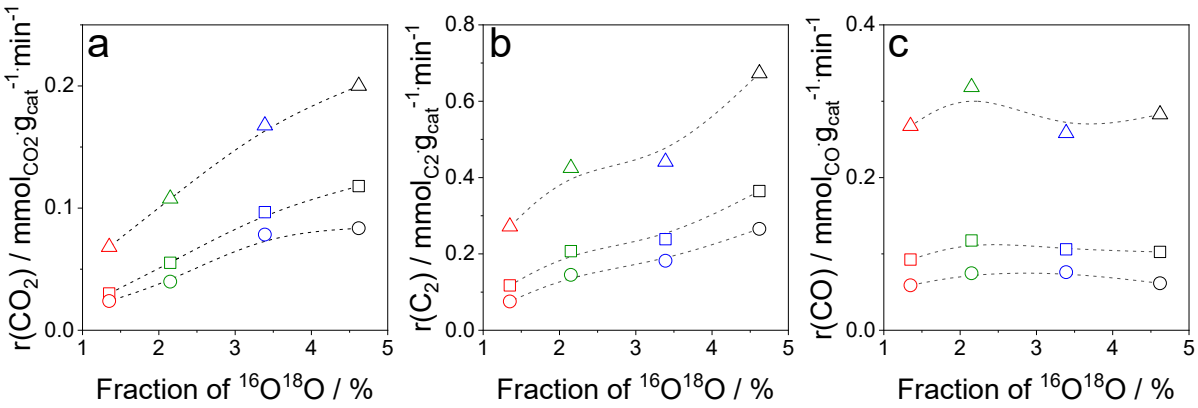

Figure S12. The dependence of the rate of CH_4 conversion into (a) CO_2, (b) C_2 hydrocarbons, (c) CO over the M_2WO_4/SiO_2 (M=Na (■), K(■), Rb (■), Cs (■)) catalysts at different CH_4/O_2 ratios (circle 12:1, square 8:1, triangle 4:1) at 800°C on the amount of formed $^{16}O^{18}O$ oxygen in the isotopic exchange tests (Figure S6).

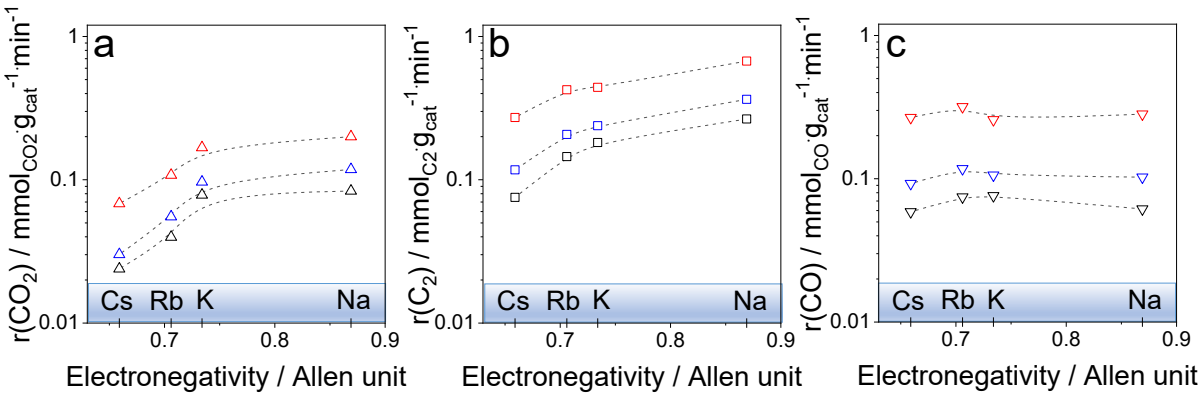

Figure S13. The dependence of the rate of CH_4 conversion into (a) CO_2, (b) C_2 hydrocarbons, (c) CO over the M_2WO_4/SiO_2 (M=Na, K, Rb, Cs) catalysts at 800°C using feeds with different CH_4/O_2 ratios (black 12:1, blue 8:1, red 4:1) on the electronegativity of the alkali metal.

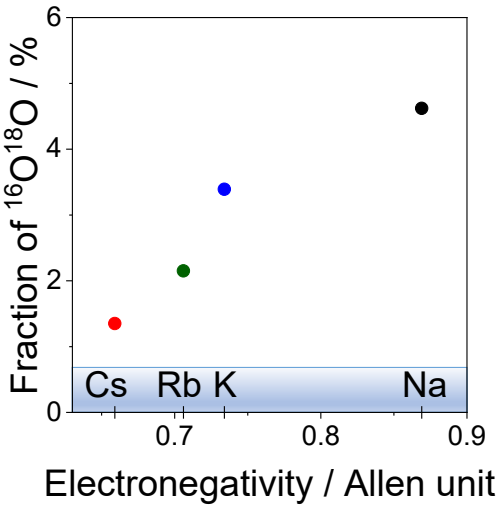

Figure S14. The correlation of fraction of $^{16}O^{18}O$ formed during the oxygen isotopic exchange experiment over the M_2WO_4/SiO_2 (M=Na (●), K (●), Rb (●), Cs (●)) catalysts with the electronegativity of the alkali metal.

Journal of Catalysis 419 (2023) 68–79

Contents lists available at ScienceDirect

Journal of Catalysis

journal homepage: www.elsevier.com/locate/jcat

Performance-defining factors of (MnO_x)-M_2WO_4/SiO_2 (M = Na, K, Rb, or Cs) catalysts in oxidative coupling of methane

Anna Zanina [a], Vita A. Kondratenko [a], Henrik Lund [a], Jianshu Li [b], Juan Chen [b], Yuming Li [b], Guiyuan Jiang [b,*], Evgenii V. Kondratenko [a,*]

[a] Leibniz Institut für Katalyse e.V., Albert-Einstein-Str. 29a, 18059 Rostock, Germany
[b] State Key Laboratory of Heavy Oil Processing, China University of Petroleum Beijing, Beijing 102249, People's Republic of China

ARTICLE INFO

Article history:
Received 5 December 2022
Revised 20 January 2023
Accepted 4 February 2023
Available online 8 February 2023

Keywords:
Oxidative coupling of methane
In situ characterization
Alkali metals
Oxygen species
Active sites
Transient experiments

ABSTRACT

This work unveils the fundamentals relevant for activity and product selectivity in the oxidative coupling of methane (OCM) over the (MnO_x)-M_2WO_4/SiO_2 (M = Na, K, Rb, or Cs) catalysts. The presence of the molten phase of Na_2WO_4 and the ability of the catalysts to release lattice oxygen were not found to be the performance-governing factors. As proven by oxygen isotopic exchange experiments combined with thorough catalytic tests, the performance of both tri- and bimetallic catalysts is defined by the involvement of adsorbed oxygen species formed from gas-phase O_2. Lattice oxygen of M_2WO_4/SiO_2 is not capable of converting CH_4 to C_2H_6, while that of MnO_x-M_2WO_4/SiO_2 is active for this reaction. The OCM activity of M_2WO_4/SiO_2 decreases with the atomic weight of alkali metal, whereas there is no such effect in the presence of MnO_x, which, however, increases the activity. The enhancing effect was explained by improving the active site turnover.

© 2023 Elsevier Inc. All rights reserved.

1. Introduction

Direct conversion of methane into value-added products is attractive both from fundamental and applied viewpoints [1–3]. The production of ethylene and ethane (C_2-hydrocarbons) through oxidative coupling of methane (OCM) is highly important in this regard. Since typical temperature of OCM is 750–900 °C, the catalyst must have high thermostability in addition to the predominant formation of the desired C_2 hydrocarbons. The multicomponent MnO_x-Na_2WO_4/SiO_2 catalyst fulfills these requirements [4–6]. However, unknown structure–activity-selectivity relationships and the ambiguity about the role and the kind of oxygen species participating in the formation of selective and unselective products limit further developments to achieve industrially attractive performance.

There is no doubt that all components of the MnO_x-Na_2WO_4/SiO_2 system must co-exist to ensure high selectivity to C_2-hydrocarbons [7], although Mn-free Na_2WO_4/SiO_2 does not significantly differ from its Mn-containing counterpart in this regard [8–10]. From recent in situ/operando characterization studies, Mn in MnO_x is known to be in the +3 oxidation state under OCM conditions [11–13]. The oxidation state of W is close to +6 [12,14]. It is important to note that the Na_2WO_4 phase exists in a molten state at temperatures above 700 °C, as evidenced by various in situ studies using Raman spectroscopy [11,12,15], X-ray diffraction analysis (XRD) or XRD-CT (computed tomography) [9,16–19]. This molten phase was suggested to be crucial for high catalyst activity due to higher rates of chemical and mass-transport processes [20]. Our very recent OCM study using M_2WO_4/SiO_2 (M = Na, K, Rb, or Cs) demonstrated that only Na_2WO_4 was present in the molten state under reaction conditions [21]. Nevertheless, no obvious differences between the catalysts were established in terms C_2-hydrocarbons selectivity. Catalyst activity decreased, however, with a decrease in the electronegativity of alkali metals.

There exist various mechanistic concepts about the kind and the origin of oxygen species participating in the formation of C_2 hydrocarbons and carbon oxides. For example, atomic oxygen species associated with surface Na-WO_x sites was suggested to convert CH_4 into C_2H_6 and CO [15,22]. It was also assumed that molecular O_2 dissolved in the molten Na_2WO_4 phase can oxidize CH_4 to CO_2. However, we have recently demonstrated that lattice oxygen of M_2WO_4 (M = Na, K, Rb, Cs) cannot oxidize methane to C_2-hydrocarbons but to carbon oxides [21]. Such materials are active and selective only in the presence of adsorbed oxygen species formed from gas-phase oxygen. For MnO_x-Na_2WO_4/SiO_2 the importance of oxygen released through the interaction of Mn^{3+}

* Corresponding authors.
E-mail addresses: jianggy@cup.edu.cn (G. Jiang), evgenii.kondratenko@catalysis.de (E.V. Kondratenko).

https://doi.org/10.1016/j.jcat.2023.02.004
0021-9517/© 2023 Elsevier Inc. All rights reserved.

Supporting information

Performance-defining factors of (MnO_x)-M_2WO_4/SiO_2 (M=Na, K, Rb or Cs) catalysts in oxidative coupling of methane

Anna Zanina[1], Vita A. Kondratenko[1], Henrik Lund[1], Jianshu Li[2], Juan Chen[2], Yuming Li[2],

Guiyuan Jiang[2,*], Evgenii V. Kondratenko[1,*]

[1]Leibniz Institut für Katalyse e.V., Albert-Einstein-Str. 29a, 18059 Rostock, Germany

[2]State Key Laboratory of Heavy Oil Processing, China University of Petroleum Beijing, Beijing 102249, People's Republic of China

*Corresponding author: jianggy@cup.edu.cn (GJ)

*Corresponding author: evgenii.kondratenko@catalysis.de (EVK)

Table of content

Table S1. Catalyst elemental composition determined by ICP-OES and AAS. The theoretical values are given in brackets.

Table S2. BET values of fresh and after OCM at 800°C under $CH_4/O_2/N_2$ and $CH_4/O_2/H_2O/N_2$ flows for 36 h.

Table S3. The obtained parameters of the fitted curves of time-resolved changes in Kubelka-Munk function at 420 nm from in situ UV-vis tests at 750 °C in H_2/N_2 flow.

Fig. S1. STEM-EDX images of fresh (a) MnO_x-Na_2WO_4/SiO_2, (b) MnO_x-K_2WO_4/SiO_2, (c) MnO_x-Rb_2WO_4/SiO_2 and (d) MnO_x-Cs_2WO_4/SiO_2.

Fig. S2. STEM-EDX images of spent (a) MnO_x-K_2WO_4/SiO_2 and (b) MnO_x-Cs_2WO_4/SiO_2 catalysts after OCM at 800 °C under $CH_4/O_2/N_2$ and $CH_4/O_2/H_2O/N_2$ flows.

Fig. S3. N_2 adsorption-desorption isotherms of (a) Na_2WO_4/SiO_2, (b) K_2WO_4/SiO_2, (c) Rb_2WO_4/SiO_2 and (d) Cs_2WO_4/SiO_2.

Fig. S4. N_2 adsorption-desorption isotherms of the MnO_x-M_2WO_4/SiO_2 catalysts (a) M= K, (b) Rb, (c) Cs and (d) MnO_x-WO_x/SiO_2.

Fig. S5. XRD patterns of MnO_x-M_2WO_4/SiO_2 catalysts where M = K, Rb, Cs (a) before and (b) after OCM at 800 °C under $CH_4/O_2/N_2$ and $CH_4/O_2/H_2O/N_2$ flows. Identified phases: SiO_2 tetragonal (α-cristobalite, blue bars, PDF-No. 00-039-1425), SiO_2 orthorhombic (tridymite, light blue bars, PDF-No. 00-042-1401), SiO_2 hexagonal (quartz, cyan bars, PDF-No. 01-070-2516), $MnWO_4$ monoclinic (red bars, PDF-No. 01-072-0478), Mn_2O_3 cubic (black bars, PDF-No. 01-071-3820) or $Mn_7O_8(SiO_4)$ tetragonal (magenta bars, PDF No. 01-089-5661).Fig. S5. XRD patterns of MnO_x-M_2WO_4/SiO_2 catalysts where M = K, Rb, Cs (a) before and (b) after OCM at 800 °C under $CH_4/O_2/N_2$ and $CH_4/O_2/H_2O/N_2$ flows.

Fig. S6. XRD patterns of (a) K_2O/SiO_2 and (b) Cs_2O/SiO_2 before and after OCM at 800 °C under $CH_4/O_2/N_2$ and $CH_4/O_2/H_2O/N_2$ flows. Identified phases: SiO_2 tetragonal (α-cristobalite, blue bars, PDF-No. 00-039-1425), SiO_2 orthorhombic (tridymite, light blue bars, PDF-No. 00-042-1401).

Fig. S7. In situ XRD patterns of (a) M_2WO_4/SiO_2 (M=Na, K, Rb, Cs) and (b) MnO_x-M_2WO_4/SiO_2 (Na, K) in air at 800 °C. Identified phases: SiO_2 cubic (β-cristobalite, dark blue bars, PDF-No. 01-077-8670), SiO_2 hexagonal (tridymite, light green bars, PDF-No. 01-073-0403), K_2WO_4 hexagonal (blue bars, PDF-No. 00-024-0902), Rb_2WO_4 orthorhombic (green bars, PDF-No. 00-024-0976), Cs_2WO_4 hexagonal (red bars, PDF-No. 00-030-0377), Mn_2O_3 cubic (black bars, PDF-No. 01-071-3820), or $Mn_7O_8(SiO_4)$ tetragonal (dark yellow bars, PDF No. 01-089-5661).

Fig. S8. (a) Oxygen desorption profiles of fresh M_2WO_4/SiO_2 (M= Na, K, Rb, Cs) and WO_x/SiO_2 catalysts. (b) The amount of oxygen desorbed during O_2-TPD experiments.

Fig. S9. The profiles of $^{18}O_2$ (black), $^{16}O_2$ (red), $^{16}O^{18}O$ (green) recorded during treatment of (a-d) MnO_x-M_2WO_4/SiO_2, (e-h) M_2WO_4/SiO_2 and (i) WO_x/SiO_2, (j) MnO_x/SiO_2, (k) MnO_x-WO_x/SiO_2 in a flow of (1vol%)$^{18}O_2$/Ar (7 ml/min).

Fig. S10. Transients of $C^{16}O$, $C^{18}O$, $C^{16}O_2$ recorded after CH_4-$^{18}O_2$ pulses at 800 °C over (a, c, e, g) M_2WO_4/SiO_2 and (b, d, f, h) MnO_x-M_2WO_4/SiO_2; (a), (b) M=Na; (c), (d) M=K; (e), (f) M=Rb; (g), (h) M=Cs.

Fig. S11. The spectra at 750 °C under O_2/N_2 (green), H_2/N_2 for 1 min (pink) and H_2/N_2 for 60 min (red) over (a) MnO_x-Na_2WO_4/SiO_2, (b) MnO_x-K_2WO_4/SiO_2, (c) MnO_x-Rb_2WO_4/SiO_2, (d) MnO_x-Cs_2WO_4/SiO_2; (e) temporal change in the Kubelka-Munk function at 420 nm during reduction of oxidized MnO_x/SiO_2, Na_2WO_4/SiO_2 and MnO_x-Na_2WO_4/SiO_2 catalyst at 750 °C in 40vol%H_2/N_2.

Fig. S12. The fitted curves of reduction of MnO_x-M_2WO_4/SiO_2 catalysts (a) M=Na, (b) K, (c) Rb, (d) Cs at 750 °C in 40vol%H_2/N_2 by $f(t) = (1 - A_1 \times e^{-k_1 t}) - (1 - A_2 \times e^{-k_2 t}) + B$ function.

Fig. S13. The selectivity-conversion relationship for C_2H_6, C_2H_4, CO and CO_2 formed at 800 °C and 1.2 bar over MnO_x-M_2WO_4/SiO_2 (empty symbols) and M_2WO_4/SiO_2 (crossed symbols) catalysts (a,e,i,m) M=Na, (b, f, j, n) K, (c, g, k, o) Rb, (d, h, l, p) Cs using a $CH_4/O_2/N_2$ 40/5/55 feed, after the cycle in water using $CH_4/O_2/H_2O/N_2$ 40/5/30/25.

Fig. S14. The selectivity-conversion plot for C_2 hydrocarbons (■), CO_2 (♦) and CO (▲) formed over MnO_x-WO_x/SiO_2. Reaction conditions: 800 °C, 10-100 mg catalyst, $CH_4/O_2/N_2$ 40/5/55, flow rate of 30ml/min.

Fig. S15. The experimental transient responses of $C^{16}O_2$ (black line), $C^{16}O^{18}O$ (red line) and $C^{18}O_2$ (dark green line) detected after switching from a $CH_4/^{16}O_2$/He=30/4/66 feed to a $CH_4/^{18}O_2$/Ar/He=30/4/1/65 feed at 775 °C over (a) MnO_x-Na_2WO_4/SiO_2, (b) MnO_x-K_2WO_4/SiO_2, (c) Na_2WO_4/SiO_2 and (d) K_2WO_4/SiO_2. The profiles of $C^{16}O^{18}O$ and $C^{18}O_2$ calculated using a statistical model considering only one kind of oxygen species are shown as light grey and dark grey lines, respectively.

Fig. S16. Transients of (a) Ar and CO_2 as well (b) Ar and H_2O recorded at 800 °C after switch from He to CO_2/Ar/He or H_2O/Ar/He flows. Catalyst: 25 mg MnO_x-Na_2WO_4/SiO_2.

Table S1. Catalyst elemental composition determined by ICP-OES and AAS. The theoretical values are given in brackets.

Catalyst	Element amount wt%		
	Mn	W	Alkali metal
MnO_x-Na_2WO_4/SiO_2	2.9 (2.8)	3.2 (2.8)	0.7 (0.7)
Na_2WO_4/SiO_2	-	3.1 (2.8)	0.7 (0.7)
MnO_x-K_2WO_4/SiO_2	3.0 (2.8)	2.8 (2.8)	1.1 (1.2)
K_2WO_4/SiO_2	-	3.3 (2.8)	1.2 (1.2)
MnO_x-Rb_2WO_4/SiO_2	2.9 (2.8)	2.8 (2.8)	2.6 (2.6)
Rb_2WO_4/SiO_2	-	3.0 (2.8)	2.5 (2.6)
MnO_x-Cs_2WO_4/SiO_2	3.0 (2.8)	2.8 (2.8)	4.0 (4.0)
Cs_2WO_4/SiO_2	-	3.0 (2.8)	4.1 (4.0)

Table S2. BET values of fresh and after OCM at 800°C under $CH_4/O_2/N_2$ and $CH_4/O_2/H_2O/N_2$ flows for 36 h.

Catalyst	Specific surface area, m^2/g_{cat}	
	Before reaction	After reaction
MnO_x-Na_2WO_4/SiO_2	4.0	1.0
Na_2WO_4/SiO_2	5.1	1.4
MnO_x-K_2WO_4/SiO_2	4.3	2.4
K_2WO_4/SiO_2	15.5	1.6
MnO_x-Rb_2WO_4/SiO_2	5.0	2.5
Rb_2WO_4/SiO_2	14.8	2.8
MnO_x-Cs_2WO_4/SiO_2	4.7	1.9
Cs_2WO_4/SiO_2	9.8	2.0
Mn-WO_X/SiO_2	226.6	56.7

Table S3. The obtained parameters of the fitted curves of time-resolved changes in Kubelka-Munk function at 420 nm from in situ UV-vis tests at 750 °C in H_2/N_2 flow.

Catalysts	k_1	A_1	k_2	A_2	B	R^2
$MnNaWO_x/SiO_2$	0.0015±0.0004	2.48±0.04	0.025±0.001	3.38±0.08	14.16±0.08	0.97
$MnKWO_x/SiO_2$	0.0020±0.0000	2.43±0.03	0.044±0.002	2.33±0.06	14.85±0.06	0.98
$MnRbWO_x/SiO_2$	0.0013±0.0000	1.51±0.02	0.057±0.005	1.31±0.05	12.48±0.05	0.98
$MnCsWO_x/SiO_2$	0.00096±0.00003	1.00±0.01	104.90±0	0.17±0.06	13.17±0.06	0.96

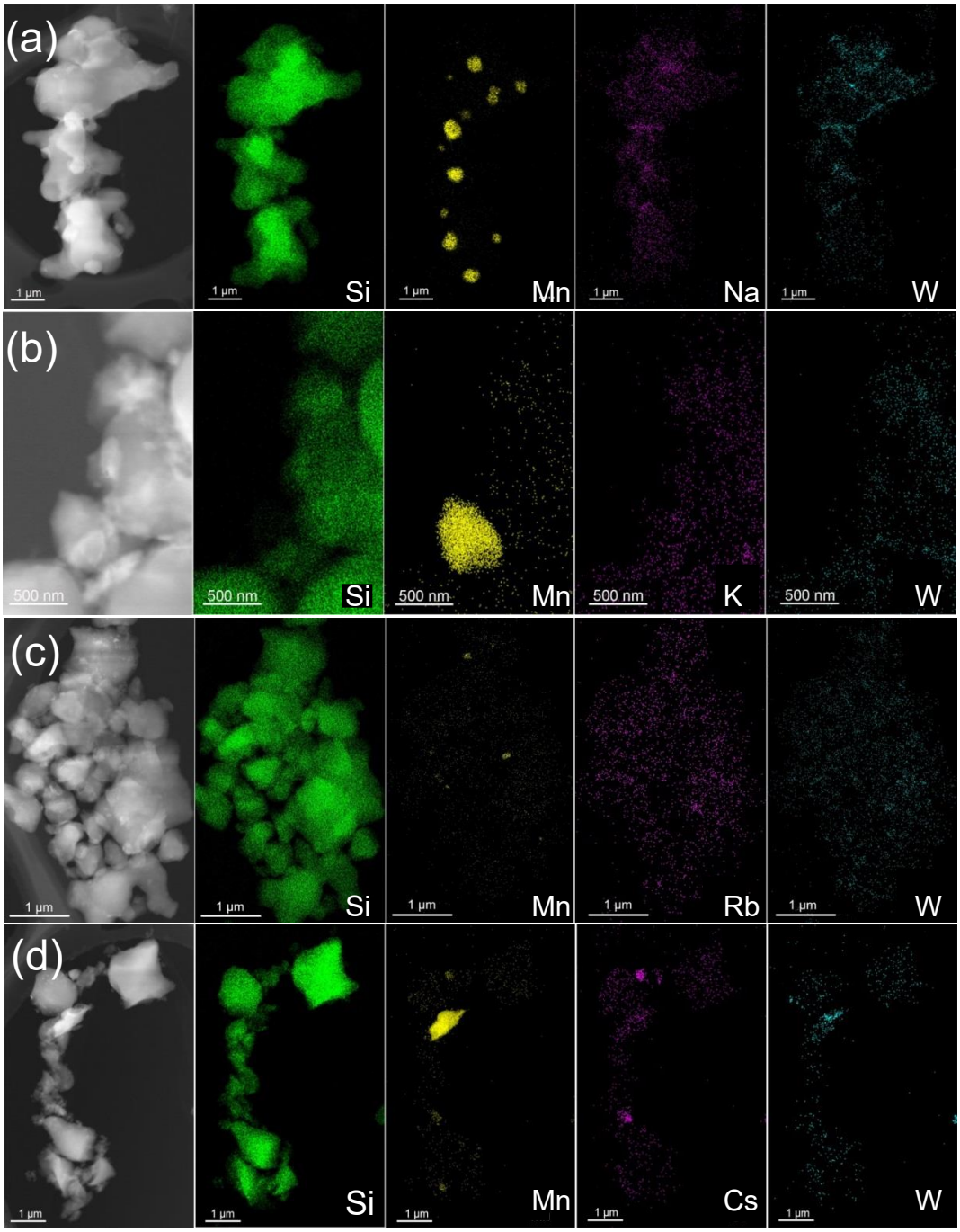

Fig. S1. STEM-EDX images of fresh (a) MnO_x-Na_2WO_4/SiO_2, (b) MnO_x-K_2WO_4/SiO_2, (c) MnO_x-Rb_2WO_4/SiO_2 and (d) MnO_x-Cs_2WO_4/SiO_2.

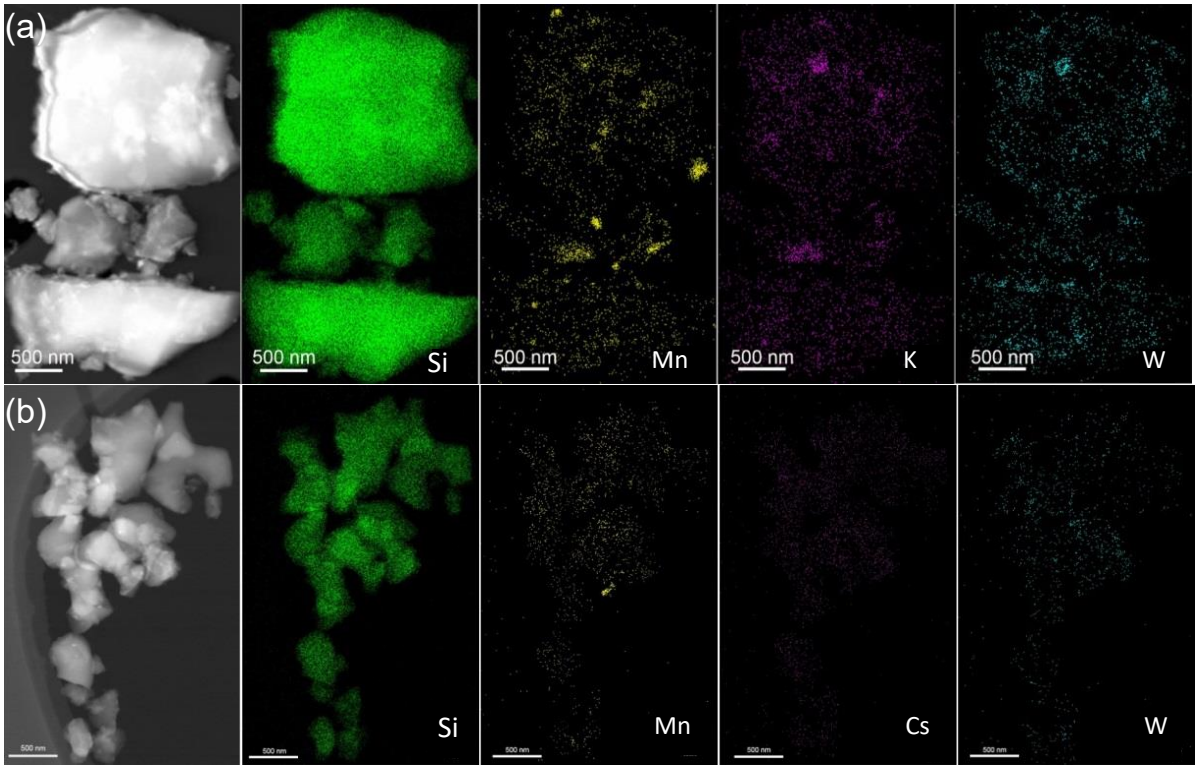

Fig. S2. STEM-EDX images of spent (a) MnO_x-K_2WO_4/SiO_2 and (b) MnO_x-Cs_2WO_4/SiO_2 catalysts after OCM at 800 °C under $CH_4/O_2/N_2$ and $CH_4/O_2/H_2O/N_2$ flows.

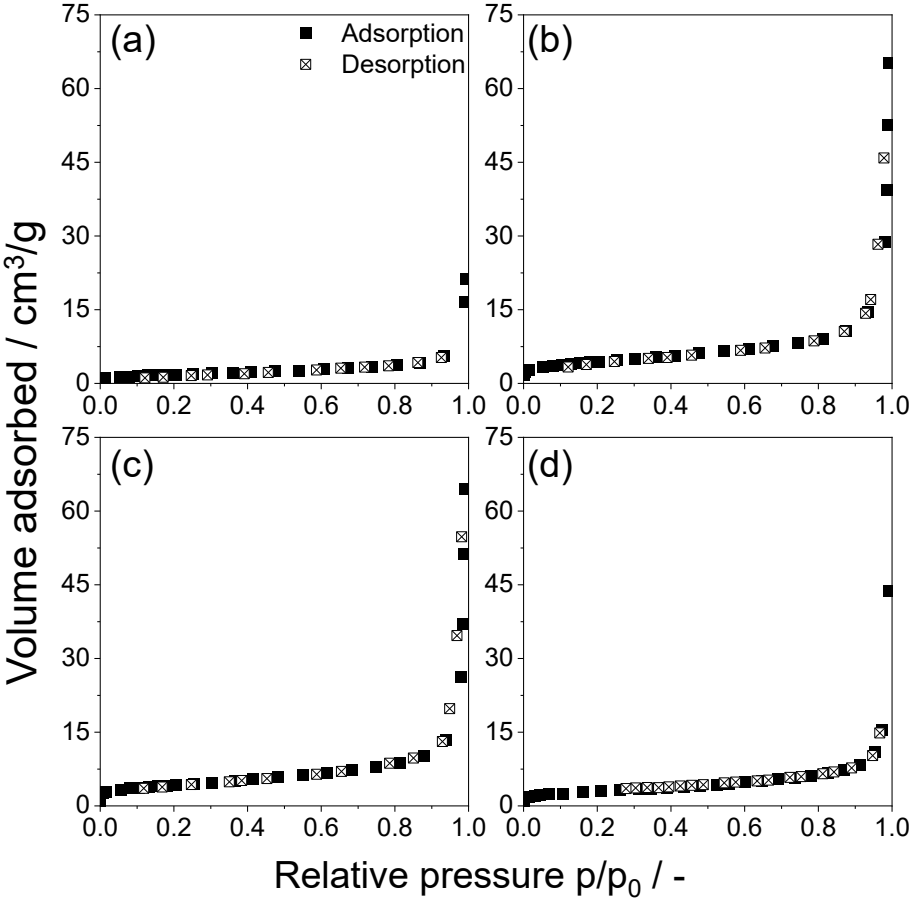

Fig. S3. N_2 adsorption-desorption isotherms of (a) Na_2WO_4/SiO_2, (b) K_2WO_4/SiO_2, (c) Rb_2WO_4/SiO_2 and (d) Cs_2WO_4/SiO_2.

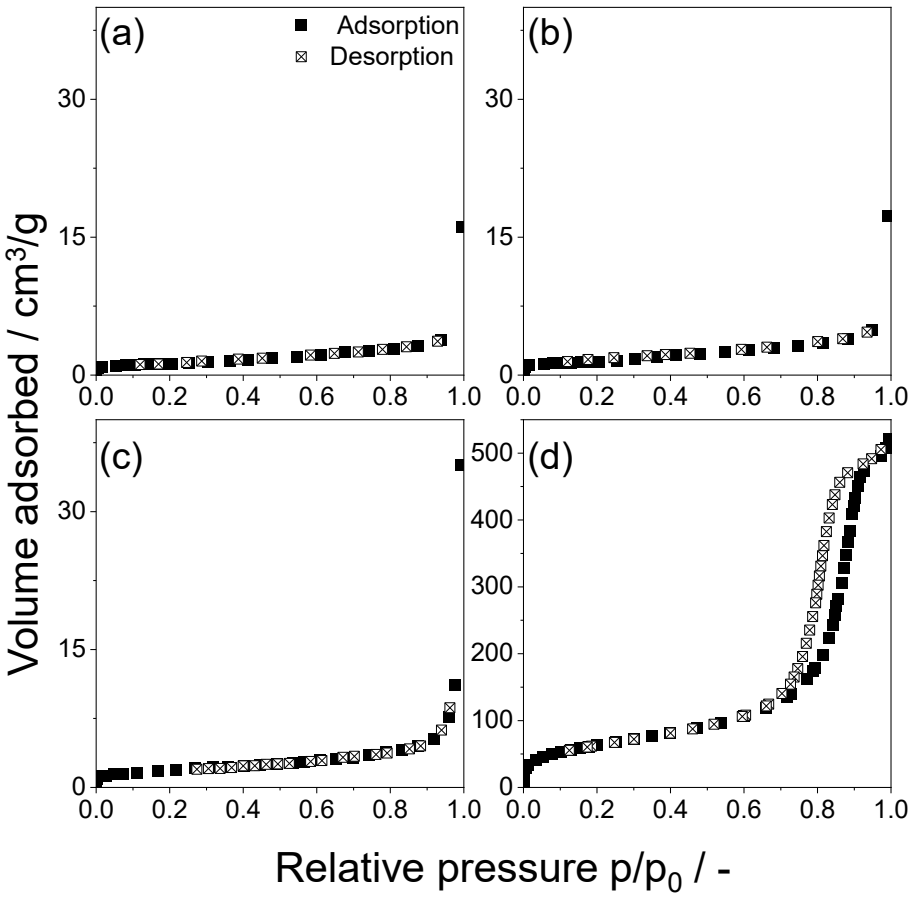

Fig. S4. N_2 adsorption-desorption isotherms of the MnO_x-M_2WO_4/SiO_2 catalysts (a) M= K, (b) Rb, (c) Cs and (d) MnO_x-WO_x/SiO_2.

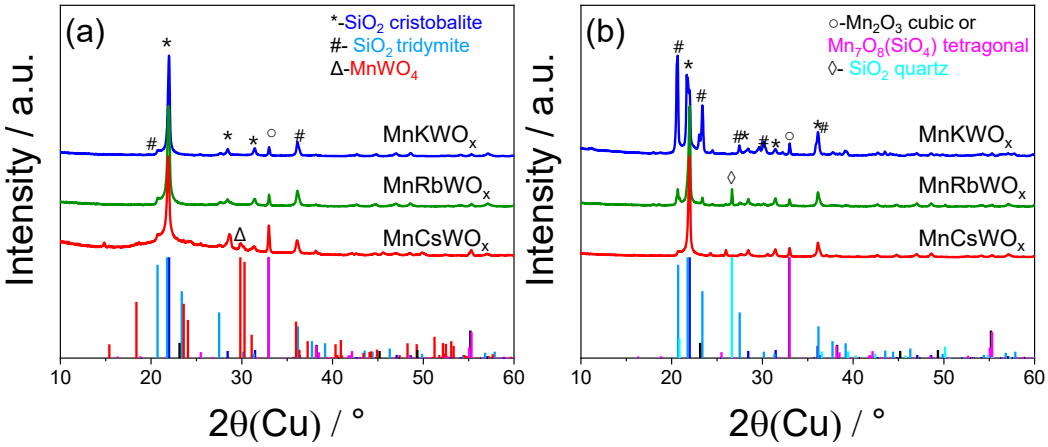

Fig. S5. XRD patterns of MnO_x-M_2WO_4/SiO_2 catalysts where M = K, Rb, Cs (a) before and (b) after OCM at 800 °C under $CH_4/O_2/N_2$ and $CH_4/O_2/H_2O/N_2$ flows. Identified phases: SiO_2 tetragonal (α-cristobalite, blue bars, PDF-No. 00-039-1425), SiO_2 orthorhombic (tridymite, light blue bars, PDF-No. 00-042-1401), SiO_2 hexagonal (quartz, cyan bars, PDF-No. 01-070-2516), $MnWO_4$ monoclinic (red bars, PDF-No. 01-072-0478), Mn_2O_3 cubic (black bars, PDF-No. 01-071-3820) or $Mn_7O_8(SiO_4)$ tetragonal (magenta bars, PDF No. 01-089-5661).

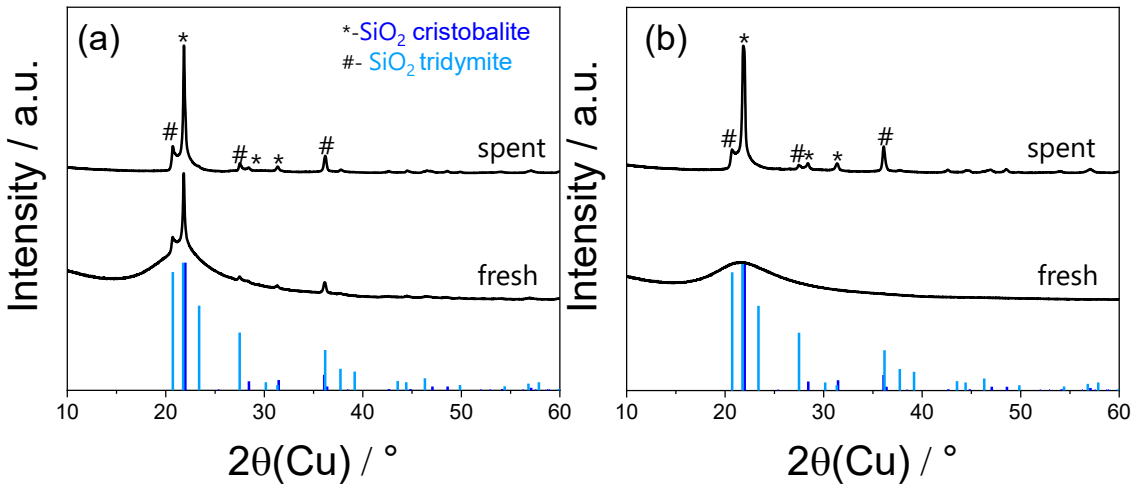

Fig. S6. XRD patterns of (a) K_2O/SiO_2 and (b) Cs_2O/SiO_2 before and after OCM at 800 °C under $CH_4/O_2/N_2$ and $CH_4/O_2/H_2O/N_2$ flows. Identified phases: SiO_2 tetragonal (α-cristobalite, blue bars, PDF-No. 00-039-1425), SiO_2 orthorhombic (tridymite, light blue bars, PDF-No. 00-042-1401).

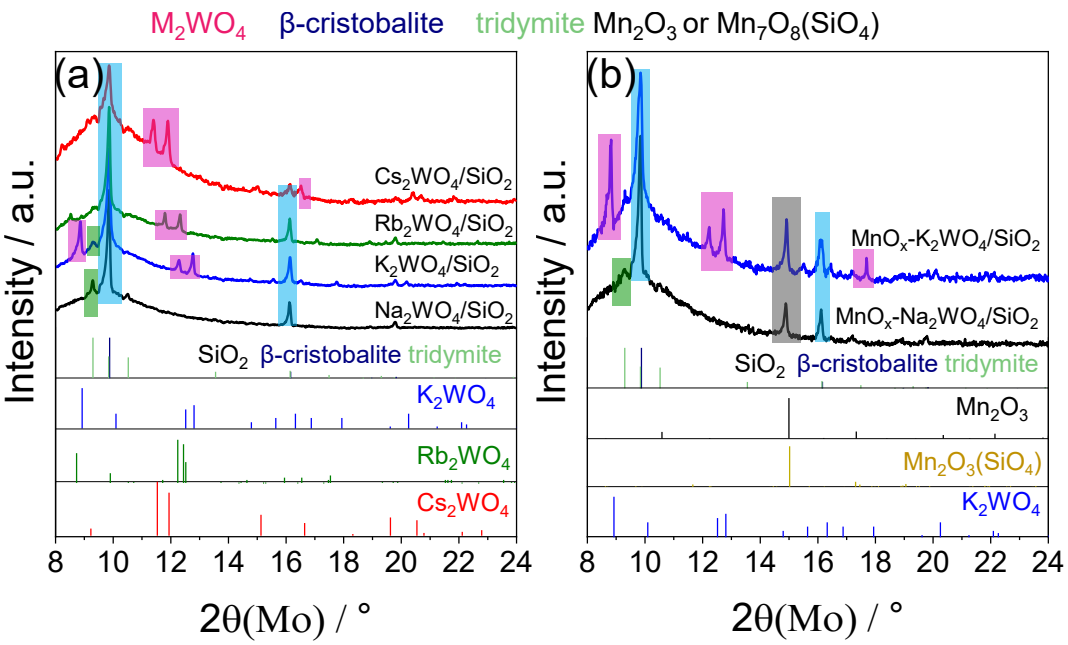

Fig. S7. In situ XRD patterns of (a) M_2WO_4/SiO_2 (M=Na, K, Rb, Cs) and (b) MnO_x-M_2WO_4/SiO_2 (Na, K) in air at 800 °C. Identified phases: SiO_2 cubic (β-cristobalite, dark blue bars, PDF-No. 01-077-8670), SiO_2 hexagonal (tridymite, light green bars, PDF-No. 01-073-0403), K_2WO_4 hexagonal (blue bars, PDF-No. 00-024-0902), Rb_2WO_4 orthorhombic (green bars, PDF-No. 00-024-0976), Cs_2WO_4 hexagonal (red bars, PDF-No. 00-030-0377), Mn_2O_3 cubic (black bars, PDF-No. 01-071-3820), or $Mn_7O_8(SiO_4)$ tetragonal (dark yellow bars, PDF No. 01-089-5661).

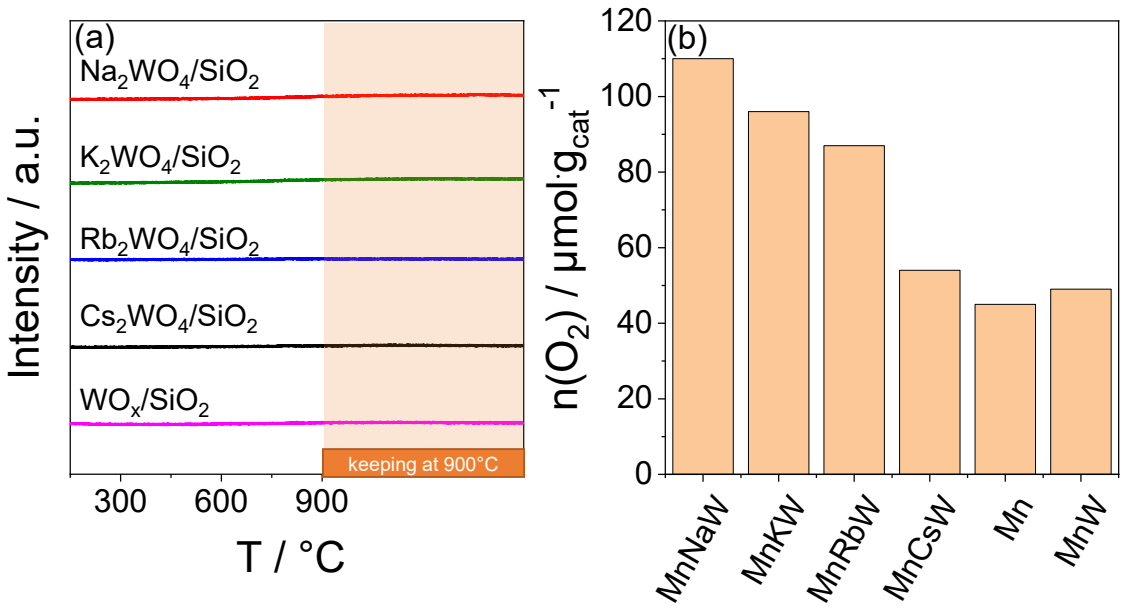

Fig. S8. (a) Oxygen desorption profiles of fresh M_2WO_4/SiO_2 (M= Na, K, Rb, Cs) and WO_x/SiO_2 catalysts. (b) The amount of oxygen desorbed during O_2-TPD experiments.

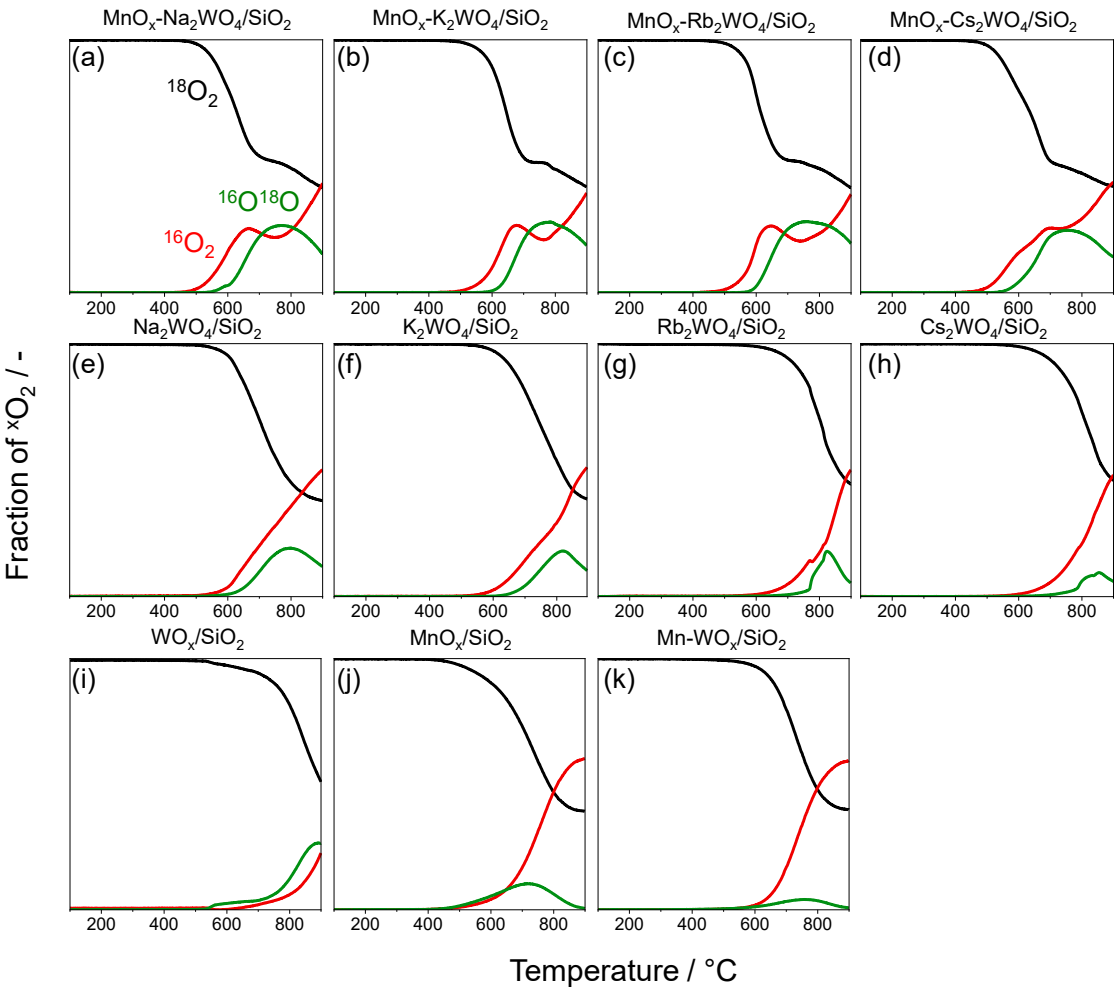

Fig. S9. The profiles of $^{18}O_2$ (black), $^{16}O_2$ (red), $^{16}O^{18}O$ (green) recorded during treatment of (a-d) MnO_x-M_2WO_4/SiO_2, (e-h) M_2WO_4/SiO_2 and (i) WO_x/SiO_2, (j) MnO_x/SiO_2, (k) MnO_x-WO_x/SiO_2 in a flow of (1vol%)$^{18}O_2$/Ar (7 ml/min).

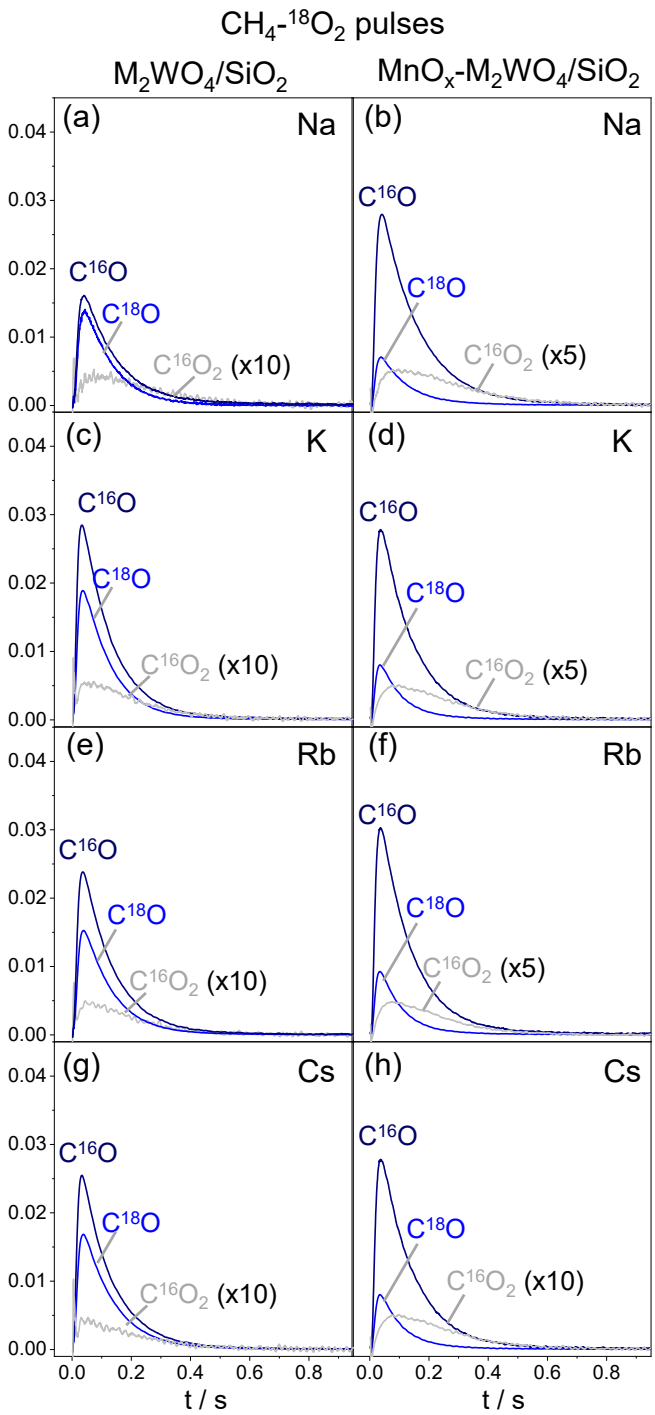

Fig. S10. Transients of $C^{16}O$, $C^{18}O$, $C^{16}O_2$ recorded after CH_4-$^{18}O_2$ pulses at 800 °C over (a, c, e, g) M_2WO_4/SiO_2 and (b, d, f, h) MnO_x-M_2WO_4/SiO_2; (a), (b) M=Na; (c), (d) M=K; (e), (f) M=Rb; (g), (h) M=Cs.

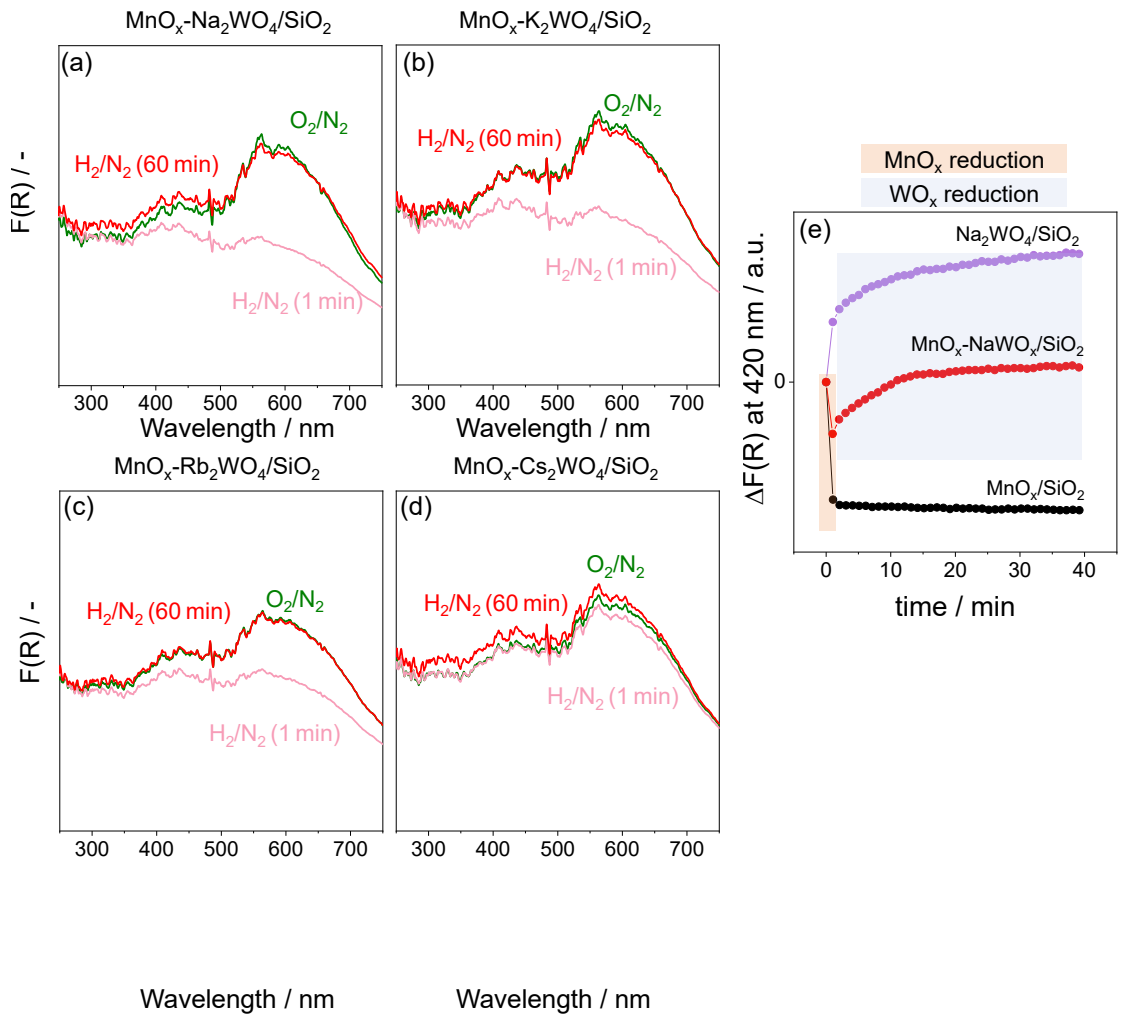

Fig. S11. The spectra at 750 °C under O_2/N_2 (green), H_2/N_2 for 1 min (pink) and H_2/N_2 for 60 min (red) over (a) MnO_x-Na_2WO_4/SiO_2, (b) MnO_x-K_2WO_4/SiO_2, (c) MnO_x-Rb_2WO_4/SiO_2, (d) MnO_x-Cs_2WO_4/SiO_2; (e) temporal change in the Kubelka-Munk function at 420 nm during reduction of oxidized MnO_x/SiO_2, Na_2WO_4/SiO_2 and MnO_x-Na_2WO_4/SiO_2 catalyst at 750 °C in 40vol%H_2/N_2.

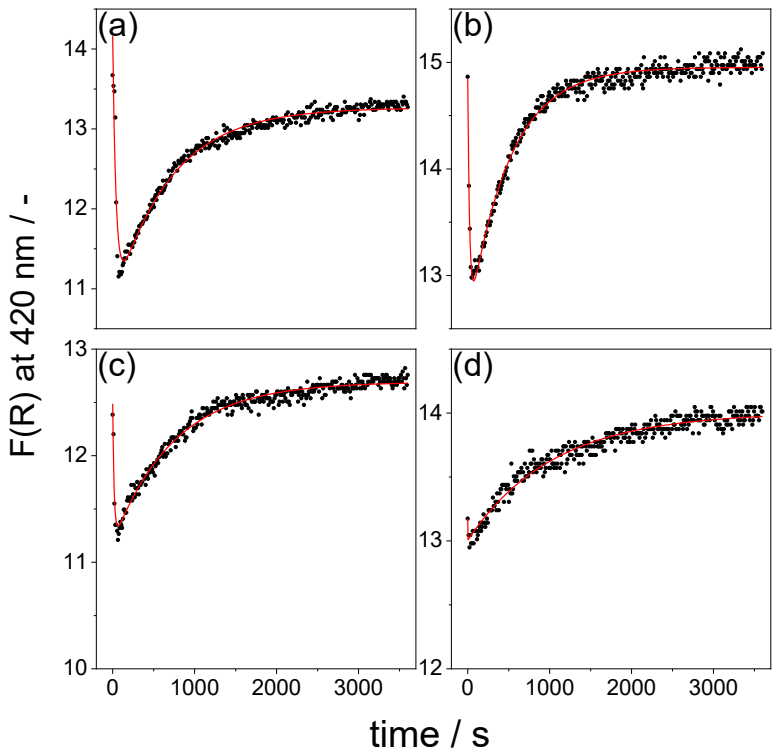

Fig. S12. The fitted curves of reduction of MnO_x-M_2WO_4/SiO_2 catalysts (a) M=Na, (b) K, (c) Rb, (d) Cs at 750 °C in 40vol%H_2/N_2 by $f(t) = (1 - A_1 \times e^{-k_1 t}) - (1 - A_2 \times e^{-k_2 t})$ +B function.

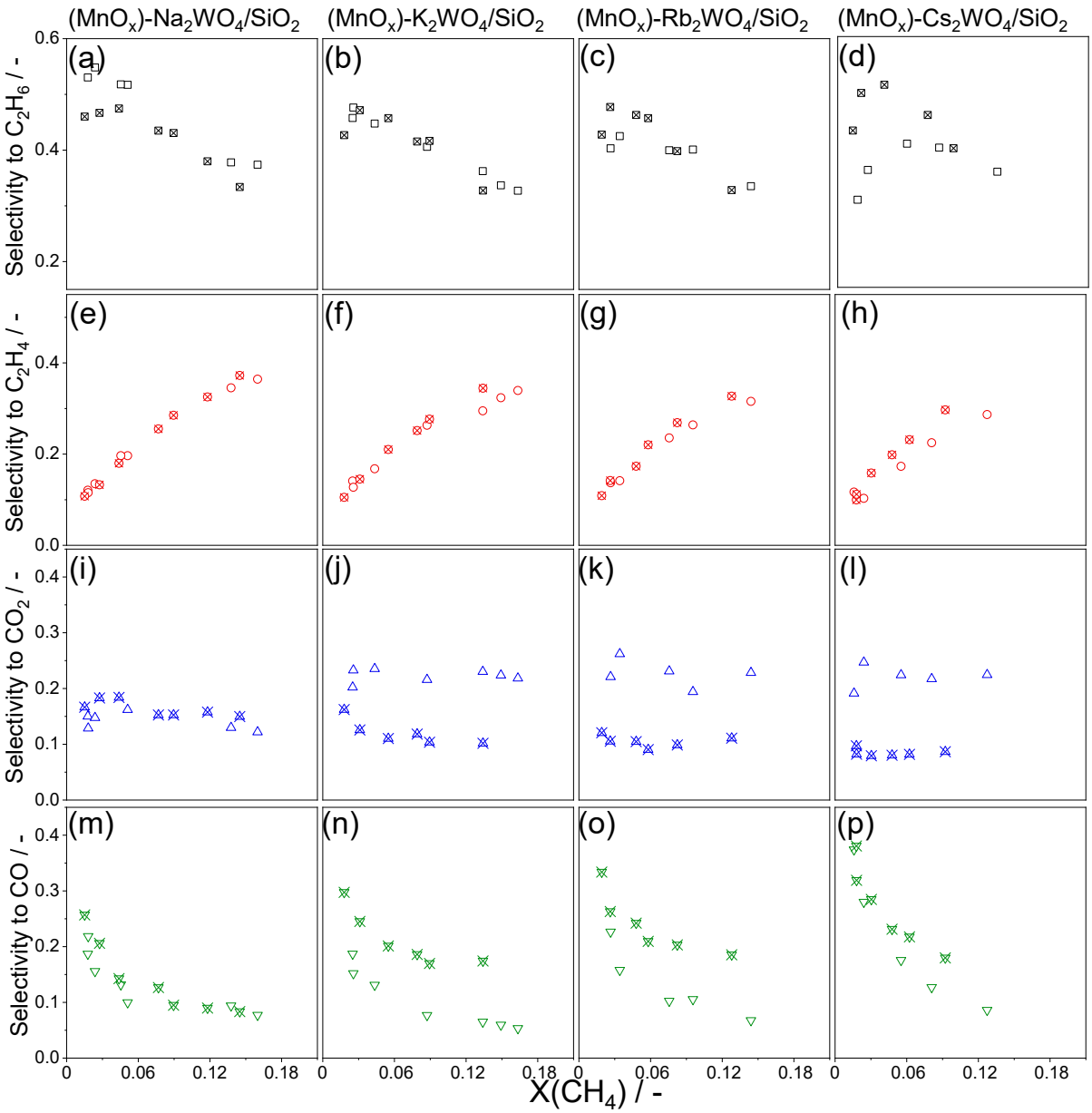

Fig. S13. The selectivity-conversion relationship for C_2H_6, C_2H_4, CO and CO_2 formed at 800 °C and 1.2 bar over MnO_x-M_2WO_4/SiO_2 (empty symbols) and M_2WO_4/SiO_2 (crossed symbols) catalysts (a,e,i,m) M=Na, (b, f, j, n) K, (c, g, k, o) Rb, (d, h, l, p) Cs using a $CH_4/O_2/N_2$ 40/5/55 feed, after the cycle in water using $CH_4/O_2/H_2O/N_2$ 40/5/30/25.

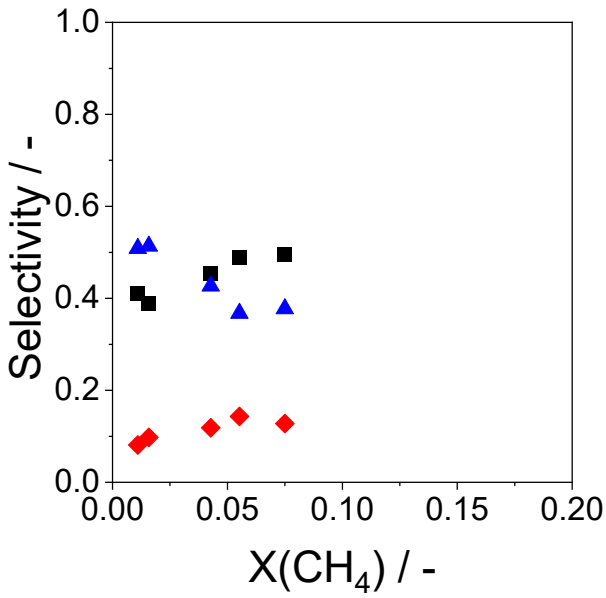

Fig. S14. The selectivity-conversion plot for C_2 hydrocarbons (■), CO_2 (♦) and CO (▲) formed over MnO_x-WO_x/SiO_2. Reaction conditions: 800 °C, 10-100 mg catalyst, $CH_4/O_2/N_2$ 40/5/55, flow rate of 30ml/min.

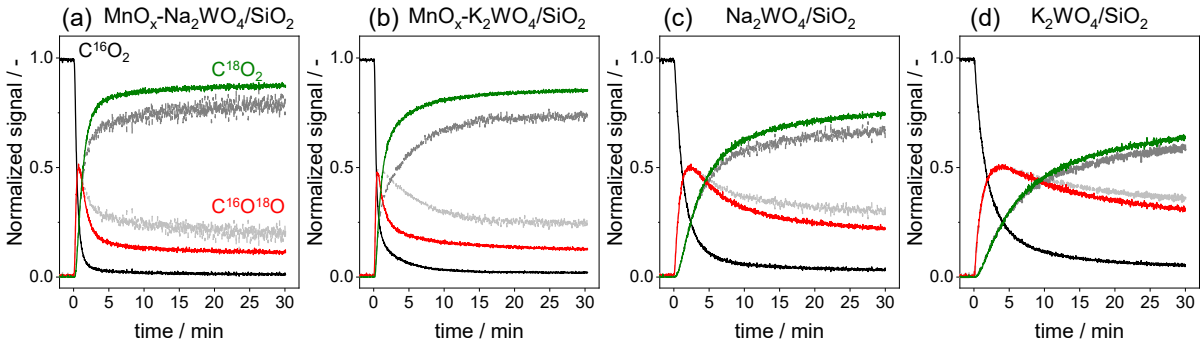

Fig. S15. The experimental transient responses of $C^{16}O_2$ (black line), $C^{16}O^{18}O$ (red line) and $C^{18}O_2$ (dark green line) detected after switching from a $CH_4/^{16}O_2$/He=30/4/66 feed to a $CH_4/^{18}O_2$/Ar/He=30/4/1/65 feed at 775 °C over (a) MnO_x-Na_2WO_4/SiO_2, (b) MnO_x-K_2WO_4/SiO_2, (c) Na_2WO_4/SiO_2 and (d) K_2WO_4/SiO_2. The profiles of $C^{16}O^{18}O$ and $C^{18}O_2$ calculated using a statistical model considering only one kind of oxygen species are shown as light grey and dark grey lines, respectively.

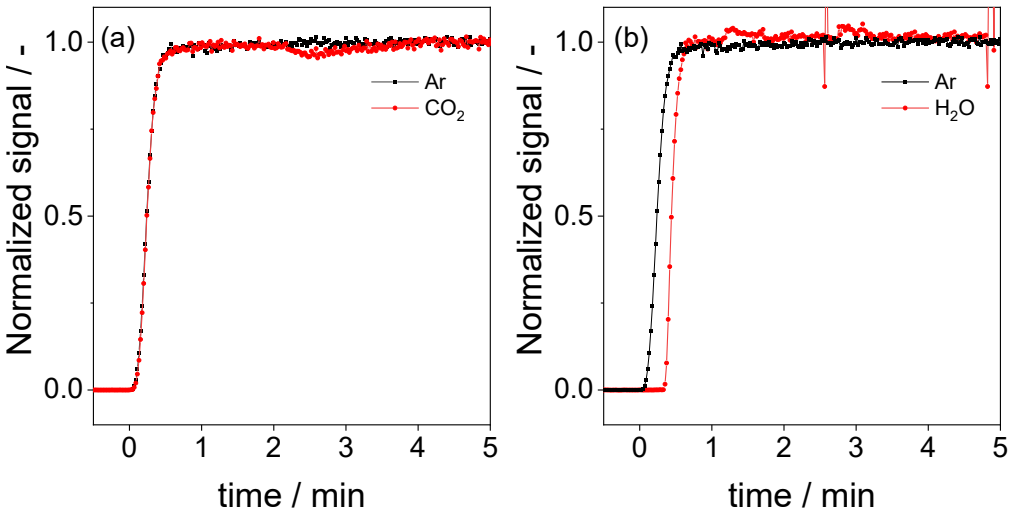

Fig. S16. Transients of (a) Ar and CO_2 as well (b) Ar and H_2O recorded at 800 °C after switch from He to CO_2/Ar/He or H_2O/Ar/He flows. Catalyst: 25 mg MnO_x-Na_2WO_4/SiO_2.

8. Curriculum vitae

Personal details:

Name	Anna Zanina
Date of birth	16.01.1994
Place of birth	Irkutsk, Russia
Email:	anna.zanina@catalysis.de

Education

07/2020 – present	Doctoral Student Leibniz-Institut für Katalyse e.V. (Rostock, Germany) Final qualifying paper: Fundamentals determining activity and product selectivity in the oxidative coupling of methane over MnO_x-M_2WO_4/SiO_2 (M=Na, K, Rb, or Cs)
09/2012-06/2018	Diploma in Fundamental and Applied Chemistry Qualification: Chemist. Lecturer in Chemistry Lomonosov Moscow State University (Moscow, Russia) Final qualifying paper: Nickel-Molybdenum sulfide catalysts based on mesoporous aluminosilicates in hydrogenation of aromatic compounds in water-carbon monoxide system
09/2011-06/2012	High school certificate The Specialized Educational Scientific Center on Physics, Mathematics, Chemistry and Biology of Novosibirsk State University (Novosibirsk, Russia)

List of publications:

1. **A. Zanina**, V.A. Kondratenko, H. Lund, J. Li, J. Chen, Y. Li, G. Jiang, E.V. Kondratenko, Performance-defining factors of (MnO_x)-M_2WO_4/SiO_2 (M = Na, K, Rb, or Cs) catalysts in oxidative coupling of methane, J. Catal., 419 (2023) 68-79.

2. **A. Zanina**, V.A. Kondratenko, H. Lund, J. Li, J. Chen, Y. Li, G. Jiang, E.V. Kondratenko, The Role of Adsorbed and Lattice Oxygen Species in Product Formation in the Oxidative Coupling of Methane over M_2WO_4/SiO_2 (M = Na, K, Rb, Cs), ACS Catal., (2022) 15361-15372.

3. Z. Aydin, **A. Zanina**, V.A. Kondratenko, J. Rabeah, J. Li, J. Chen, Y. Li, G. Jiang, H. Lund, S. Bartling, D. Linke, E.V. Kondratenko, Effects of N_2O and Water on Activity and Selectivity in the Oxidative Coupling of Methane over Mn–Na_2WO_4/SiO_2: Role of Oxygen Species, ACS Catal., 12 (2022) 1298-1309.

4. Z. Aydin, **A. Zanina**, V.A. Kondratenko, R. Eckelt, S. Bartling, H. Lund, N. Rockstroh, C.R. Kreyenschulte, D. Linke, E.V. Kondratenko, Elucidating the effects of individual components in K_xMnO_y/SiO_2 and water on selectivity enhancement in the oxidative coupling of methane, Catal. Sci. Tech., 11 (2021) 5827-5838.

5. A. Vutolkina, A. Glotov, **A. Zanina**, D. Makhmutov, A. Maximov, S. Egazar'yants, E. Karakhanov, Mesoporous Al-HMS and Al-MCM-41 supported Ni-Mo sulfide catalysts for HYD and HDS via in situ hydrogen generation through a WGSR, Catal. Today, 329 (2019) 156-166.

6. Y. Li, Q. Zhang, S. Fu, V.A. Kondratenko, T. Otroshchenko, S. Bartling, Y. Zhang, **A. Zanina**, Y. Wang, G. Cui, M. Zhou, Z. Zhao, C. Xu, G. Jiang, E.V. Kondratenko, Active species and fundamentals of their creation in Co-containing catalysts for efficient propane dehydrogenation to propylene, Chem. Eng. J., 460 (2023) 141778.

Conference participation

Talks

A. Zanina, V.A. Kondratenko, H. Lund, E.V. Kondratenko, "Role of oxygen species in the oxidative coupling of methane over M_2WO_4/SiO_2 (M=Na, K, Rb, Cs) catalysts", 9th World Congress on Oxidation Catalysis: Oxidation for a Sustainable Future and Clean Environment, Cardiff, September 4-8th 2022.

Posters

A. Zanina, D. Makhmutov, A. Vutolkina, Hydrocracking of shale oil over bimetallic sulfide catalysts based on mesoporous Al-HMS aluminosilicates, International scientific conference of students, graduate students, and young scientists Lomonosov-2016, Moscow State University, Russia, 11.04-15.04.2016.

A. Zanina, D. Makhmutov, A. Vutolkina, A Glotov, Ni-Mo sulfide catalysts based on mesoporous aluminosilicates in hydrogenation of model compounds via WSGR, 5th International School-Conference on Catalysis for Young Scientists "Catalyst Design: From Molecular to industrial Level", Moscow, Russia, 20.05.-23.05.2018.

A. Zanina, D. Makhmutov, E.V. Kondratenko, Oxidative coupling of methane over Mn-M(M=K, Rb or Cs)$_2WO_4/SiO_2$: Effects of alkali metal and water, 54. Jahrestreffen Deutscher Katalytiker, Online Event, 2021

A. Zanina, D. Makhmutov, E. V. Kondratenko, Study of catalyst activity and selectivity in oxidative coupling of methane in presence of water, 6th International School-Conference of Young Scientists "Catalyst Design: From Molecular to Industrial Level", Online Event, 16.05-19.05.2021

A. Zanina, E. V. Kondratenko, "Does molten tungstate in M_2WO_4/SiO_2 catalyst play a decisive role in the oxidative coupling of methane?", 55. Jahrestreffen Deutscher Katalytiker, Weimar, Germany, 27.06-29.06.2022.

A. Zanina, V.A. Kondratenko, H. Lund, E. V. Kondratenko, "Understanding of multiphase catalysts by time-resolved in situ catalyst characterization combined with temporal analysis of products for oxidative coupling of methane", 56. Jahrestreffen Deutscher Katalytiker, Weimar, Germany, 15.03-17.03.2023.